FeCrAl as a Catalyst Support

FeCrAl as a catalyst support

Gianluca Pauletto,[†,‡] Angelo Vaccari,[¶] Gianpiero Groppi,[§] Lauriane Bricaud,[‖,†] Patricia Benito,[¶] Daria C. Boffito,[†] Johannes A. Lercher,[‡,⊥] and Gregory S. Patience[*,†]

†*Chemical Engineering Department, École Polytechnique de Montréal, 2900 Boulevard Édourd-Montpetit, Montréal, Canada*

‡*Department of Chemistry, Technical University of Munich, 4 Lichtenbergstr, 85747 Garching, Germany*

¶ *Department of Industrial Chemistry "Toso Montanari", University of Bologna, Viale Risorgimento 4, 41036 Bologna, Italy*

§*Laboratory of Catalysis and Catalytic Processes, Dipartimento di Energia, Politecnico di Milano, via La Masa 34, 20156 Milano, Italy*

‖*Ecole Nationale Superieure des Mines, 158 Cours Fauriel, 42023 St Etienne, France*

⊥*Pacific Northwest National Laboratory, Institute for Integrated Catalysis, 902 Battelle Boulevard, WA 99352 Richland, USA*

E-mail: gregory-s.patience@polymtl.ca

Phone: +1 514 340 4711 ext 3439. Fax: +1 514 340 4059

Abstract

Fe, Cr, Al alloy (FeCrAl) is an exceptional support for highly exothermic and endothermic reactions that operate above 700 °C in chemically aggressive environments, where low heat and mass transfer rates limit reaction yield. FeCrAl two- and three-dimensional structured networks—monoliths, foams and fibers—maximize mass transfer rates while their remarkable thermal conductivity minimizes hot spots and thermal

gradients. Another advantage of the open FeCrAl structure is the low pressure drop due to the high void fraction and regularity of the internal path. The surface Al_2O_3 layer, formed after an initial thermal-oxidative, supports a wide range of metal and metal oxide active phases. This aluminum oxide that adheres to the metal surface protects it from corrosive atmospheres and carbon (carburization) thus allowing FeCrAl to operate at higher temperature.

Top applications are industrial burners, in which compact knitted metal fibers distribute heat over large surface areas, and automotive tail gas converters. Future applications include producing H_2 and syngas from remote natural gas in modular units. This review summarizes the specific preparation techniques, details process operating conditions and catalyst performance of a several classes of reactions, and highlights positive and challenging aspects of FeCrAl.

Contents

1 Introduction

To meet societies aspirations of sustainable development requires innovation to substitute petroleum with renewable bio-sourced feedstocks and catalysis will figure prominently in this paradigm shift. Already, industry applies catalysis in over 80 % of the chemical processes, which represents 30 % of the global gross product.[1,2] Solid catalysts have replaced harmful mineral acids and chloro-containing ones with the extra benefit of re-use compared to homogeneous systems. The incredible potential of heterogeneous catalysts, consists in their porous

nature that can be optimized to meet reaction conditions—high temperature, pressure, and corrosive environments, for example. Consequently the share of solid catalysts in the chemical industry will continue to rise as a result of the growth in world population and the escalation of the global energy demand, which was forecast to double from 2000 to 2035.[1,3] Heterogeneous catalysis is a key component of new processes targeting green chemistry and sustainability.[4,5] Indeed, in the last twenty years the field of environmental catalysts boosted the design of new solid materials capable of converting air and water pollutants generated by anthropogenic activities, as well as catalysts capable of converting heterogeneous substrates selectively—those derived from biomass.[4–7] Despite their numerous and indisputable advantages, heterogeneous catalyst design faces challenges to develop new sustainable processes and increase efficiency/decrease harmful and toxic byproducts in current processes. Catalyst comprising particles, pellets, and gauzes add complexity to plant operations; mass and heat transfer resistance around the catalyst limits the reagent throughput and introduces uncertainty with respect to scale-up and modelling;[8] and, narrow pores limit applications to less bulky molecules.[9] The latter limitation is particularly true for emerging biorefineries, which involves molecules such as lignin, polysaccharides and triglycerides. Synthesizing systems with interconnected micro- and mesopores, combining high specific surface area and improved mass transport remains major challenges in heterogeneous catalysis.[10]

Process intensification (PI) principles suggest introducing structure or modular catalytic units to minimize spatial randomness and control preferential mass and heat transfer pathways.[1,11,12] The structure can fit molecular, micro-, meso- and macro-scales. In this context, besides choosing a material that is inert at the operating pressure and temperature, and act synergistically with the active component, selecting a support facilitates modularization. Industry requires high flow rates, short contact times, tight temperature control, and low pressure drop across the bed.[13] Pressure drop across structured catalysts are two orders of magnitude lower than across packed beds and radial and axial temperature gradients (local hot spots) are lower due to the higher effective thermal conductivity and the regularity of

the internal path, which makes it possible to operate in the laminar regime.[11]

Cordierite—a mixture of Mg, Si and Al oxides extruded as a monolith for automotive tail gas treatments—is the most common high temperature structured support.[14] However, when hot spots affect the conversion and selectivity, materials with high heat transfer capacity, such as metallic supports, improve performance.

The metallurgy industry developed a Fe, Cr (up to 20 %), Al (0.5 % to 12 %) and Y (0.1 % to 3 %) alloy, which is commercialized under the name of FeCralloy® or Khantal®. Hans von Kantzow, engineer and CEO at Bultfabriks AB, discovered it in 1931, after a sample was left for years inside an oven in Hallstahammar, Sweden. FeCralloy® is a high temperature resistant steel in which Al diffuses to the surface above 800 °C. The surface Al oxidizes to Al_2O_3 in air and forms a resistant layer. The first applications were for furnaces, heating systems and electronic components. Yttrium prevents high temperature phase changes as it oxidizes first during the synthesis steps, therefore the melting steps require vacuum furnaces, which impacts the final cost of the material.[15] The ductility of FeCrAl makes it easy to shape into monoliths, fibers, foams and porous materials.[16,17] The most common structures are monoliths followed by foams and fibers that are all suitable for fixed bed reactors (Figure 1). Changing temperatures (during process start-up and shut-down, for example) dilates the materials that would crack the surface coating if it were not for the mechanical characteristics that release the stress. This property confers its high stability.[18]

Since 1976, the automotive industry has been using this material as a catalyst support but FeCrAl burners remain the most common application. In this review, we summarize the state of the art of FeCrAl in catalysis. We have structured our review of the FeCrAl adopted as a catalyst support by type of chemistry and active phase supported.

Conductivity is the controlling radial heat transfer mechanism in the case of low void fraction systems (high solids fraction) that maximize contact between the catalyst and reactor wall.[19–21] In traditional packed bed reactors, fluid dynamics contribute most to the heat

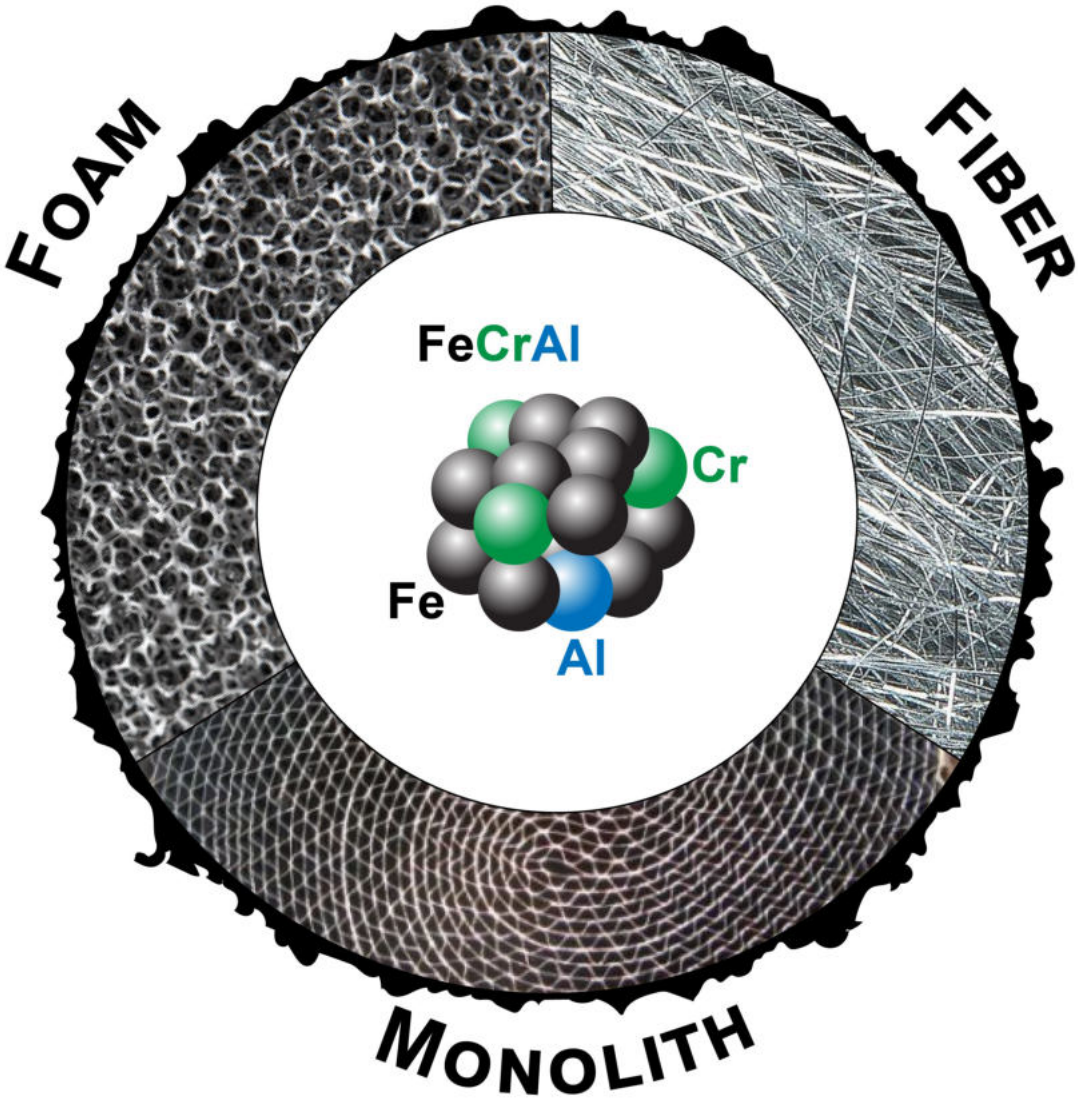

Figure 1: FeCrAl alloy. Structured supports: monolith, foam, fiber. External black coating Al_2O_3.

transfer coefficient, h, while it contributes much less to structured beds. Since $h_{\text{cond}} >> h_{\text{conv}}$, structured beds transfer more heat in smaller volumes minimizing reactor dimensions, which respects the principles of process intensification.[22] Even for highly exothermic and endothermic reactions, these beds operate isothermally, which is ideal to study reaction kinetics.[23]

Carbon preferentially forms on α-Fe,[24,25] but the Al_2O_3 surface layer minimizes contact between the gas phase and Fe thus minimizing coke deposition and carbon erosion.[26,27] Branched and bamboo nanotubes (carbon filaments) growing perpendicular to the surface

of the FeCrAl indicate the presence of exposed reduced iron.[28] During methane pyrolysis, a strong reducing environment together with the carbon deposition on the surface destabilize the protective Al_2O_3 coating. As result the reduced Fe is exposed and carbon diffusing through the particle detaches the metal from the bulk and carburizes the support with deleterious consequences.[29] Temperature also has an influence and the optimal growth appears at 700 °C. Less coke forms above 700 °C.[30] Additional and different coatings make FeCrAl a versatile material and in some cases they enhance the thermal resistance but influence carbon deposition, which carburizes the substrate with consequences on the mechanical behavior.[31] Stainless steel supports for heterogeneous catalysts are sufficient for low temperature reactions (less than 700 °C), while at higher temperatures the steel degrades with time as it has no stable protective superficial oxide.[32,33] The similar problem is also encountered in austenitic NiCr and NiCrAl form superficial chromia rather than Al_2O_3 layers and have higher density, lower electrical resistivity compared to ferretic FeCrAl. Superficial Al_2O_3 doping by Cr_2O_3 and Fe_2O_3 further stabilizes the stable alfa phase.[34] The maximum operating temperature of FeCrAl approaches 1400 °C, 200 °C higher than Ni containing alloys; superficial alumina protects the bulk metal better than chromia against sulfur and carbon diffusion.[35] While traditional Ni-based materials have higher strength and creep resistance, important in the manufacturing of structural parts, the new generation of FeCrAl now have comparable mechanical properties. As little as 0.15 % by mass of Y, Zr, Mo, Mn and Si reduce elongation caused by the interaction between bulk metal and superficial ceramic layer that are, however, less important when the material has reached high hot strength as in the case of commercial Kanthal® APM or APMT. Moreover, the higher density Ni-based alloys deform more at high temperature. Aluchrom is the commercial name of another FeCrAl alloy containing 70 %, 25 % Cr, and 5 % Al. However, micro-alloying with yttrium and zirconium is absent.[36,37] Only in the last decade has the scientific community begun to apply FeCrAl beyond furnace elements (Figure 2). From 1990, the number of articles has been increasing linearly from 50 per year and now exceeds 250 per year with about 80 dedicated to catalysis.[38] The most

prominent research cluster relates to microstructure and mechanical properties (red cluster in Figure 2), followed by oxidation (green cluster), metal composition (blue cluster with keywords Fe, Cr, Al, and Ni), and alloys, coatings, and steel (yellow cluster). Web of Science assigned 2424 journals with articles referencing FeCrAl to multidisciplinary materials science followed by metallurgy & metallurgical engineering (2225), physical chemistry (546), applied physics (418) nanoscience & nanotechnology (318), coatings & films materials science (311), and condensed matter physics (307). The most prolific journals were *J. Alloy. Compd.* with 170 articles, *Corrosion Sci.* with 100, and *Acta Mater.* with 98. Three articles, published in the 1990s, have garnered over 500 citations.[39–41]

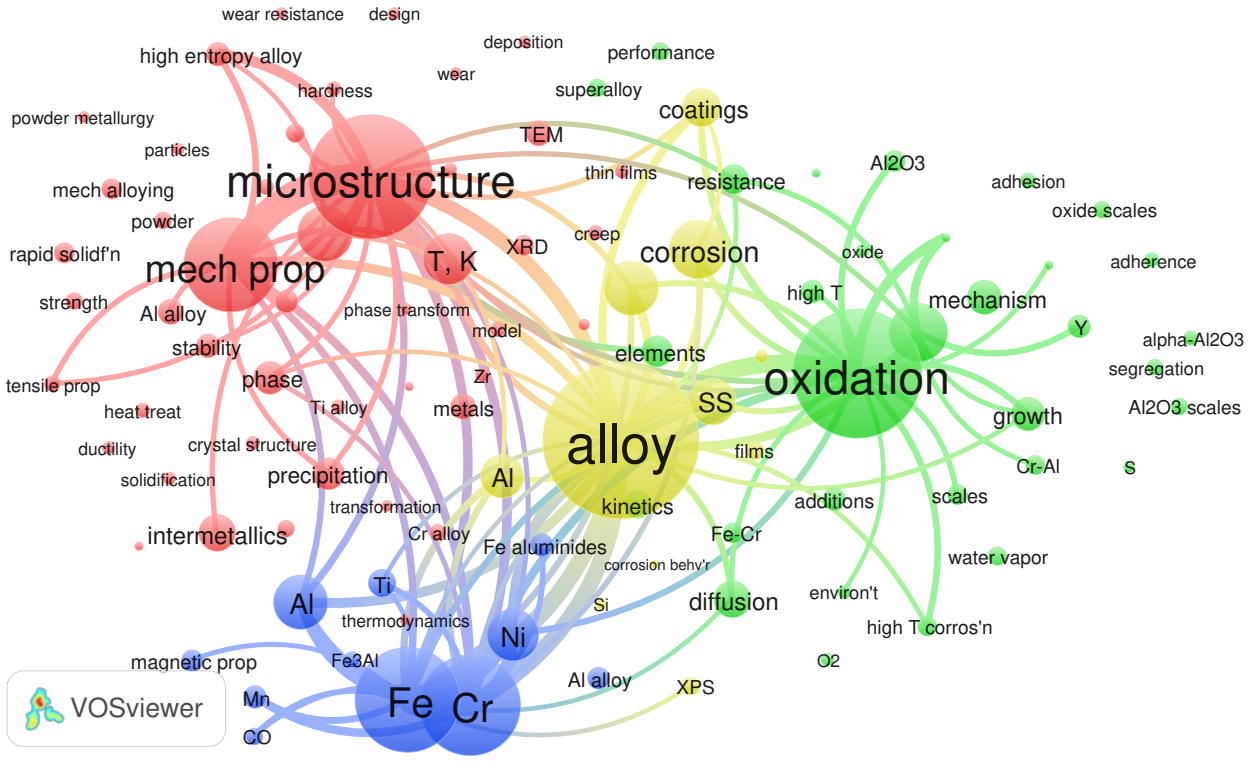

Figure 2: Bibliometric map generated by VOSviewer based on Web of Science Core Collection.[38,42] Keywords were FeCrAl, Kahntal and Fe Cr Al alloy. The size of each circle correlates with the occurrences in 4350 articles WoS indexed from 1989 to September 2018. VoSViewer groups the research into four clusters: microstructure (562 occurrences), oxidation (479 occurrences), Fe (476 occurrences), and alloy (709 occurrences) The smallest circles corresponds to 50 occurrences.

2 Heat and mass transfer in FeCrAl structures

Metal oxides as Al_2O_3, SiO_2, TiO_2, CeO_2, ZrO_2, CaO_2 are chemical resistant substrates for the synthesis of supported catalysts that operate at temperatures higher than 300 °C in the format of powder, sphere or pellet (Figure 3).[43–48]

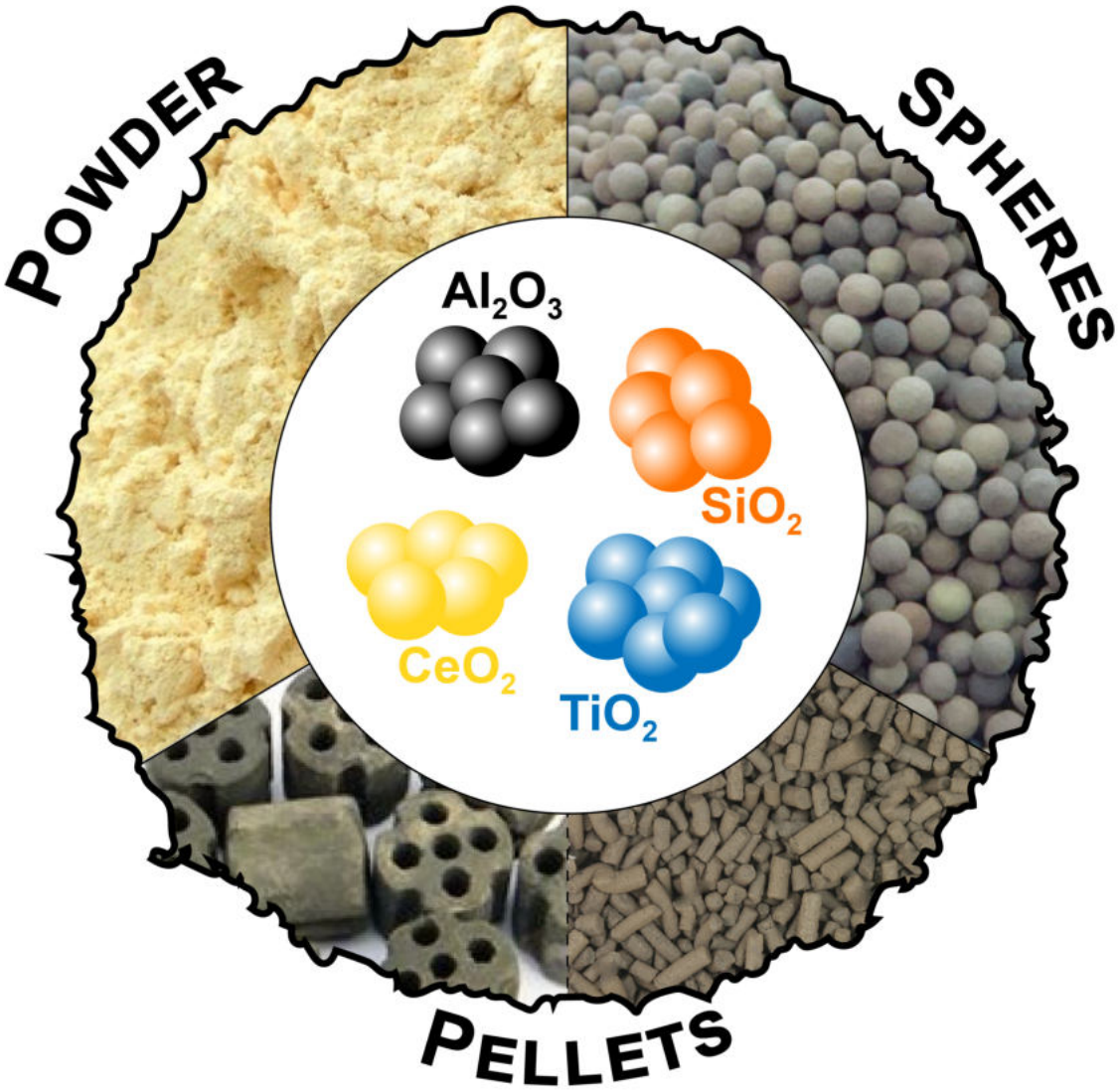

Figure 3: Most common ceramic supports.

During catalyst design, before hypothesizing synergies between support and active phases, considerations on the reaction such as temperature, pressure, energetic requirements, chemical properties of reagents and products help in identifying possible supports. The format

of the substrates is a relevant parameter to consider, but usually in a second step, at scale larger than the lab one. However, when high flow rates, short contact times, tight temperature control, low pressure drops across the bed, high heat and mass transfer are required, traditional packed bed reactors are unsuitable.[11,49,50] Moreover, when the reaction conversion and selectivity suffer from hot spots and temperature gradients, high heat transfer capacity of metallic supports improves the performance. FeCrAl is the reference material for the manufacture of structured substrates (Figure 4) for catalytic applications at high temperatures in oxidizing environments. One feature of these structured substrates is the possibility to fine tune heat and mass transfer properties to maximize catalyst performance. This is related both to thermal conductivity, specific heat and density of the material and to the geometrical characteristics of the substrates.

2.1 Geometrical properties

Honeycomb structures have been the benchmark solution for after-treatment catalytic technologies over the last several decades. They consist of a multiplicity of identical parallel channels through which gas passes in a straight path, typically in the laminar flow regime. Metal FeCrAl honeycombs are manufactured by rolling a crimped sheet coupled with a flat foil around a mandrel, while ceramic substrates are extruded. Standard cell densities range from 400 cpsi to 600 cpsi (cell per square inch) with 40 µm to 50 µm thick foils,[51] while advanced designs reach 900 cpsi to 1600 cpsi with 25 µm to 30 µm thick foils with an open frontal area in excess of 90 %.[52]

Figure 4: Most common examples of FeCrAl structures. Monoliths, foams and fibers (random sintered or knitted). Adapted with permission from reference.[53]

The geometrical properties of the assembly are evaluated based on a single channel. The surface to volume ratio, S_V, is the proportion (Eq. 1) of the void fraction (or open frontal area of the honeycomb), ε, and the hydraulic diameter d_h (typically a triangular or sinusoidal shape) and is the determining factor in gas-solid heat and mass transfer:

$$S_\mathrm{v} = \frac{4\varepsilon}{d_\mathrm{h}} \tag{1}$$

S_V up to $4000\,\mathrm{m}^{-1}$ to $6000\,\mathrm{m}^{-1}$ are standard in conventional and advanced designs, respectively.

Sintered metal fibers substrates have been applied in catalytic burners and particulate filters. Felts are manufactured starting from small diameter fibers ($d_\mathrm{f} = 10\,\mu\mathrm{m}$ to $50\,\mu\mathrm{m}$) that are sintered via high temperature diffusion bonding and reach porosities in the 80 % to 85 % range. The disordered structure creates a complex flow path, and assuming the base elements are infinitely long cylindrical fibres, the surface to volume ratio is:[54,55]

$$S_\mathrm{V} = \frac{4\,(1-\varepsilon)}{d_\mathrm{f}} \tag{2}$$

With 25 µm fibers and $\varepsilon = 85\,\%$, S_V exceeds $20\,000\,\mathrm{m}^{-1}$.[54]

Open cell metal foams consist of cavities (cells) accessible through windows (pores) in an interconnected 3D solid matrix made of struts that intersect in nodes. In FeCrAl foams, porosity reaches 95 % with pore densities in the range of 10 ppi to 100 ppi (pore per inch). Geometrical models assume that the structure consists of repeating unit cells—cubic,[56] dodecahedral,[57] and tetrakaidecahedral.[58] The latter polyhedron, also called a Kelvin cell, characterizes the foam geometry best.[59] Refinements of the geometrical model include the shape of the strut cross-section that, due to minimum surface energy reasons, changes from circular to triangular and to triangular concave with increasing void fraction[58] and the node-strut distribution of the solid material.[60] In general, S_V increases with pore density and solid fraction of the foam: $S_\mathrm{V} > 5000\,\mathrm{m}^{-1}$ for a 100 ppi foam at $\varepsilon = 0.9$.[60]

2.2 Gas-solid heat and mass transfer

Gas-solid heat and mass transfer rate coefficients, h and k_m, like S_v, depend on structure substrate geometry. Researchers apply the Colburn analogy for heat and mass transfer in ducts of honeycomb monoliths. The classical Hawthorn correlations relate the non-dimensional Nusselt number (N_Nu) for heat transfer and Sherwood number (N_Sh) for mass transfer to the Reynolds number (N_Re), Schmidt number (N_Sc) and Prandtl number (N_Pr), assuming that the characteristic length is d_h:[61]

$$N_\mathrm{Nu} = 3.66 \left(1 + 0.095 \frac{N_\mathrm{Re} N_\mathrm{Pr}}{z} d_\mathrm{h}\right)^{0.45} \tag{3}$$

$$N_\mathrm{Sh} = 3.66 \left(1 + 0.095 \frac{N_\mathrm{Re} N_\mathrm{Sc}}{z} d_\mathrm{h}\right)^{0.45} \tag{4}$$

The coefficient 3.66 represents the asymptotic solution for fully developed laminar flow in ducts, while the N_Re term accounts for the development of the velocity, temperature (Eq. 3), or concentration profiles (Eq. 4), which decrease along the channel coordinate, z. These

Hawthorn correlations apply to average transfer coefficients in circular channels but have been adapted to local heat transfer coefficients[62] and alternative geometries including triangular and sinusoidal channels typical of FeCrAl honeycombs.[63] Correlations mainly refer to laminar flow conditions which cover most of the practical applications, however, advanced configurations have been developed for FeCrAl honeycombs, which enhances heat and mass transfer coefficients by repeated disruption of the laminar flow structure.[64]

The assessment of the gas-solid heat and mass transfer performance of open cell foams is still debated in the literature. The choice of the characteristic length to be adopted in N_{Nu} and N_{Sh} correlations is a key issue. Originally, the equivalent channel diameter was assumed to be the pore size.[65] Later, the mean pore diameter was defined as the size of the internal pore window and the strut diameter.[66] For metallic foams, Giani et al.[19,67] stated that the average strut diameter, $d_{\mathrm{s,av}}$, was a more representative characteristic length when considering the flow path in the foam structure and they developed a correlation based on the analogy with convective heat transfer in bundles of tubes. The approach was further refined by combining experimental tests on CO oxidation with computational fluid dynamic simulations (CFD) developing a correlation (Equation. 5) based on the combination of asymptotic contributions associated with creeping and turbulent flow, respectively:[68]

$$N_{\mathrm{Sh}} = \varepsilon^{-2}\left(0.566 N_{\mathrm{Re}}^{0.33} + 0.039 N_{\mathrm{Re}}^{0.8}\right) N_{\mathrm{Sc}}^{\frac{1}{3}} \tag{5}$$

Few studies have been performed on sintered metal fibers[61,69] but foam and fiber felt performance correlate with the same equation with Sauter mean diameter, d_{sauter} as the characteristic length:

$$d_{\mathrm{Sauter}} = \frac{6\,(1-\varepsilon)}{S_{\mathrm{V}}} \tag{6}$$

$$N_{\mathrm{Sh}} = 1.26 \left[\frac{1-(1-\varepsilon)^{\frac{5}{3}}}{2-3(1-\varepsilon)^{\frac{1}{3}}+3(1-\varepsilon)^{\frac{5}{3}}-2(1-\varepsilon)^{2}} \right]^{\frac{1}{3}} \left(0.991 N_{\mathrm{Re}}^{\frac{1}{3}} N_{\mathrm{Sc}}^{\frac{1}{3}} + \frac{0.037 N_{\mathrm{Re}}^{0.8} N_{\mathrm{Sc}}}{1+2.44 N_{\mathrm{Re}}^{-0.1}\left(N_{\mathrm{Sc}}^{\frac{2}{3}}-1\right)} \right) \tag{7}$$

Internal mass transfer in the porous washcoat is as important as external mass transfer because the effective intraporous diffusivity is low. However, it is negligible when considering heat transfer: the gas phase boundary layer is much larger than the porous washcoat thickness and its thermal conductivity is one order of magnitude lower ($0.05\,\mathrm{W\,m^{-1}\,^{\circ}C^{-1}}$ for air vs. $0.2\,\mathrm{W\,m^{-1}\,^{\circ}C^{-1}}$ for a porous ceramic layer).

2.3 Heat transfer in FeCrAl structures

The effective conductivity, k_{eff} is a sum of the contributions from conduction, $k_{\mathrm{eff,cond}}$, convection, $k_{\mathrm{eff,conv}}$, and radiation, $k_{\mathrm{eff,rad}}$:

$$k_{\mathrm{eff}} = k_{\mathrm{eff,cond}} + k_{\mathrm{eff,conv}} + k_{\mathrm{eff,rad}} \tag{8}$$

Referring to the cross sectional direction of a honeycomb structure, the convective term is absent as the flow path is segregated in the parallel channels. Also radiation is negligible because the channel wall shielding and the large aspect ratio of the channel geometry, results in very low view factors along the axial direction. With respect to conduction, geometric anisotropy of the honeycomb structure must be considered. In the axial coordinate heat flows along the gas and the solid phases, so the axial effective thermal conductivity $k_{\mathrm{eff,ax}}$ is the sum of the intrinsic gas conductivity, k_{g} and solid conductivity k_{s} weighted by their geometrical fraction:[70]

$$k_{\mathrm{eff,ax}} = k_{\mathrm{g}}\varepsilon + k_{\mathrm{s}}(1-\varepsilon) \tag{9}$$

Because of FeCrAl's relative high thermal conductivity, which increases from $12\,\mathrm{W\,m^{-1}\,K^{-1}}$

at room temperature to 25 $W\,m^{-1}\,K^{-1}$ at 1200 °C (Figure 5), the solid term dominates.[71]

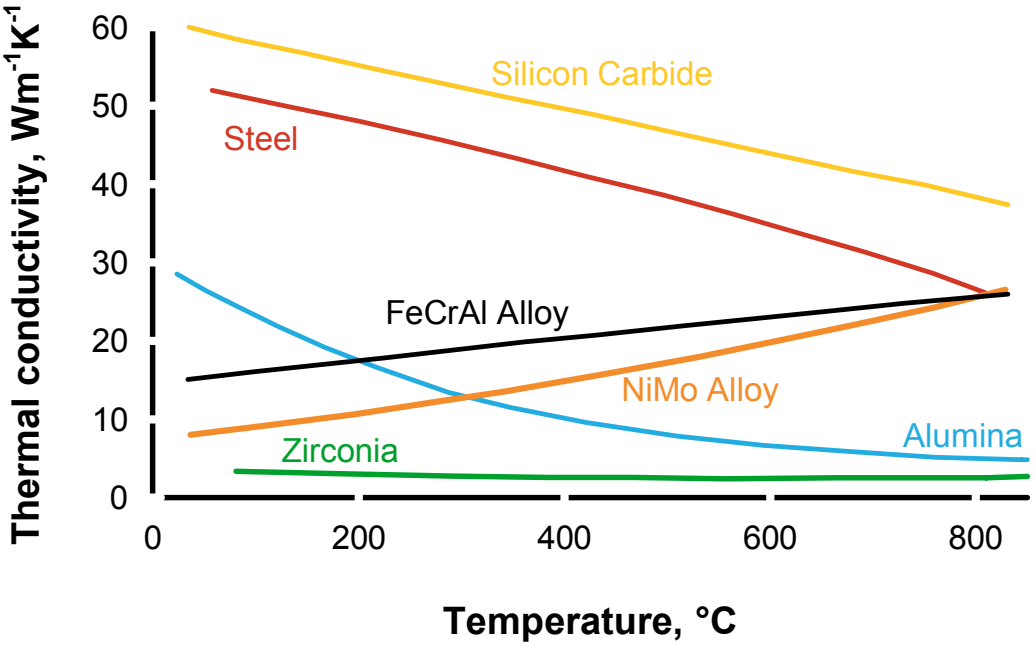

Figure 5: Thermal conductivity vs temperature of some of the most used catalyst supports. Adapted with permission from reference.[72]

On the other hand, heat conduction along the cross sectional direction is limited due to the more tortuous path along the solid walls and, mainly, to the lack of continuity of the structure associated with the manufacturing process of FeCrAl monoliths. The equations developed for extruded honeycombs are inapplicable since the lower contact points between the rolled layers result in a major resistance to heat transfer along the transversal coordinate.[70,73]

As opposed to honeycombs, open cell foams are isotropic, which guarantees the same effective conductivity in all directions. Two approaches account for the heat transport term: one approach, adapted from porous media literature, assumes that the effective conductivity is a weighted average of in-series in-parallel heat conduction paths in the solid and gas phases:

$$k_{\mathrm{eff,cond}} = b k_{\mathrm{serial}} + (1-b)\, k_{\mathrm{parallel}} \tag{10}$$

where

$$k_{\mathrm{parallel}} = k_{\mathrm{g}}\varepsilon + k_{\mathrm{s}}\,(1-\varepsilon) \tag{11}$$

and

$$k_{\mathrm{serial}} = \left(\frac{\varepsilon}{k_{\mathrm{g}}} + \frac{(1-\varepsilon)}{k_{\mathrm{s}}}\right)^{-1} \tag{12}$$

Several studies report that b varies from 0.63 to 0.65 for metallic[74] and ceramic foams.[75,76]

The second approach considers the tortuosity, τ, of the heat flow path along the solid interconnected structure:

$$k_{\mathrm{eff,ax}} = k_{\mathrm{g}}\varepsilon + \frac{k_{\mathrm{s}}\,(1-\varepsilon)}{\tau} \tag{13}$$

where τ depends on void fraction according to:[77]

$$\tau = \left(\frac{1}{3} + \frac{2}{3}\,(1-\varepsilon)\right)^{-1} \tag{14}$$

which respects the theoretical asymptotes, $\tau = 3$ as $\varepsilon \to 1$ and $\tau = 1$ as $\varepsilon \to 0$.[78]

Because foams are open, both convective dispersion and radiation contribute to Eq. 8. For the convective dispersion terms, the few available literature correlations include the Peclet number, N_{Pe}:

$$\frac{k_{\mathrm{eff,conv}}}{k_{\mathrm{g}}} = \frac{N_{\mathrm{Pe}}, x}{K_{\mathrm{r}}} \tag{15}$$

where x is the characteristic length and K_{r} is the radial dispersion coefficient. The square root of the permeability,[79] the cell size[75] and the mean pore diameter[76] have been used as characteristic lengths, with K_{r} equal to 16.67, 14.5 and 8, respectively. Considering air as the flow medium, the convective dispersion term is comparable with the conductive term at $10\,\mathrm{m\,s^{-1}}$ in a 60 ppi FeCrAl foam with $\epsilon = 0.9$. The Rosseland approximation applies for the

radiation term:

$$k_{\text{eff,rad}} = \frac{16\sigma_B T^3}{3E_{\text{r}}} \tag{16}$$

where σ_{B} is the Stefan-Boltzmann constant and E_{r}, the Rosseland extinction coefficient, which is a function of the foam geometrical properties where d_{c} is the diameter of the foam cell:

$$E_{\text{r}} = C_{\text{r}} \frac{(1-\varepsilon)^{0.5}}{d_c} \tag{17}$$

with $C_{\text{r}} = 2.65$ as proposed by Bianchi et al.,[20] the radiation term is negligible with respect to the conduction and convection except for FeCrAl foams with high void fraction ($\epsilon > 95\,\%$) and low pore density 10 ppi to 20 ppi operating below 500 °C.

When honeycomb and foams are loaded in a tube casing, the local resistance at the wall-structure interface contribute to the overall heat transfer rates towards the external environment.[20,80]

3 Catalyst preparation

Nijhuis et al., Avila et al. and Meille et al. reviewed structured catalyst support preparation, including FeCrAl.[81–84] The two main approaches to coat a catalytic layer on a 3D support include (Figure 6):

i) deposition of a ready-made catalyst (and/or support), and

ii) in situ growth of the catalyst (and/or support).[85–87]

Catalytic films comprise metal oxides containing the active phase, metallic particles, or zeolites; in situ syntheses of hydroxides form a layer of metal oxides after calcination.

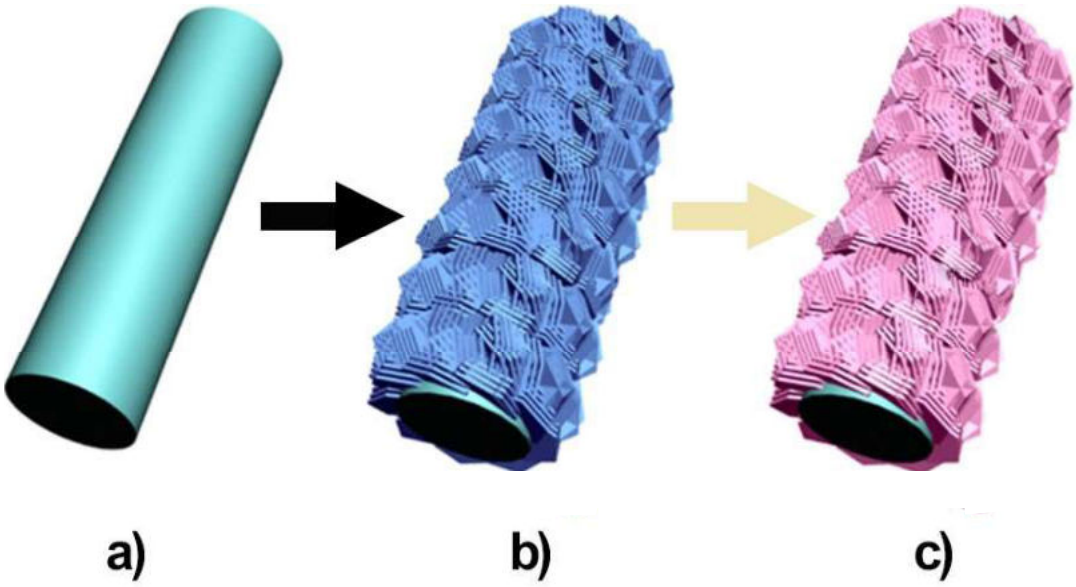

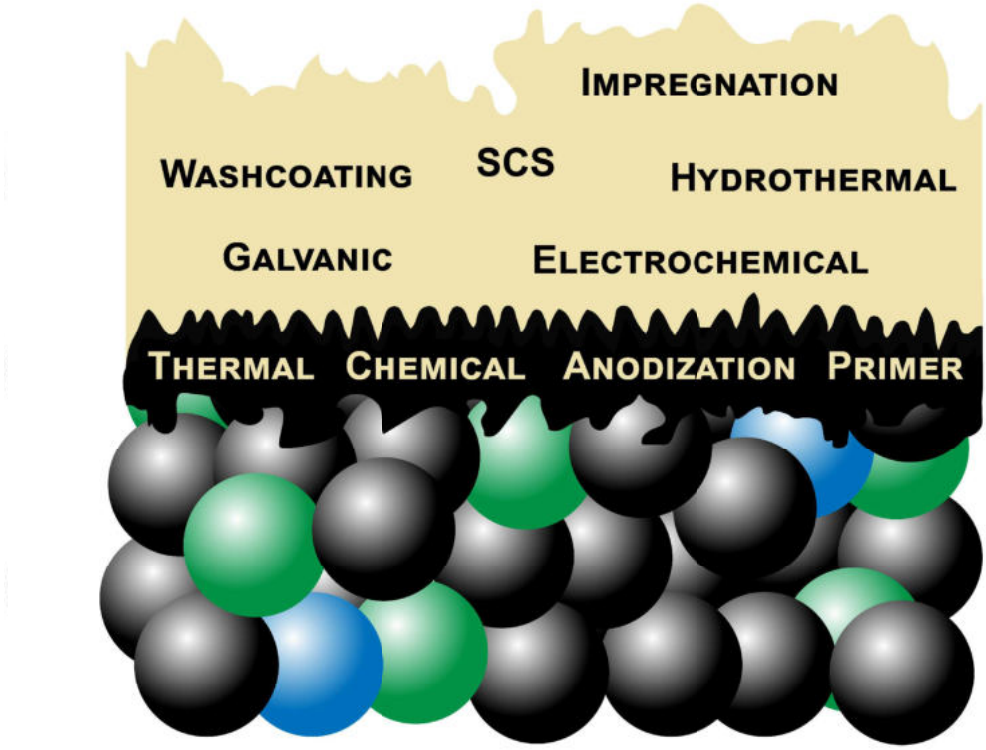

Figure 6: FeCrAl catalyst preparation: a) FeCrAl, b) FeCrAl after pretreatment, c) FeCrAl after coating of catalytic layer. Pretratments (black layer): thermal and chemical treatment, anodization and primer deposition. Coating of catalytic layer (ochre): i) washcoating; ii) impregnation followed by calcination, solution combustion synthesis (SCS), hydrothemal methods, galvanic displacement and electrochemical processes. Adapted with permission from reference.[88] Copyright 2017 American Chemical Society.

Herein, we describe methods to coat FeCrAl materials—honeycomb monoliths, fibers, meshes and open-cell foams—and focus on the in situ synthesis techniques developed in the last few years. In the sections dealing with the application of the structured catalysts, we report the specific preparation technique and its effect on the catalytic activity.

3.1 Pretreatment of the FeCrAl

Low surface area, low chemical interaction, and a mismatch between thermal expansion coefficients of the ceramic coating and the metallic support compromise the stability of structured catalyst on metallic supports. Consequently, the catalytic film creeps and peels during preparation and under reaction conditions. Pretreating and preoxidizing the metallic supports increase the available surface area and improve coating adhesion, which protects the metal.[15,18,55,89] The parent FeCrAl surfaces are smooth on a µm length scale and chemical species bind poorly to it (Figure 7). After the preoxidation step, the surface has a rough sandpaper like quality with ridges and valleys. Thus, preoxidition produces a surface Al_2O_3 layer that promotes chemical interactions between the substrate and active phase.

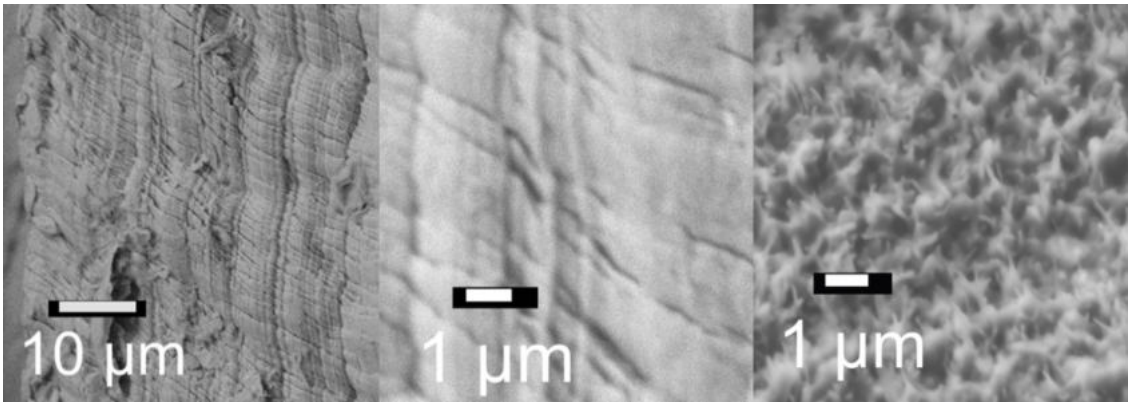

Figure 7: FeCrAl fiber surface before preoxidation (two picture on the left) and after (right).

Aluminum oxide is a common support because of its versatility to stabilize catalytically active materials for a variety of reactions. Production procedures consists of the thermal dehydration of aluminum hydroxide that produces eight Al_2O_3 allotropes but only the α,

γ, δ and θ phases are common. Temperature influences the physical conformation and the transitions from one phase to the other.[90]

3.1.1 Thermal and chemical treatment

In the case of FeCrAl metal support, the thickness and homogeneity of the Al_2O_3 produced during the initial thermal pretreatment is important but insufficient for every chemical system where precise catalyst formulations are required, as is the case of environmental reactions.[91] In a 500 h stability experiment for preferential CO oxidation operating between 100 °C to 300 °C Fe, Cr and Y migrated from the bulk to the wash coating and there deactivated the catalyst.[92] A 22 h-preoxidation treatment at 950 °C was insufficient to create an Al_2O_3 barrier between the metal support and washcoat so cations continued to migrate from the bulk.[91] Cr from a FeCrNi support migrated within 24 h on-stream operation after a 650 °C peroxidation step, while migration in a FeCrAl was undetected.[93] During thermal pretreatment of FeCrAl (above 800 °C), Al migrates to the surface and oxidizes to create a Al_2O_3 coating (Figure 8).[15,35,94,95] This coating binds compounds and has high heat shock resistance without shelling after 5000 cycles at 1000 °C (Figure 9(a)).[96]

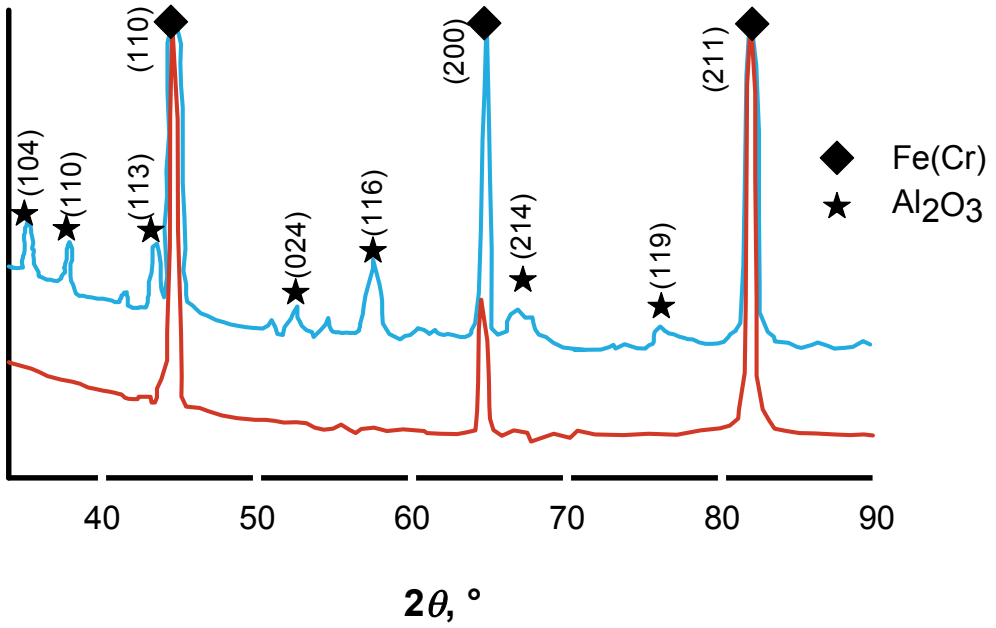

Figure 8: X-ray diffraction (XRD) analysis of FeCrAl before (red) and after (blue) preoxidation. Adapted with permission from reference.[97] Copyright 2012 Elsevier.

Additional FeCrAl pretreatment is however necessary, because the Al_2O_3 layer (after preoxidation) is rarely thick enough to protect the metal, and the surface area is too low for catalysis (Figure 9(b)). Chemical pretreatment of FeCrAl increases the oxidation rate as well as the superficial roughness that creates mechanical junctions (Figure 9(c)).[98] Thermal pretreatment is more effective than the chemical, but combining both is best (Figure 9(d)).[99]

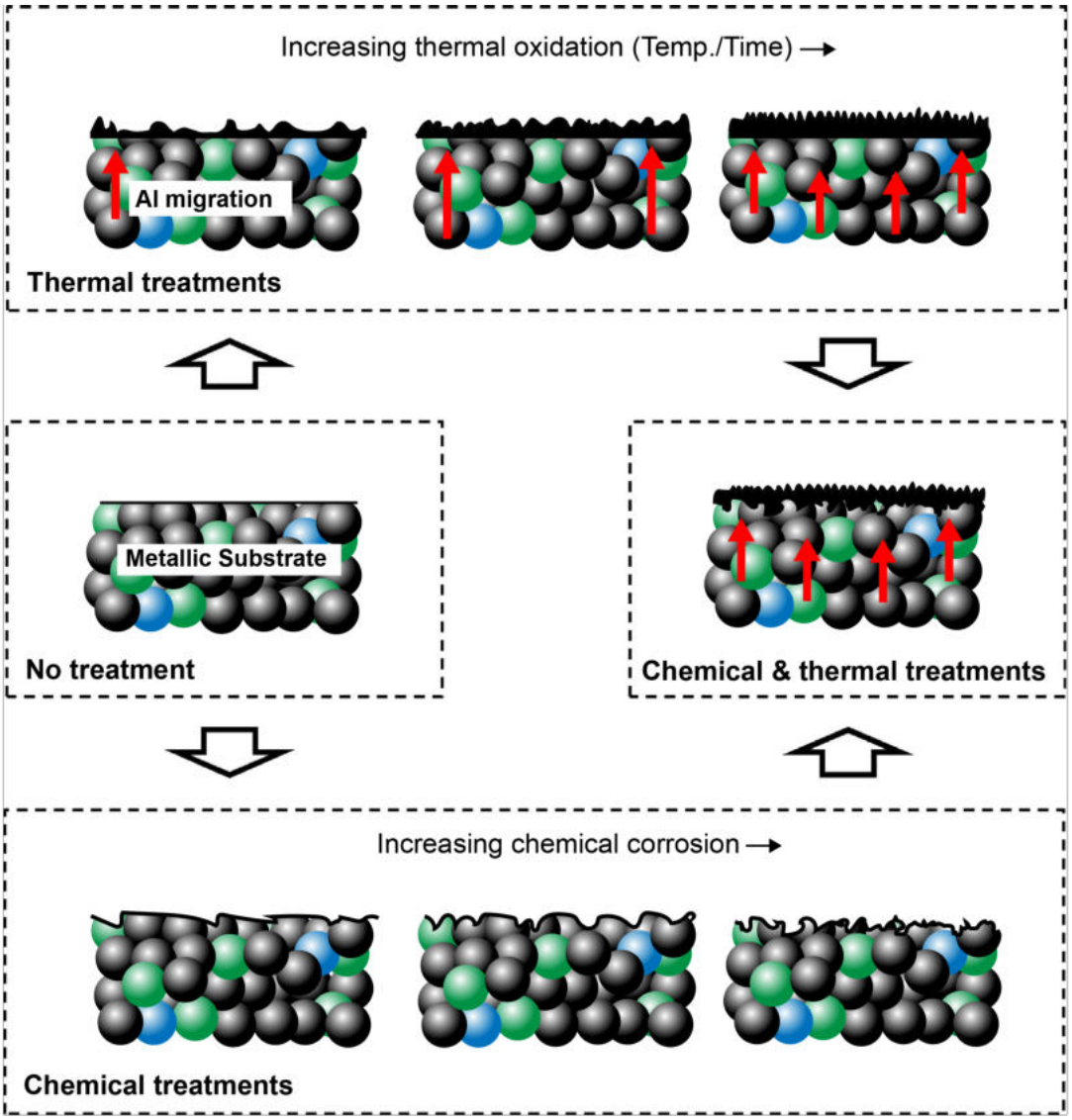

Figure 9: Morphological changes as a function of thermal pretreatment time and temperature (a), chemical pretreatment and corrosion (c) on the untreated FeCrAl (b). Al migration to the surface (red arrows) and Al_2O_3 (black). Adapted with permission from reference.[99] Copyright 2017 Elsevier.

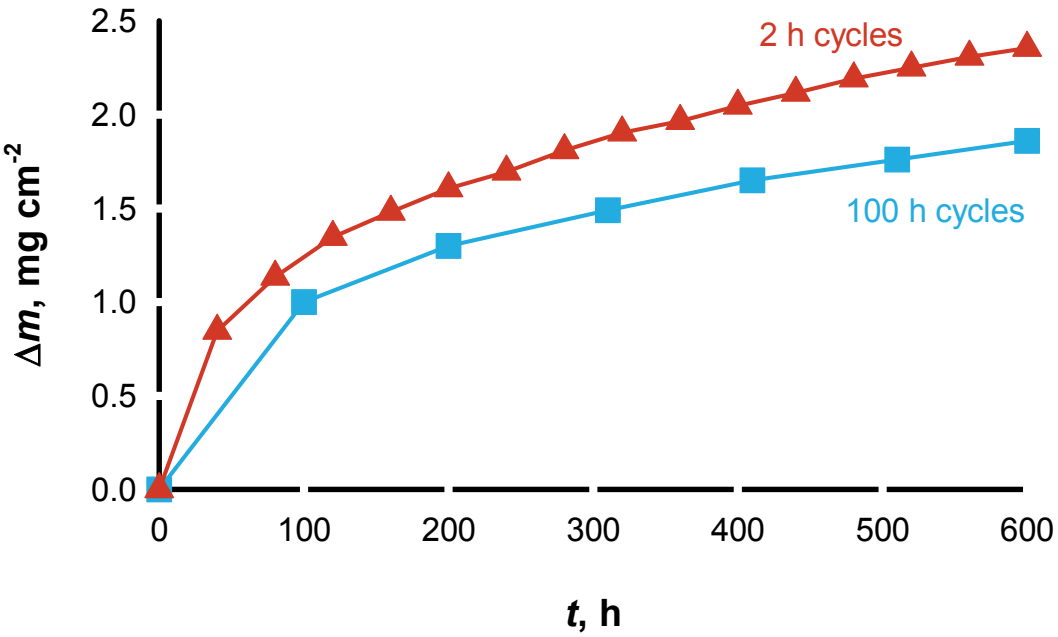

Figure 10: Mass increase depending on the air oxidation cycle duration at 1200 °C. Adapted with permission from reference.[100] Copyright 2004 Springer Nature.

FeCrAl preferentially begins to degrade at points where the Al_2O_3 surface has defects or inhomogeneities.[101] Cr_2O_3 between the bulk metal and alumina coating provides additional stability to the support, but the mass fraction of Al in the alloy is the determining factor for life-time.[102] α-Al_2O_3 preserves the metal better than γ, δ, and θ phases, because it minimizes oxygen diffusion.[103]

α-Fe, body-centered cubic, in the FeCrAl bulk determines the morphology of the Al_2O_3 formed during oxidation. Folding, stretching, and bending (mechanical deformations) of the support changes the shape and the orientation of Fe and therefore the thickness of the final Al_2O_3.[104] The oxidation rate, and thus the nature and thickness of the coating, varies with the oxidative environment composition—air, H_2O, O_2, and O_2 plus SO_2—temperature, time, substrate origins, and geometry. The chemical composition of the superficial coating changes with temperature: below 900 °C mixtures of Fe, Cr and Al oxides form. At 900 °C

the coating consists mostly of α-Al_2O_3 with some γ or θ- Al_2O_3 and a rich intra layer of Cr oxide. The mass fraction of Al metal hovers at 80 % up to a depth of 350 nm then drops to below 10 % at 600 nm. H_2O in the oxidizing mixture favors metastable phases.[105] The α phase forms in the range of 900 °C to 1100 °C while several allotropes co-exist at lower temperatures.[101]

The oxide layer grows following a cubic time dependence even if possible discrepancies might appear as a result of thermal cycling cracks and support inhomogeneity.[100] Higher quantities of Al in the alloy increase the thermal stability of FeCrAl, because Al oxidizes into a thicker protective layer.[106] However, not all Al diffused to the surface oxidizes because the growing Al_2O_3 thickness blocks metal-oxygen contact.

In short-time thermal cycles, the oxide layer cracks and exposes additional Al (Figure 10) that reacts and forms a Al_2O_3 grain. More Al_2O_3 increases oxidation resistance but, on the other hand, a higher number of grain boundaries decreases it as O_2 diffusion increases. After H_2 annealing, La-Zr and La-Hf in the bulk reduce the oxidation state of the alloy and they reduce the presence of both Fe and Cr in the oxide layers.[107]

Thermal oxidation in O_2 and SO_2 atmospheres, or deposition of active catalyst and alumina via magnetron sputtering creates acid and basic sites that change the catalytic activity.[103,108] Even though the magnetron radio frequency (RF) is six times more efficient than direct current (DC), it operates on a small surface area limited by the geometry of the source.[109] Magnetron sputtering supplies superficial Al_2O_3 that helps to control the morphology but powder embedded techniques also increase superficial aluminium that produces nanowires during oxidation. In this case, thermal stress does not crack the additional alumina washcoat that is often added.[110]

3.1.2 Anodization

Anodic oxidation applies an electric field to an electrolyte, usually an acid (H_2SO_4), in contact with a material that generates a porous oxide layer at the surface, while dissolving

the support. Time, current density, temperature, type of electrolyte, and its concentration determine morphology, porosity, and thickness of the oxide layer. This result is different from that produced by calcination. During anodization of FeCrAl, the metals component dissolve generating channels of ca. 1 µm to 4 µm perpendicular to the surface and simultaneously an amorphous oxide film develops with cavities at the nanometeric scale; iron preferentially dissolves compared to chromium.[111,112]

3.1.3 Deposition of a primer

Calcined substrates coated with an intermediate layer (primer) have higher chemical affinity between the coating and FeCrAl. Boehmite (AlOOH) sol, the precursor for Al_2O_3, can be prepared by dispersion of DisperalTM in an HNO_3 aqueous solution. The viscosity of the slurry depends on the concentration of the acid, the HNO_3/Al_2O_3 ratio, pH and particle dimensions; the concentration of the solid phase in the slurry influences the adhesion of the particles on metal fibers.[113] Alternatively, an AlOOH sol is produced by direct reaction between aluminum foils and an HCl solution (a mass fraction of 10 % HCl).[114] A dip-coating methodology (vide infra), controlling the withdrawal rate, is used to deposit the sols on foams or plates.

Some authors reported the synthesis of metal supported catalysts after the intermediate deposition of enamel layers that creates a barrier between metal support and superficial coating. This technique, normally used in the manufacturing of steel reactors for corrosive atmosphere, has mainly been reported for metals structures that do not form a protective superficial Al_2O_3 layer.[115] Even if the barrier properties of dense enamel to cation migration are higher compared to Al_2O_3, the final stability of the coating is negatively affected by a low thermal expansion coefficient of the enamel.[116] Syngas type reactions are to be avoided as the Si in the enamel reacts with hydrogen. This is a similar challenge that the refractory industry solved with applying high purity alumina.[92,117,118] Enamel coatings work best at lower temperatures but lack mechanical stability above 800 °C.[35,37] Coating surfaces with

enamel introduces interesting barrier properties for precise catalyst formulations. Annealing enamel requires precise operating conditions to minimize Cr migration as the enamel densifies.[87,92,119]

3.2 Washcoating of a ready-made catalyst or support

Washcoating with ready-made catalysts and supports has evolved over time to improve adhesion and loading and to preserve the properties of the powder catalysts. This process includes:

i) filling the voids of the structured support with a powder slurry or a sol-gel dispersion (liquid-like material) by dipping it for seconds;

ii) removing the excess fluid;

iii) drying and calcining;

iv) repeating the procedure to reach the desired catalyst loading.

The resulting film thickness depends on the balance between fluid viscosity (rheology), and the slurry removal procedure.[83,86,87] Final cladding adhesion depends on preoxidation, binder and slurry composition (Figure 11).[114,120]

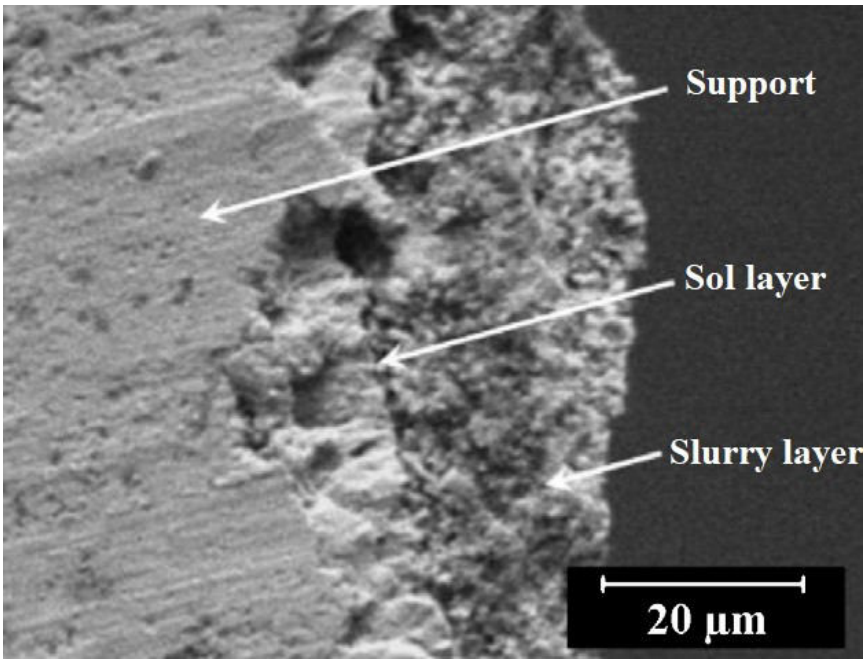

Figure 11: Scanning electron microscope (SEM) image of sample section after 10 h pre-oxidation at 900 °C, sol layer 2 % $g\,g^{-1}$ and slurry 25.3% $g\,g^{-1}$ deposition. Adapted with permission from reference.[120] Copyright 2017 Elsevier.

High temperature decreases the BET surface area and changes the Al_2O_3 phase. However, porosity and superficial area remain constant with stabilizers like CeO_2, La_2O_3, ZrO_2 (Figure 12).[121] Adding $Ce_{0.68}Zr_{0.32}O_2$ in Al_2O_3 increases the binding strength with the support and inhibits the phase transformation of the Al_2O_3 giving a high and stable surface area.[122,123]

Sample	Slurry formulation	Solid content
A	35% γ-Al_2O_3	35%
B	30% γ-Al_2O_3 5% $Ce_{0.68}Zr_{0.32}O_2$	35%
C	28% γ-Al_2O_3 7% $Ce_{0.68}Zr_{0.32}O_2$	35%
D	17.5% γ-Al_2O_3 17.5% $Ce_{0.68}Zr_{0.32}O_2$	35%

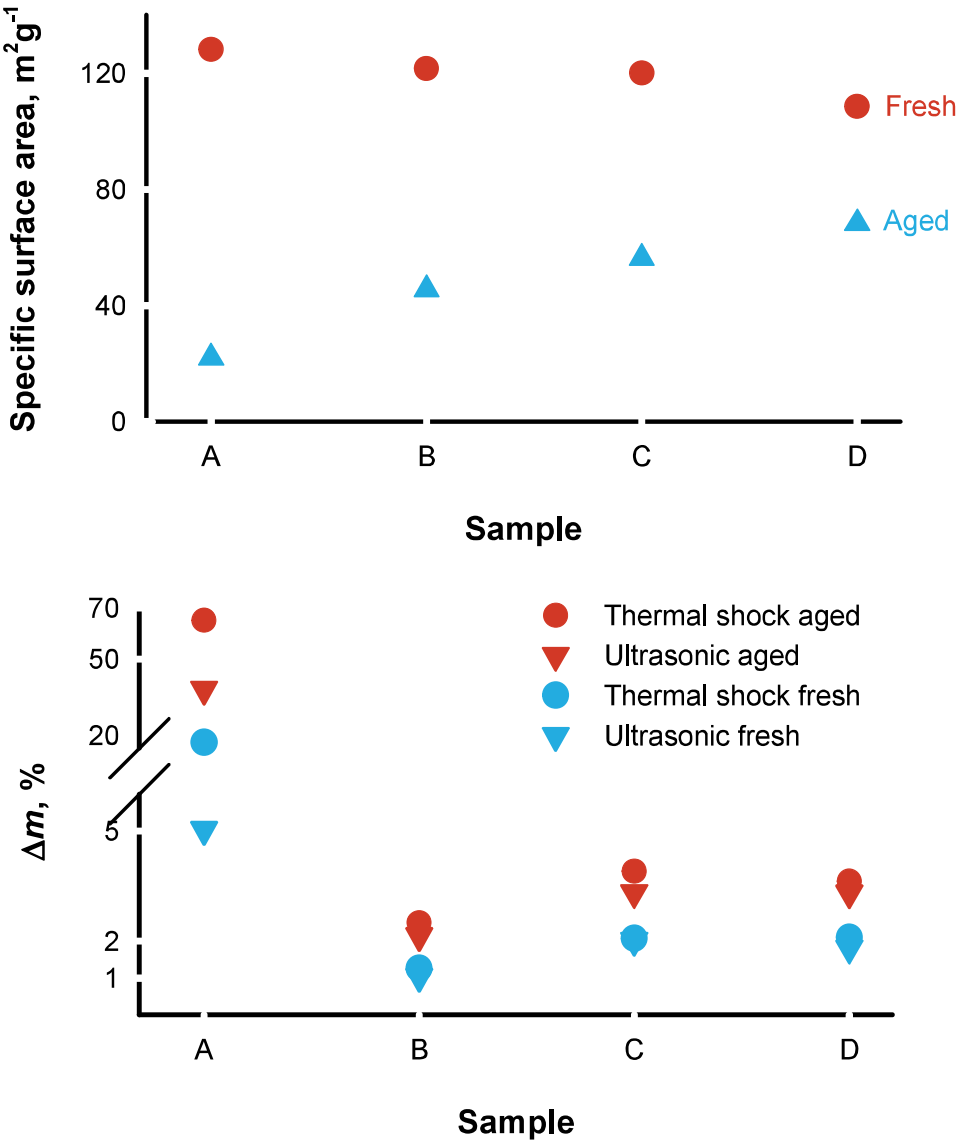

Figure 12: Specific surface area before and after washcoat aging. Percentage mass loss of the washcoat before and after aging for thermal shock and ultrasonic tests. Sample composition reported on the table.

Thermal shock tests at 700 °C and mechanical test under sonication in petroleum ether

demonstrated that the support geometry has a stronger influence than pretreatment. The adheshion of the protective layer was best on the high porosity foam compared to preoxidized foils, coated foils and coated foams (Figure 13).[97,110,114,120,124] In any case, pretreatment increases the interfacial forces between support and coating. Sol gel coating of fibers with Al_2O_3 behaves differently compared to flat foils and alcohol, as a solvent, is better for fibers because of its lower surface tension and boiling point compared to water.[124,125]

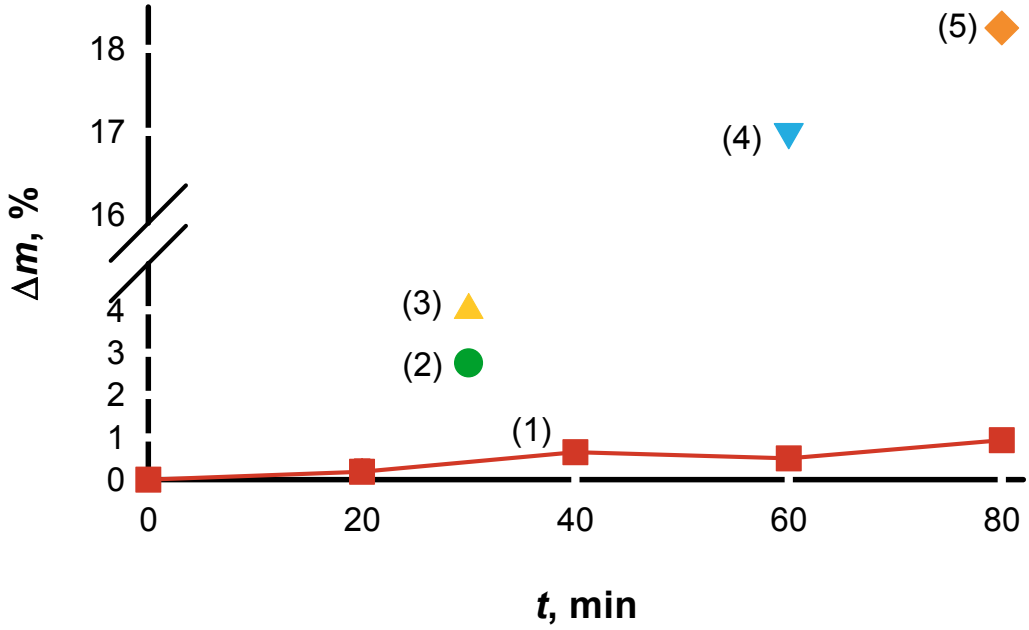

Figure 13: Weight loss comparison during mechanical stress test at 40 kHz in ultrasonic bath. (1),[97] (2),[114] (3),[110] (4)[124] and (5).[120] Adapted with permission from reference.[97] Copyright 2012 Elsevier.

A mass fraction of 2 % $g\,g^{-1}$ La in the Al_2O_3 slurry stabilizes the metastable phase at 950 °C. La also minimizes cracks in the cladding and reacts with the metal substrates enhancing the adhesion (Figure 14).[126] Introducing a $LaMnAl_{11}O_{19}$ hexaaluminate (HA) in Al_2O_3 layer on FeCrAl foil enhances the adhesion stability of the catalyst and maintains its high activity.[127] The HA is vertically embedded in Al_2O_3 intermediate layer.[128]

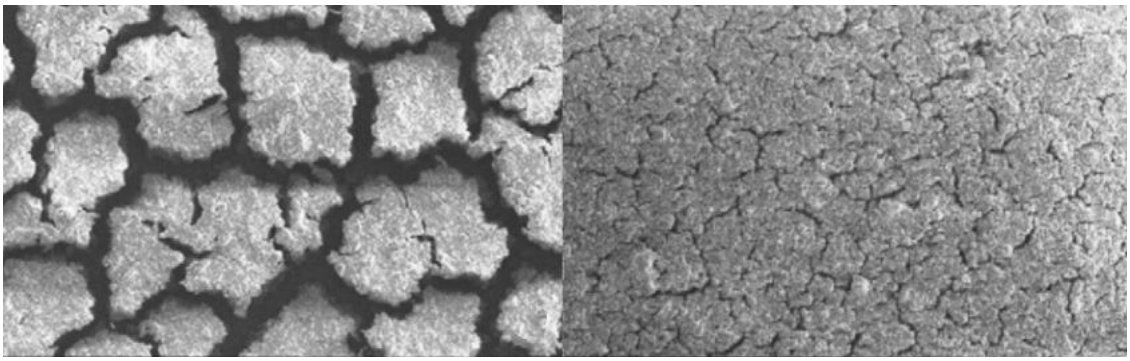

Figure 14: FeCrAl surface micrographs after 2 h at 1200 °C. With (right) and without (left) 2% $g\,g^{-1}$ La. Adapted with permission from reference.[126] Copyright 2015 Elsevier.

Adhesion of plasma sprayed Al_2O_3 and TiO_2 is superior to that of traditional dip coating. Plasma electrolytic oxidation is a promising technique, because it creates a protective cladding without any pretreatment although the dispersion remains more heterogeneous than traditional deposition methods.[129] Silica SBA-15 is an alternative to alumina as a protective layer, but requires colloidal silica rather than Al_2O_3 as a binder to favor the interaction between cladding and the metal support.[130] The elements of the slurry that affect its rheology include: solvent type (usually water), particle size and distribution, binder (e.g. colloidal silica/alumina), dispersant (mainly acids), and additives (e.g. long-chain surfactants containing hydrophilic and hydrophobic groups).

The recipe depends on the type of powder to be coated and determines the amount, homogeneity, and adhesion of the film. Low slurry viscosity lead to low loading and high adhesion, while high-viscosity formulations generate thicker washcoat layers that adhere poorly.[86] A drawback to the coating method is that it modifies catalyst morphology.[131] For instance, SBA-15 agglomerates with a wheat-like appearance break down under magnetic stirring into rods.[132]

The preparation method of a colloidal dispersion of a ready-made catalyst is similar to the binder deposition step. Driving out liquid is easy for simple shaped supports since only viscous force resists the fluid movement. Blowing (dip-blowing) and centrifugation (spin-coating) are appropriate for complex shapes like open-cell foams, especially with a high

pore density. Air jets and centrifugation complement gravitational forces to overcome capillary forces in draining liquid from the channels and cells .[132–134] For instance, spin coating controls the $Pd-CeO_2$ coating formation on FeCrAl open cell foams with cell diameters down to 500 µm. The higher shear stresses induced by rotation during wet film deposition reduces clogging and increases the film homogeneity with respect to ordinary dip-coating (Figure 15).[134]

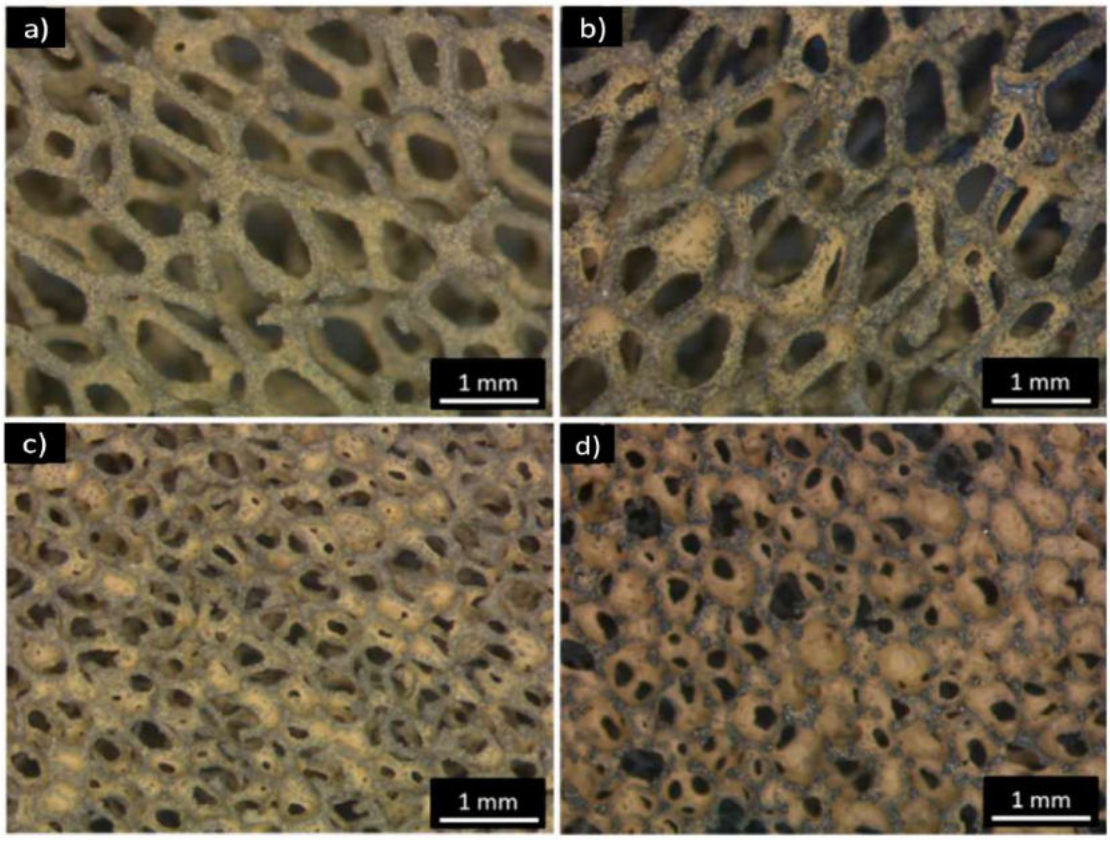

Figure 15: Optical microscope images of spin-coated (a,d) and dip-coated (b,e) foams of 1200 µm (a,b) and 580 µm (d,e) cell diameters. Adapted with permission from reference.[134] Copyright 2007 Elsevier.

3.3 In situ-growth of active phases

In direct deposition routes, catalyst (metal particles, metal oxide, and zeolites) and precursor (hydroxides) grow directly on the surface of the structured support. These methods can be considered as a heterogeneous precipitation where the growing seeds form on the

metal support surface rather than in the liquid phase. While in-situ growth techniques avoid modifications of the catalyst during slurry preparation, producing materials like those from conventional synthesis methods (without a structured metal support), requires special attention.

3.3.1 Impregnation followed by calcination

The simplest way to develop in situ catalytic materials is to impregnate a solution of a precursor (mainly metal salts) on a pretreated FeCrAl, i.e with a porous alumina coating, followed by calcination, like in the conventional preparation of powder catalysts. The immersion of a pretreated foil in a solution containing La^{3+} and Mn^{2+} leads to their adsorption on the porous Al_2O_3 layer, which generates a firmly adhered $LaMnAl_{11}O_{19}$ hexa-aluminate after calcination due to solid state reactions.[127,128] Alternatively, when dealing with more complex shapes, such as fibers, wherein the immersion may lead to inhomogenous species adsorption, the precursor solutions can be sprayed on the support, which oxidizes to Al_2O_3 or Al_2O_3-CeO_2 during calcination.[135]

3.3.2 Solution combustion synthesis

Solution combustion synthesis (SCS) produces adhesive coatings of inorganic nanomaterials. It is a self-propagating redox reaction between metal precursors (oxidizers) and organic fuel in aqueous solution.[136,137] The solution heated until 300 °C to 600 °C initiates reaction that rises to temperature from 750 °C to 1500 °C, for a very short time. Consequently, a highly crystalline and pure film develops consisting of nanosized powder with relative high specific surface area and low tendency to sinter. The fuel-to-oxidizer ratio, φ (elemental stoichiometric coefficient), controls the heat released and the crystalline structure of the final product. Metal nitrates are common oxidizers while urea and glycine are conventional fuels. Compared to washcoating, in SCS crystal lattice parameters can be regulated and reactants are cheaper.

$CuO\text{-}CeO_2$ on FeCrAl monolith thermally pretreated are prepared from Cu/Ce nitrate and urea. The solid loading increases with the concentration of the solution but the detachment of the film is also more noticeable—200 g L^{-1} concentration balances both phenomena. Pr and La improve the adhesion of the catalytic film as Nd and Zr influence copper and CeO_2 dispersion.[138,139]

The aqueous solution of the nitrate precursors with glycine as fuel is sprayed over the gauze surface at 400 °C. One step in situ spray pyrolysis SCS on pre-oxidized gauzes produces a highly corrugated and porous $Pd(LaMnO_3 \cdot 2ZrO_2)$ catalytic layer (Figure 16).[140] Pt-Rh/MgO on pretreated woven fibers are prepared by a two-step SCS; MgO first deposits from a $Mg(NO_3)_2$ and urea solution and afterwards the SCS of Pt-Rh is done using $Pt(NH_3)_4(NO_3)_2$, $RhCl_3$ with the same fuel.[141] Usually after SCS the material is calcined to confer additional stability. To achieve the desired catalyst loadings, the deposition cycles are repeated several times, as in the case of washcoating.

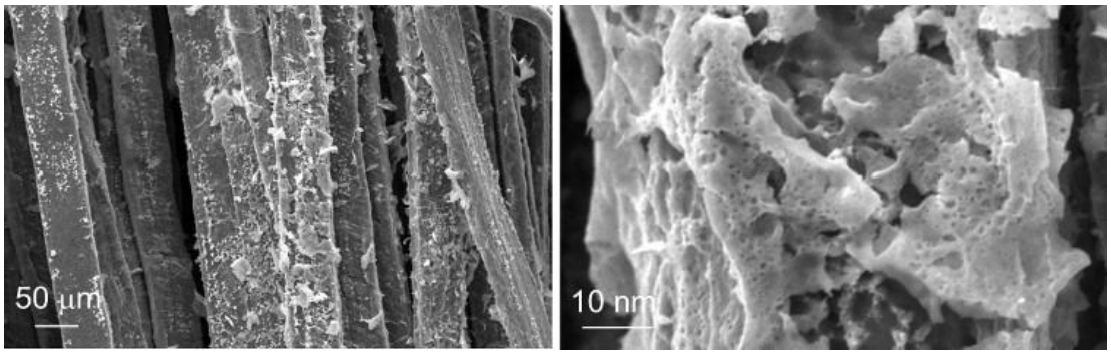

Figure 16: SEM micro-graphs of FeCrAl fibers supporting $Pd(LaMnO_3 \cdot 2ZrO_2)$ prepared by in situ SCS.[140]

3.3.3 Hydrothermal methods

The synthesis and deposition of catalytic species under hydrothermal conditions is typically used to prepare zeolites or the urea assisted co-precipitation of single or mixed hydroxides on structured supports. Its main advantage is the control of the crystal growth and, therefore, the orientation of the particles on the coating. On the other hand, yield on the support is

low, since the solids precipitate in the bulk solution at the same time as on the support. This is particularly costly when dealing with noble-metal catalysts.

The in situ synthesis of zeolites on the surface of structured supports generates a binderless and oriented microporous film of zeolite crystals, while washcoating forms a disordered meso- (due to the binders) and microporous zeolite film.[83,84,142] The coating procedure consists of immersing the pretreated support in a zeolite gel that is hydrothermally treated at 140 °C to 160 °C. The gel is prepared from an aqueous solution containing zeolite precursors (e.g. sodium silicate, SiO_2, $Na_2Al_2O_4$), a structure directing or pore filling agent and a base mobilizing agent (e.g. OH^-, F^-). Zeolite nucleates and grows homogeneously in the mother liquid while nucleation and nuclei growth on the support surface, relevant for the in situ zeolite synthesis, is heterogeneous. The subsequent calcination step removes structure directing agents and binders.

Likewise for conventional (homogeneous) preparation of zeolites, type of precursors, Si/Al and H_2O/Si ratio, pH, type and amount of additives as well as crystallization temperature and time determine the growth kinetics and, therefore, the properties of the zeolitic materials. These parameters control the shape and size of crystals and, as a consequence, the coating stability. Zeolitic material properties depend on Si/Al ratio, which also determines nucleation and crystallization rates.[143] The concentration of the gel controls the ratio homogeneous/heterogeneous precipitation; the hydrothermal treatment pH can dissolve the Al_2O_3 from FeCrAl.[142,144]

The surface accessibility and the support pretreatment affect the synthesis of the zeolite, but in micro-channels and pores, diffusive limitations of the gel may create non-homogeneous coatings with unstable over-growths. The FeCrAl pretreatment provides chemical compatibility, increases hydrophilicity and irregularities (roughness) on the surface that favor the zeolite growth and promote coating adhesion. At the same time α-Al_2O_3, formed during pretreatments, acts as an Al precursor in the zeolite synthesis.[142,144,145,145–147]

Crystals of ferrierite are synthesized on foils pretreated at 800 °C starting from alumina,

silica and piperidine. Nucleation time and temperature are two factors that control crystal size, small crystals improve contact with the metal foil.[147]

Seeding pretreated supports avoid organic templates.[146,148] In the synthesis of ZSM-5 over sheets, the alumina layer increases the amount and stability of zeolite. Similarly, ZSM-5 and SSZ-13 bind to the Al_2O_3 layer developed on open-cell foams pretreated at 1000 °C.[149,150]

In the synthesis of mordenite, the preoxidized surface at 700 °C of corrugated foils is impregnated with a cationic polymer (poly-diallyldimethilammonium chloride) prior to seeding—charge reversion procedure.[144] Deposits are polycrystalline, dense, continuous, adherent, and producible quickly with a *c*-axis orientation perpendicular to the support surface. A marked preferential growth on the metallic surface at the expense of a negligible growth within the synthesis solution is an advantage of seeding, but the type and concentration of the seed as well as the calcination temperature influence the properties of the film (Figure 17).[144] To obtain Cu-Ce/mordenite coatings, Cu is introduced by ionic exchange, while Ce by impregnation.

Table 1: Zeolite synthesis performed on FeCrAl foils pretreated at 900 °C.

Catalyst name	**Synthesis time** h	**Seeding suspension** $g\,L^{-1}$	**Mass variation** $\%g\,g^{-1}$
F900-1	3	5	0.3
F900-2	6	5	1.5
F900-3	24	5	14.3
F900-4	24	10	8.4

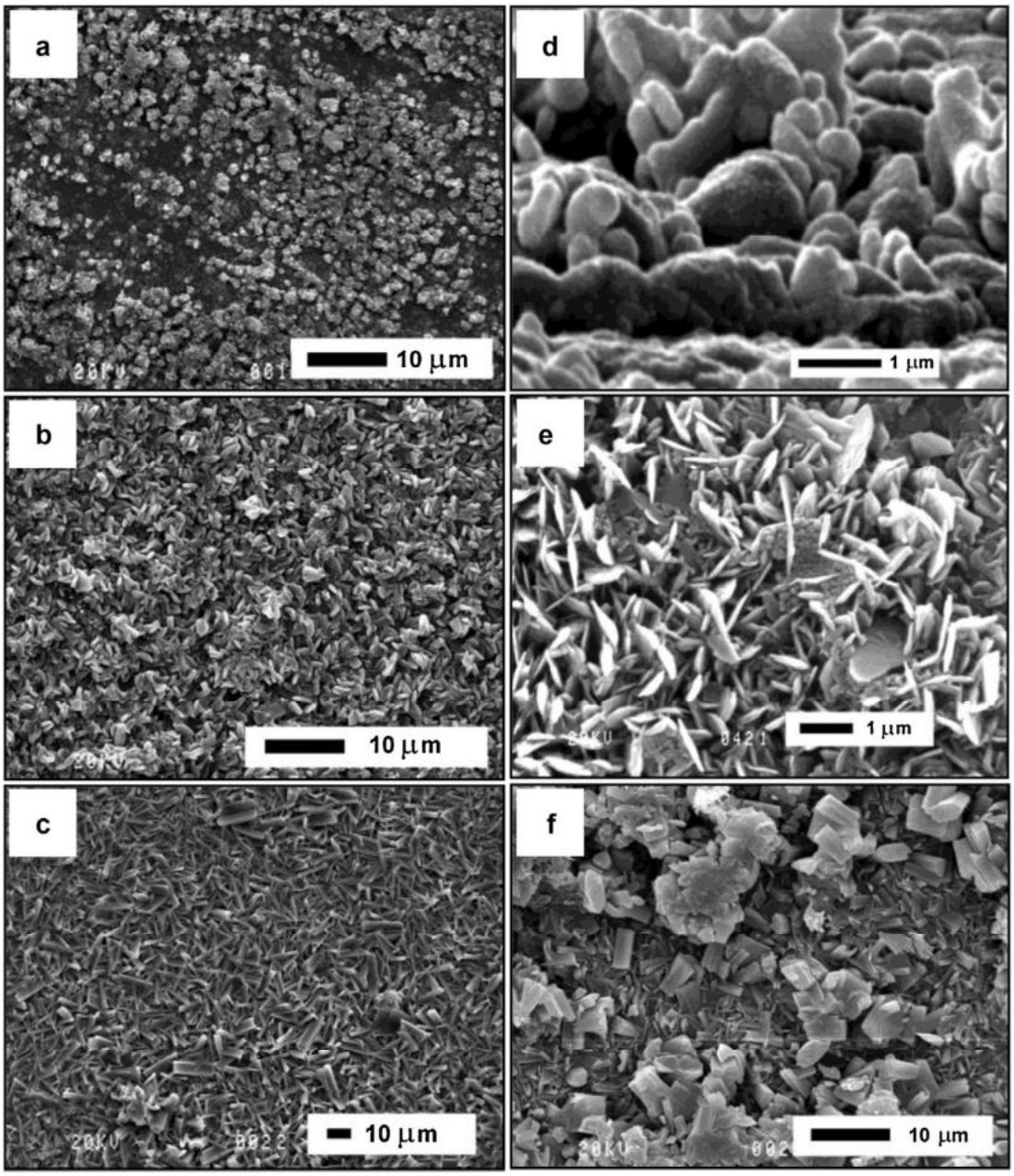

Figure 17: Growths obtained under various syntheses conditions (Table 1): (a) F900-1, (b) F900-2, (c) F900-3, (d) close view on sample F900-1, (e) seeding of nanocrystals on substrate with alumina whiskers and (f) F900-4.[144] Copyright 2013 Elsevier.

The precipitation of hydroxides on FeCralloys with urea as a homogeneous base is also conducted under hydrothermal conditions. Like for zeolite synthesis, the pretreatment of the support plays a key role. Ni/Mg/Al layered double hydroxides (LDHs), catalyst precursors, do not crystallize onto pristine FeCrAl-fiber, while through a $\gamma-Al_2O_3$/water interface-

assisted method homogeneously distributed and vertically aligned LDH nanoplatelets deposit.[88] The process involves:

i) FeCrAl preoxidation;

ii) hydrothermal reaction to embed AlOOH nanosheets on the $\alpha-Al_2O_3$ film and calcination from 450 °C to 600 °C;

iii) LDHs synthesis under hydrothermal conditions at about 150 °C for several hours (∼12 h) starting from nitrate salts and urea later calcinated above 500 °C.

The method strongly depends on the Al_2O_3 nanosheets, which are grown from a solution of sodium aluminate and urea at 160 °C for 12 h. Increasing the amount of Al_2O_3 nanosheets improves the LDH growth. AlOOH can also be obtained starting from a suspension of Al powder in a NaOH aqueous solution, while the in situ growth of LDH can be performed in the absence of Al in the mixture, since the Al_2O_3 layer acts as an Al source (Figure 18).[88]

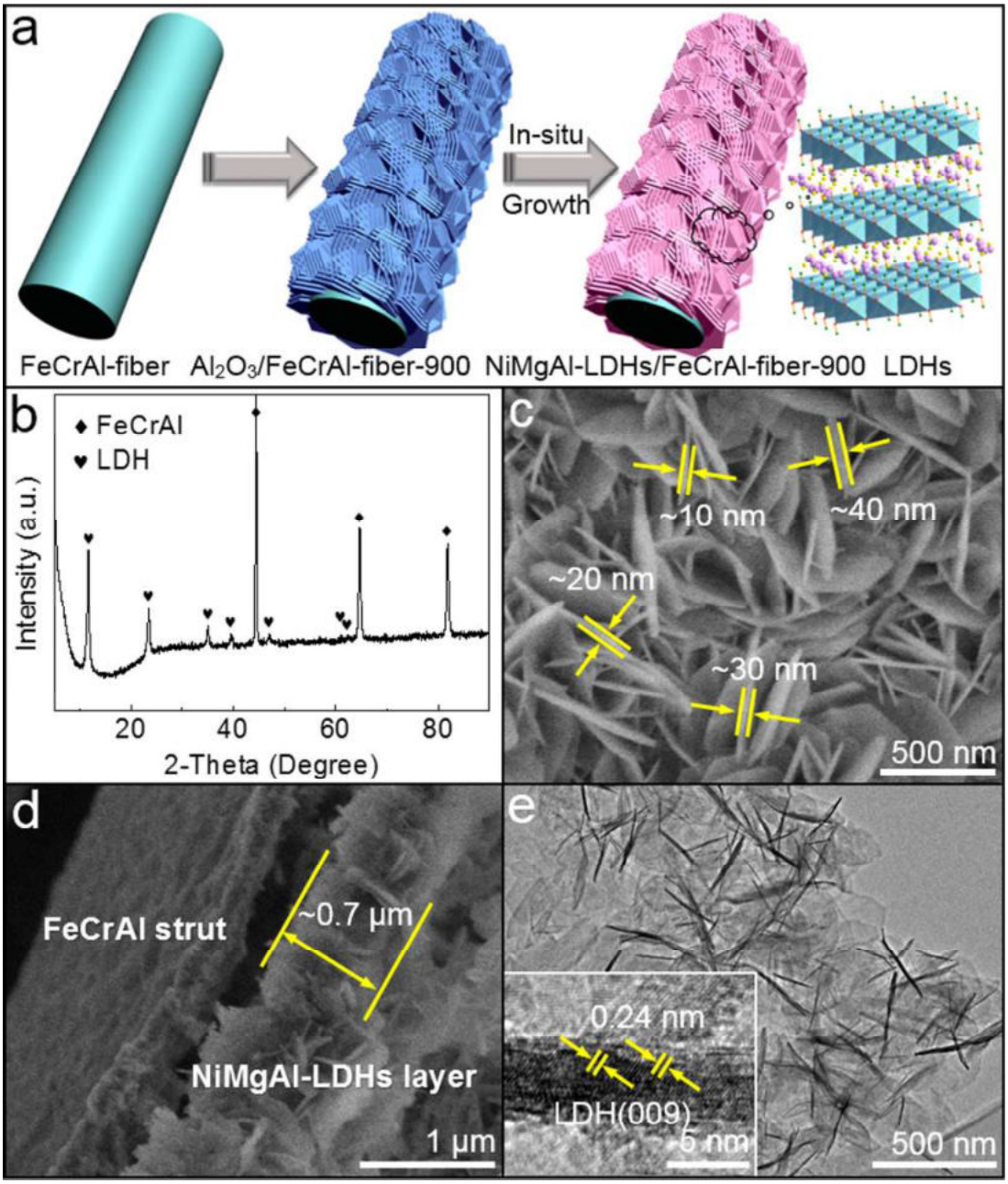

Figure 18: Fabrication strategy (a) of the NiO−MgO−Al_2O_3/FeCrAl-fiber-900 catalyst derived from the NiMgAl−LDHs/FeCrAl-fiber-900 precursor. XRD pattern (b), SEM (c,d) and TEM micro-graphs (e) of the NiMgAl−LDHs/FeCrAl-fiber-900 precursor.[88] Copyright 2017 American Chemical Society.

The method is modified to synthesize Ni@SiO_2/Al_2O_3/FeCrAl-fiber core shell catalysts. A "top-down" from "macro-micro-nano" self-assembly strategy adds to the two first steps (oxidation and AlOOH nanosheet deposition), the wet impregnation with Ni^{2+} using 3-

aminopropyltriethoxysilane as bridge molecules and as a source of SiO_2, after hydrolysis in water. Calcination at 550 °C is finally necessary to obtain the actual catalyst.[151]

3.3.4 Galvanic displacement and electrochemical processes

The methods explained in previous sections are also applied to coat ceramic supports. Indeed, besides the treatment of the FeCrAl and the migration of alloy elements into the coating, the other preparation parameters can be considered support-independent. On the contrary, in galvanic displacement and electrochemical deposition, the spontaneous reactivity of the support and its electrical conductivity are exploited to deposit catalysts or precursors.

Galvanic displacement occurs when a less noble metal template contacts a more noble metal cation and it begins as soon as the support is immersed in the solution (also called spontaneous deposition). The morphology and mass of particles deposited depends on time, precursor, concentration, and pH of the solution. The method is effective to deposit noble metals on FeCrAl, because the galvanic potentials of reductant/oxidant between two pairs are different.

Pd deposits on foam surfaces in an O_2-free aqueous solution of $PdCl_2$ in HCl; Fe, Cr, and Al are all displaced by Pd^{2+}. Concentration of the precursor, time, passive oxides on FeCrAl surface, and pH influence the Pd loading and the particle size (Figure 19).[152,153] At pH= 3, Pd loading increases with time from 5 min to 120 min, nonetheless the metal nucleates in a rather low number of sites that preferentially keep growing, resulting in large Pd particles.[152] Decreasing the pH to 1, reduces the Pd particle size and improve the dispersion.[153]

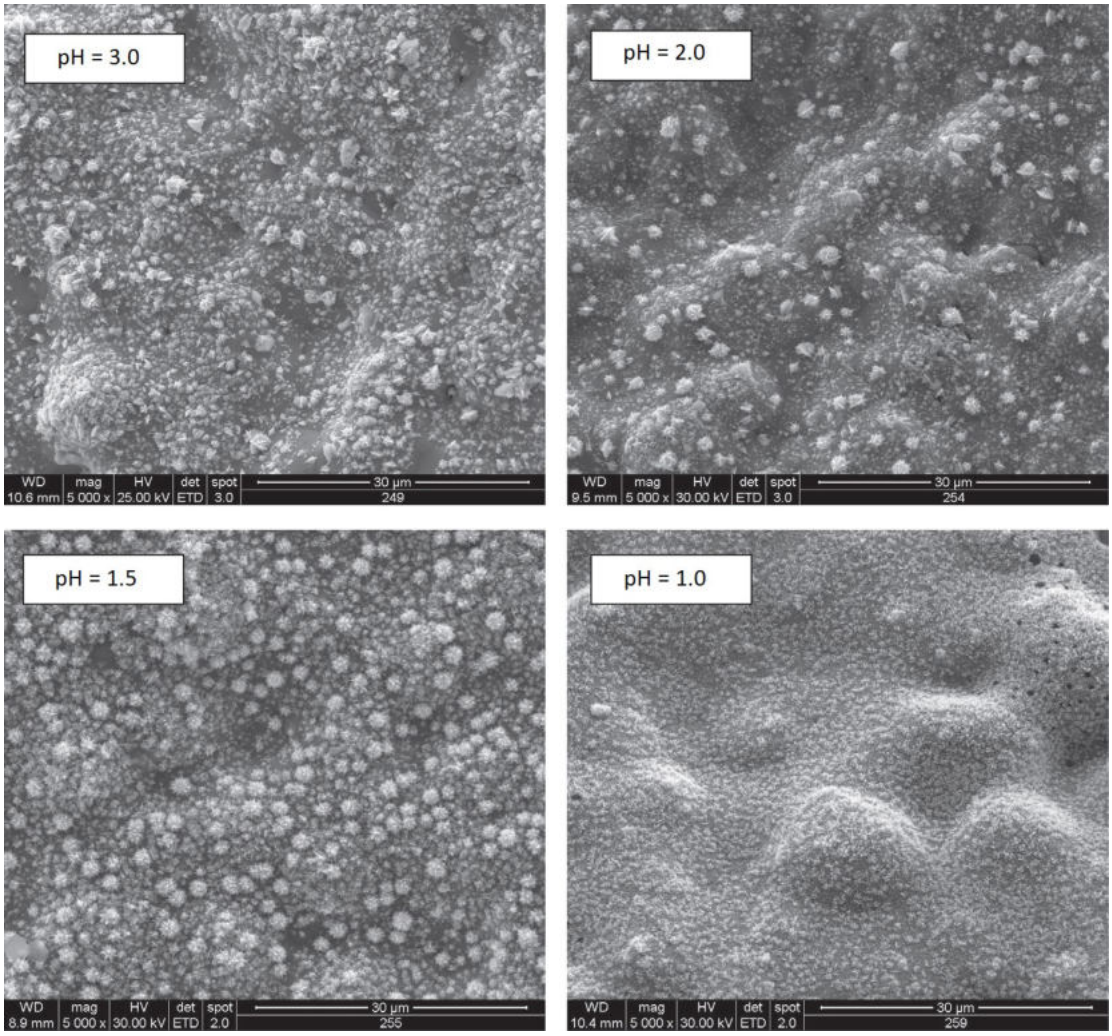

Figure 19: SEM micrographs of FeCrAl foams obtained by spontaneous deposition of Pd as a function pH. Adapted with permission from reference.[153] Copyright 2013 Elsevier.

Coating of foam surfaces with nanometric Rh requires 24 h starting from an O_2-free $RhCl_3$ in HCl aqueous solution at pH 2; however, these conditions deteriorate the mechanical properties of the foam.[154]

Electrochemical deposition coats conductive FeCrAl supports with metallic particles, hydroxides and oxides, and their combinations in one-step, at room temperature. A cathodic potential is applied in continuous or pulse mode to the metal substrate to be coated (working electrode). Rh and Pt metallic particles are deposited on bare foams (untreated) as an alternative to galvanic displacement.[154,155] Metal precursors are electrochemically reduced

at a selected cathodic potential. The concentration of the salts, applied potential, deposition charge, and roughness of the support control the nucleation and growth of metallic deposits, and therefore the particle size and distribution. Diluted chloride baths (mM concentrations) promote nucleation, while acidic pH (around 2-3) minimizes the hydrolysis of the ions of noble metals. The deposition charge controls the noble metal loading; however, under these electrodeposition conditions hydrogen evolution reaction is favored, decreasing the current efficiency.

Electroreduction of $RhCl_3$ at $-0.4\,V$ vs saturated calomel electrode (SCE) forms Rh particles of ca. 25 nm, homogeneously deposited on the surface, even if in 2.44 mL foam cylinders the local Rh loading at peripheral positions is higher than in the center. The loading and the morphology are better compared to galvanic displacement (Figure 20).[154]

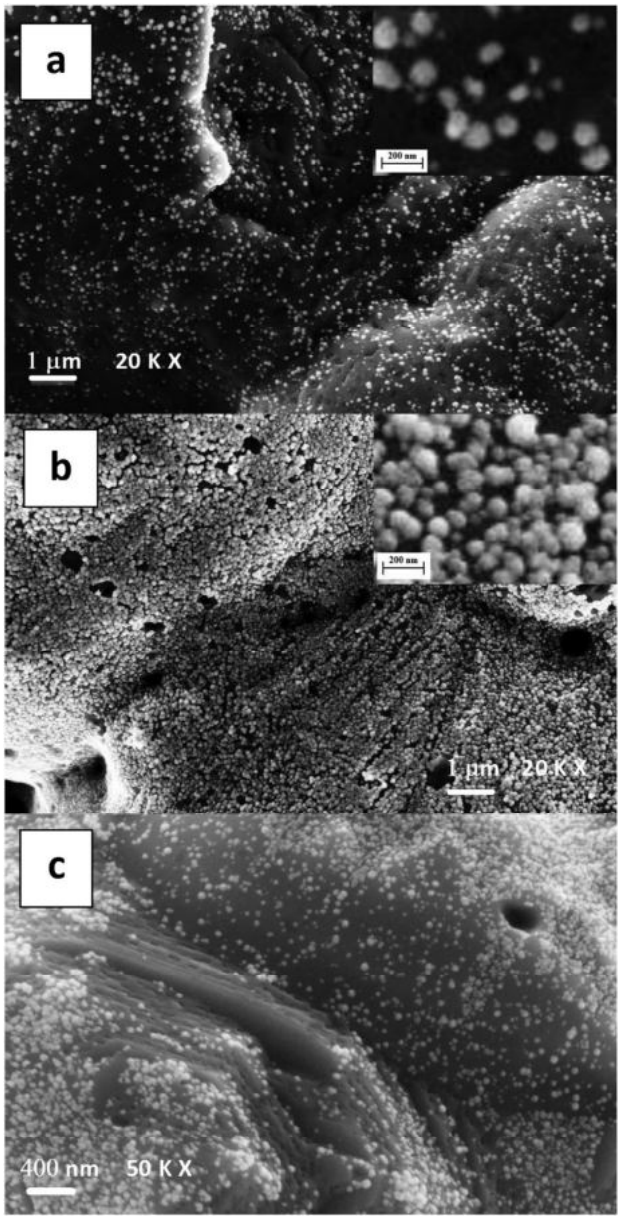

Figure 20: SEM micro-graphs of Rh-FeCrAl samples prepared following electro-deposition (a,b) or spontaneous deposition (c).[154] Copyright 2014 Elsevier.

Starting form H_2PtCl_6, the inhomogeneous reactivity of the FeCrAl surface produces a low surface density of large Pt particles (0.1 µm to 1 µm), which are composed of assemblies of small and spiky crystallites; Pt loading grows with the deposition charge.[155] Like Pd particles obtained by galvanic displacement, most Pt particles simultaneously nucleate on reactive positions and keep growing without generating new ones when increasing the noble

metal loading and/or upon prolonged electrolyses.

The electrodeposition of hydroxides or oxides occurs through the electro-base generation method—the generation of a basic medium at the electrode-electrolyte interface provokes the chemical precipitation of cations on the electrode surface. This method, consisting of applying a cathodic pulse at the foam dipped in a solution containing nitrates and cations, was developed to coat untreated open-cell foams of small pore sizes. LDHs (Ni/Al[156] and Rh/Mg/Al[157]) and $PdCeO_2$, coatings are prepared avoiding pore blockage.[158] Nitrate, water and O_2 reduction contribute to the pH increase[159] while OH^- generated from dissolved O_2 has a minor contribution. Although H_2O and NO_3^- reduction increase the pH, the former produces H_2 bubbles that detach the coating and the pH generated is low.[160] The quality of the electrodeposited catalysts is determined by:

i) the support, including electrical conductivity and roughness[159] and geometrical parameters (size and shape[160,161]);

ii) electrochemical set-up, namely electrical contact between the working electrode and the potentiostat[162] and type of cell[157]

iii) type and concentration of metal precursors, pH of the electrolyte, applied potential, and synthesis time.[161,163–166]

The potential applied controls the electrochemical reactions, though the presence of precipitating cations catalyzes the reduction processes. Prolonging the synthesis time usually increases the solid loading, but it can change the composition of the precipitates. Reaching 15 µm to 20 µm Rh/Mg/Al LDHs layers with controlled properties also depends on the size of the foam piece. For highly reducible Rh^{3+} adjusting the initial pH minimizes Rh metallic precipitation. For $PdCeO_2$ catalysts, selecting a suitable Pd^{2+} complex precursor like ($Pd(NH_3)_4(NO_3)_2$ or $PdCl_2$ in HCl), minimizes precipitation. In the synthesis of Rh/Mg/Al-LDHs, modifying the total metal concentration determines the amount of solid deposited, composition, and crystalline phases. However, as in the case of Rh/Mg/Al films

with coprecipitated-like features (Figure 21), it is required to optimize potential (−1.2 V vs SCE), time (2000 s), total metal concentration (0.06 M), number of electrical contacts, replenishment of the solution, and separation of working and counter electrode with a double-compartment flow cell. However, since actual catalysts only develop after calcination at 900 °C the properties of the materials also depend on the interaction of the coating with the metallic support.[167] Cubic fluorite CeO_2 forms on the surface and is highly reproducible (compact and platelet-like), while the task is more challenging for $PdCeO_2$ coatings. Adjusting the Pd precursor, $PdCl_2$ concentration (0.15 M), applied potential and time (−1.1 V vs SCE for 500 s) disperses well Pd species on the CeO_2 coating;

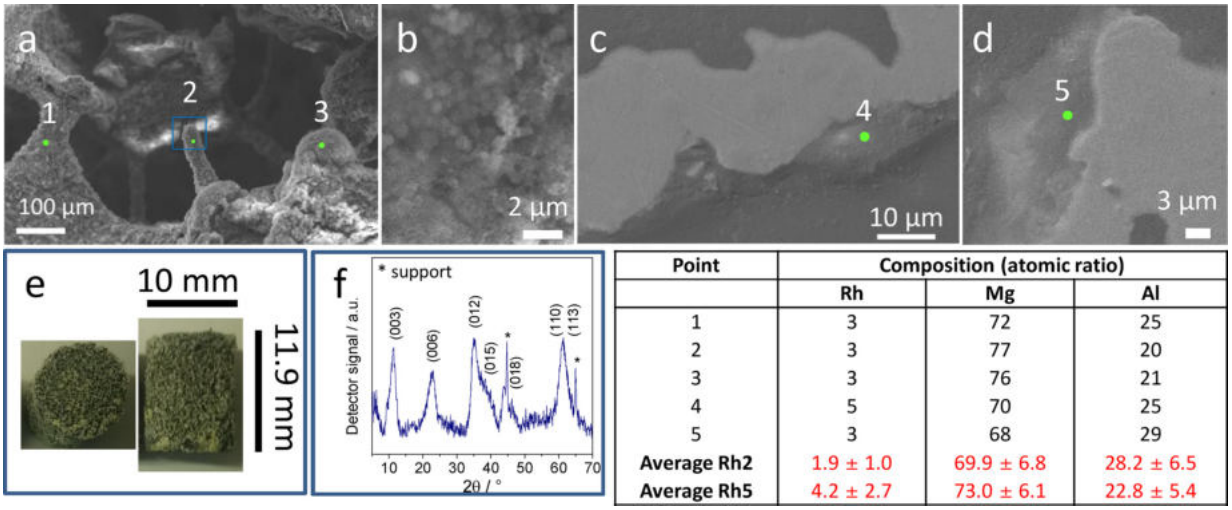

Point	Composition (atomic ratio)		
	Rh	Mg	Al
1	3	72	25
2	3	77	20
3	3	76	21
4	5	70	25
5	3	68	29
Average Rh2	1.9 ± 1.0	69.9 ± 6.8	28.2 ± 6.5
Average Rh5	4.2 ± 2.7	73.0 ± 6.1	22.8 ± 5.4

Figure 21: SEM micro-graphs and composition of Rh5 catalyst precursor: a) medium magnification; b) high magnification; c and d) cross-section of an embedded foam; e) of the prepared coated foam; f) XRD of the fresh coating. In the table EDS composition of the spots identified with the numbers 1, 2, 3, 4, 5.[157] Copyright 2018 Elsevier.

depositing of Pt-CeO_2 on foams faces similar challenges too.[168] Pulsed deposition, instead of constant-potential electrodeposition, controls size and surface distribution of nanoparticles (ca. 30 nm to 50 nm at −1.0 V and 100 nm at −0.7 V vs SCE).

In variance to electrochemical processes, electroless plating relies on redox reactions to deposit metals on objects without an electric current. The metal substrate is immersed in a solution of the metal precursor and a reducing agent is added. For the deposition of Pd and

Pt on FeCrAl wire mesh substrate with robust adhesion and uniform dispersion, electroless plating is applied after an initial galvanic displacement step on a cleaned surface to remove passivated oxides.[169,170]

4 Applications in emission control

Catalytic devices drastically reduce CO, NO_x, uncombusted hydrocarbons, and particulate emissions from gasoline and diesel engines.[171–173] Gas hourly space velocities (GHSV) in the catalytic converters approach $1\,000\,000\,h^{-1}$. They operate with noble metals (active phase) and structured supports with a high void volume, such as honeycomb monoliths, to minimize pressure drop. Cordierite ($Mg_2Al_4Si_5O_{18}$) has the added benefit of negligible thermal expansion. In the last 10 years, most research has focused on replacing ceramic supports with metallic ones that withstand 1000 °C, expand catalytic functionality and reduce noise. This configuration is easier to manufacture and it is more facile to recover precious metals. Fibres, monoliths and foam of FeCrAl have been tested and most being coated with an Al_2O_3 layer (Figure 22). Coatings are more prevalent for monoliths and include ZSM5, SBA15, modenite, bentonite, ZrO_2, CeO_2, and TiO_2. They promote the interaction with the active phase, reduce sintering and supply lattice oxygen.

Cost remains a limiting factor.[93,174,175] During the metallic support preparation Ni coming from the brazing material modifies the structure of FeCrAl. Transition metals enters the alloy and creates regions of Ni_xAl_y, that strength the support in a similar way to the precipitation hardening technique.[176] Although the deactivation strongly depends on the nature of the support, FeCrAl supporting Pt behaves in the same way as Pt supported on cordierite (Figure 23), while the same active phase on FeCrNi is poorer.[93]

FeCrAl wire meshes supporting K, from vapor chemical deposition, suppress soot emission. It combusts soot above 330 °C and remains active with a difference in the CO_2 peak of only 25 °C between the first and the fifth cycle.[177] Catalytic converters with diesel particulate

filters, currently also made of cordierite, trap the particulate matter by physical separation; when the pressure drop increases, ceria catalytically oxidizes the carbon and temperature increases.

4.1 Automotive tail gas treatment

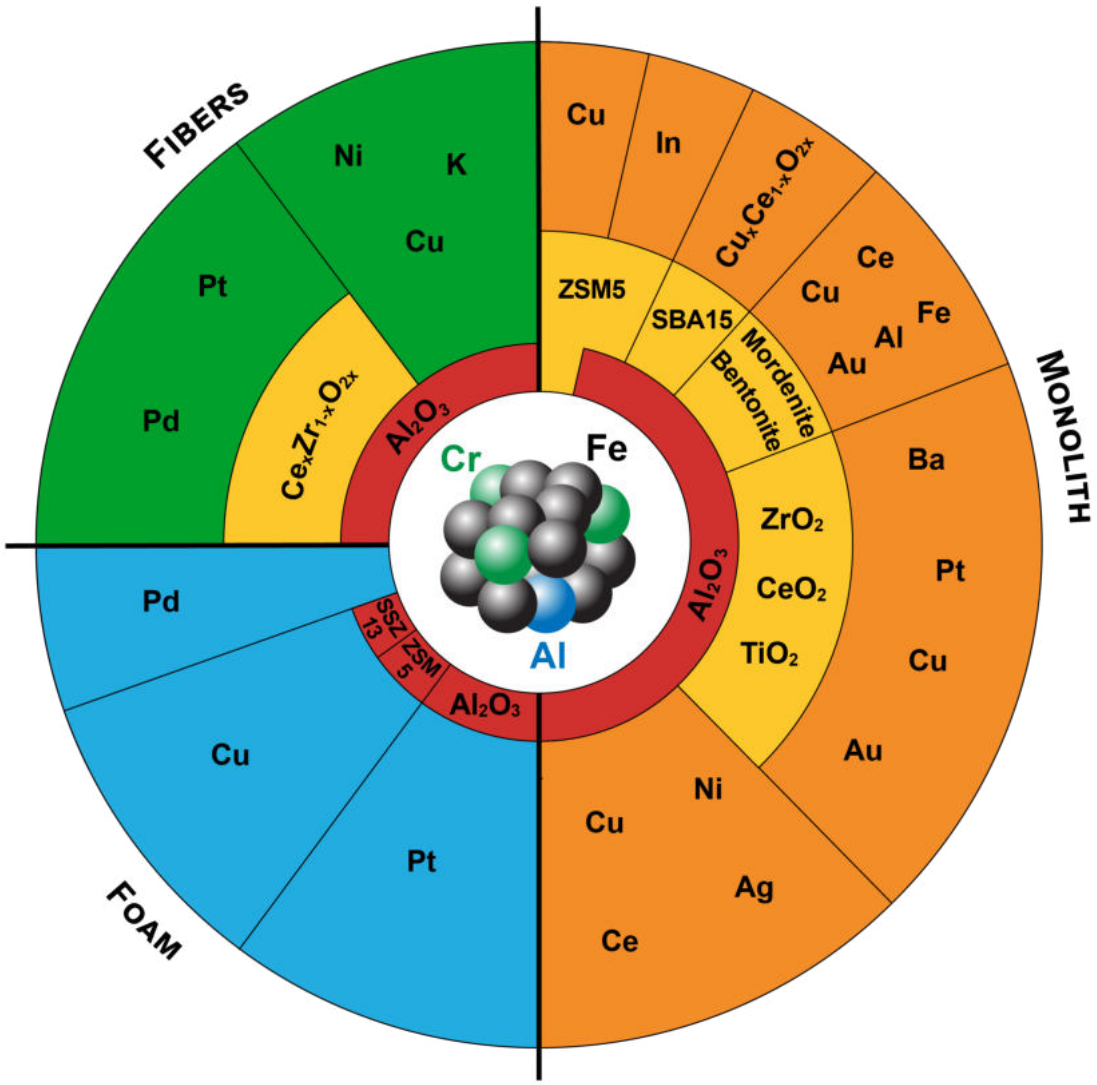

Figure 22: Catalyst structure, formulation and active phase for automotive tail gas treatment.

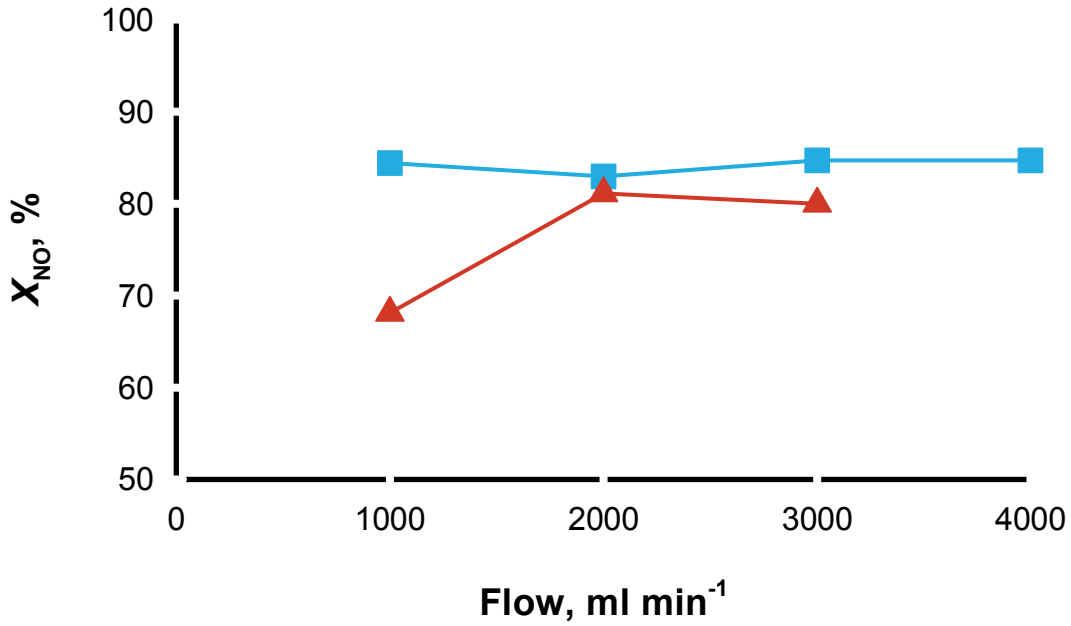

Figure 23: Conversion of NO as function of the residence time for FeCrAl hollow sphere structured bed (blue) and ceramic monolith (red). Adapted with permission from reference.[93] Copyright 2009 Elsevier.

In FeCrAl the alumina layer, formed on the surface, blocks the negative effect of the Cr that otherwise diffuses or migrates from the bulk to the active phase.[93] With Al−Fe pillared bentonites or CeO_2 coatings, cations move between external and protective oxide layers, which is deleterious in the case of precise catalyst formulations. These movements vary with elements, protective coating, ions, and the process/reaction conditions.[91,178] When supported on bentonites, Au blocks Cr in the alloy, while the contrary occurs with CeO_2 as the intermediate layer.[91] In-situ combustion synthesis produces Cu−CeO_2 on FeCrAl catalysts for the preferential oxidation of CO. Adding Pr or La improves the stability of the catalyst but La decreases CO oxidation.[138]

Oxygen treatment of silver nanoparticles on FeCrAl plate with a diameter smaller than 3 nm creates AgO_x that are active in transforming nitrite to nitrate. When the metal particles are bigger, the grains are more stable; the activation of O_2 and its consequent interaction

with the active phase does not occur, that is why only particles with a certain maximum diameter are active in the nitrogen reduction.[179] Ba and TiO_2 or ZrO_2 are active at room temperature in the reduction of NO_x and their interactions generate superficial nitrites followed by the oxidation of superficial barium or carbon. The formation of these components is more efficient in presence of zirconia.[180]

4.1.1 Noble metals

Noble metals are the most active component in catalytic automotive converters. In cycling NO_x storage-reduction (NSR) catalysts to treat diesel tail gases, Pt particles deposited on external coating of BaO, work both in lean and rich conditions. In the first case, Pt catalyzes the full oxidation of nitrogen oxides to NO_2 while forming $BaNO_3$; in the second, it catalyzes the reaction between nitrates and excess fuel.[171–173,181–184] With time, NO_x oxidizes Pt, but thermally treating the system produces coarse particles, which minimizes the oxidation rate.[185] Activity and thermal stability are higher for Pt−Pd and Pt−Rh bimetallic particles or three way catalysts (TWC)[171–173,186,187] and where successfully deposited by ionic exchange on γ-Al_2O_3 or on a mixture CeO_2-ZrO_2-γ-Al_2O_3 on preoxidized FeCrAl fibers.[184] Together with the design of the geometry of the mesh, it combines high catalytic and filtration ability without affecting the pressure drop at high flow rate.[184]

In the preparation of metallic foams, like TWC supports, spontaneous deposition of Pd avoids problems during the preparation. The specific surface area, s_A, of the active metal increases at pH= 1 (Figure 19) but s_A is higher on Ni-based foams. However, with FeCrAl the interaction with the substrates preserves the activity and the final efficiency is 10 times higher than the traditional Pd alumina washcoating.[153]

4.1.2 Copper-Indium

Although Cu has not been applied industrially in pollution control devices for vehicle exhaust, Cu is an alternative to precious metals for CO oxidation or selective catalytic reduction (SCR) of NO_x, as it is inexpensive, has acceptable mechanical properties, and is relatively stable to poisoning.[188] SCR use ammonia or urea to reduce NO_x and are usually combined with oxidation catalysts to prevent prevent leakage after the reduction step.[189] Cu is forbidden in North America because it produces traces of dioxin[190] but bulk Cu, while activates both carbon and nitrogen species, is constrained by it low melting point. When on FeCrAl fibers prepared via chemical and electrochemical methods, it has comparable performance to bulk copper fibers (Figure 24) but can operate at higher temperatures. A spinel phase forms between the Cu and fiber under layers that stabilizes Cu/CuOx nanoparticles in or on its crystallites.[188] Corrugated FeCrAl metal foils coated with 30 % ($g\,g^{-1}$) Ce/mordenite impregnated with 2 % ($g\,g^{-1}$) Cu efficiently oxidize CO in micro reactors.[144]

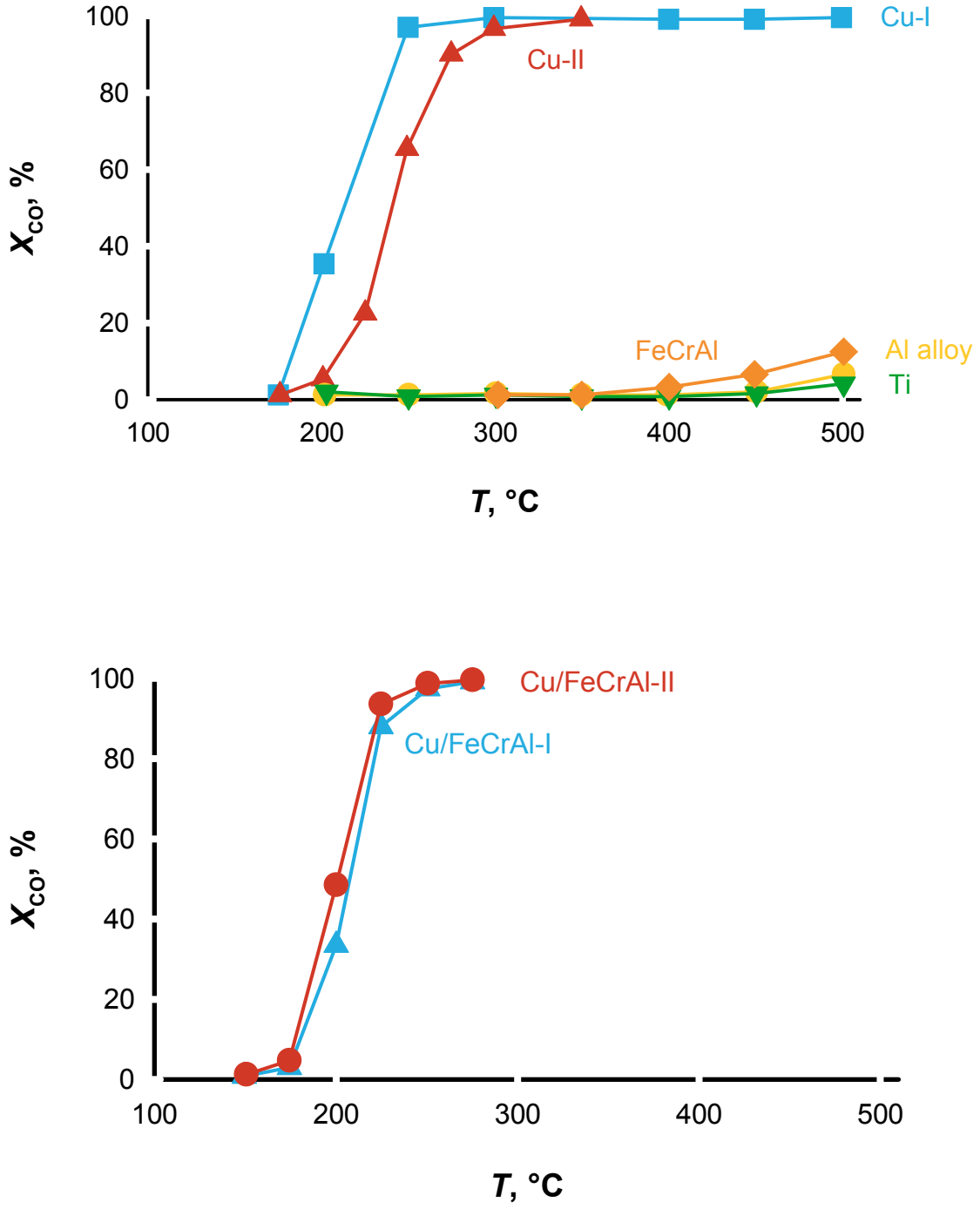

Figure 24: CO conversion vs. temperature: for bulk metal fibers (above) and for Cu-coated FeCrAl fibers (below). Adapted with permission from reference.[188] Copyright 2018 Elsevier.

Monolithic catalysts on FeCrAl foils are pretreated with basic, acidic, and ethanol solutions; boehmite primer sol improved the adhesion between the calcined metallic support and the washcoat layers of SBA-15 (mesoporous silica) co-impregnated with Cu and Ce nitrates. The strong interactions between CeO_2, CuO and the metallic substrate improve catalytic activity such that CO oxidizes completely at 160 °C.[191]

Pressure drop in FeCrAl converters are lower and the catalytic beds are shorter than ceramic monoliths for the SCR of NO_x in stationary applications.[146,150] Mechanical stability of short channel structured converters prepared by in situ synthesis of Cu-exchanged ZSM-5 zeolite on FeCrAl was superior to dip-coating. The high activity and selectivity confirm the active phase is highly dispersed.[146] FeCrAl foams (Table 2) are very active (Figure 25) in the SCR of NO_x because the deposited thin zeolite layer enhances the mass transfer. Pressure drop was 200 times lower than in traditional packed beds operating at the same conversion and catalyst loading.[192]

Table 2: Preparation conditions and composition of ZSM-5 supported on FeCrAl plate. C calcined, N no calcined metal support. S in-situ, D dip-coating.

Catalyst name	**Support**	**Deposition**	**Si/Al**	**Cu/Al**	**Loading**, $g\,m^{-2}$
25 CSO	C	S	25	0.25	14
25 NSO	N	S	25	0.35	101
15 CSO	C	S	15	0.13	10
15 CSI	C	S	15	0.25	13
37 CDO	C	D	37	1.06	4

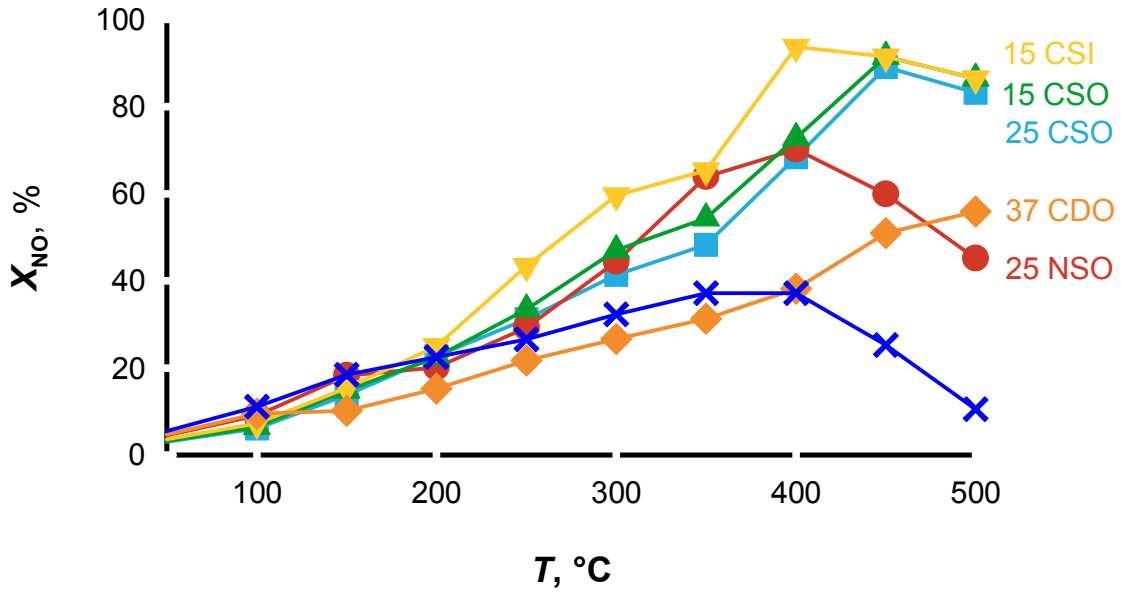

Figure 25: NO conversion vs temperature of samples (Table 2). Adapted with permission from reference.[146]

Polycrystalline ZSM5 as a dense and continuous phase on FeCrAl has *c*-axis preferred orientation orthogonal to the support surface. After In ion-exchange, it becomes less active in the SCR reaction compared to the same powdered catalyst. The orientation of the channels decreases the accessibility of the active sites with a consequent drop in performance. At the same time, the selectivity increased due to a decrease of the non-selective In and to the presence of oxidized Fe.[148] Similar results have been reported from the test of a mordenite grown on monolithic support. In this case, the b-axis was orthogonal to the surface; the metal support gives better results not only because of the orientation of the zeolite but also of the nature of In active sites compared to the results with a cordierite monolith.[193] Cu/SSZ-13 zeolite on a foam, synthesized in situ via hydro-thermal synthesis, was as active as in a packed bed reactor. This system operates at higher temperature (to the point where mass transfer rather than kinetics limits reaction rates), while maintaining a pressure drop two orders of magnitude lower than a packed bed at the same flow rate.[150]

4.1.3 Nickel

NiO catalysts obtained by electroplating combined with ultrasonic treatment of FeCrAl washcoated γ-Al_2O_3 were proposed as catalytic converters for exhaust emission control. Oxidation exhaust gas tests at 1100 °C for 100 h in a tube demonstrated the potential of Ni as the active phase.[194] It not only catalyzed the reaction but also improved the thermal stability of the FeCrAl. Al_2O_3 deposited at the same time as the electroplating, as an ultrasonic bath effectively replaces a magnetic impeller. The final material had a homogeneous layer of alumina with higher superficial roughness.[195] The mass of a FeCrAl monolith support after three 20 h cycles in a furnace at 1100 °C changed marginally, indicating it is resistant toward support oxidation. Combined coating and electroplating in the catalyst preparation performed best.[196]

4.2 CH_4 oxidation

The global warming potential of CH_4 is 21 times greater than CO_2,[197,198] so it has stricter emission limits for natural gas power plants, automotive engines, chemical industry flares, landfills, and oil operations.[197,198] Standard flares operate readily at methane concentrations above ~30 % ($L\,L^{-1}$) but generate NO_x because of the high temperature flame. Reacting low methane concentrations requires catalysts, which, coincidentally, reduces the operating temperature thus minimizing NO_x.[199–202] Active metals include Pd and Pt supported on SiO_2 or Al_2O_3, but also rare earth oxides and perovskites have proven high effictive at lower cost.[203–205]

Below 800 °C, intrinsic surface kinetics control the reaction rate in coventional packed bed reactors and at higher temperature, mass-transfer limits the activity. Structured beds operate better at both low and high CH_4 concentration. In the first case, pressure drop is lower at high volumetric flow rates, and in the second case adapting the structured bed geometry to the reaction conditions increases heat transfer rates.[11,206] FeCrAl as fibers and a monolith have been applied more than foams to support both noble and and transition

metals for such applications (Figure. 26).

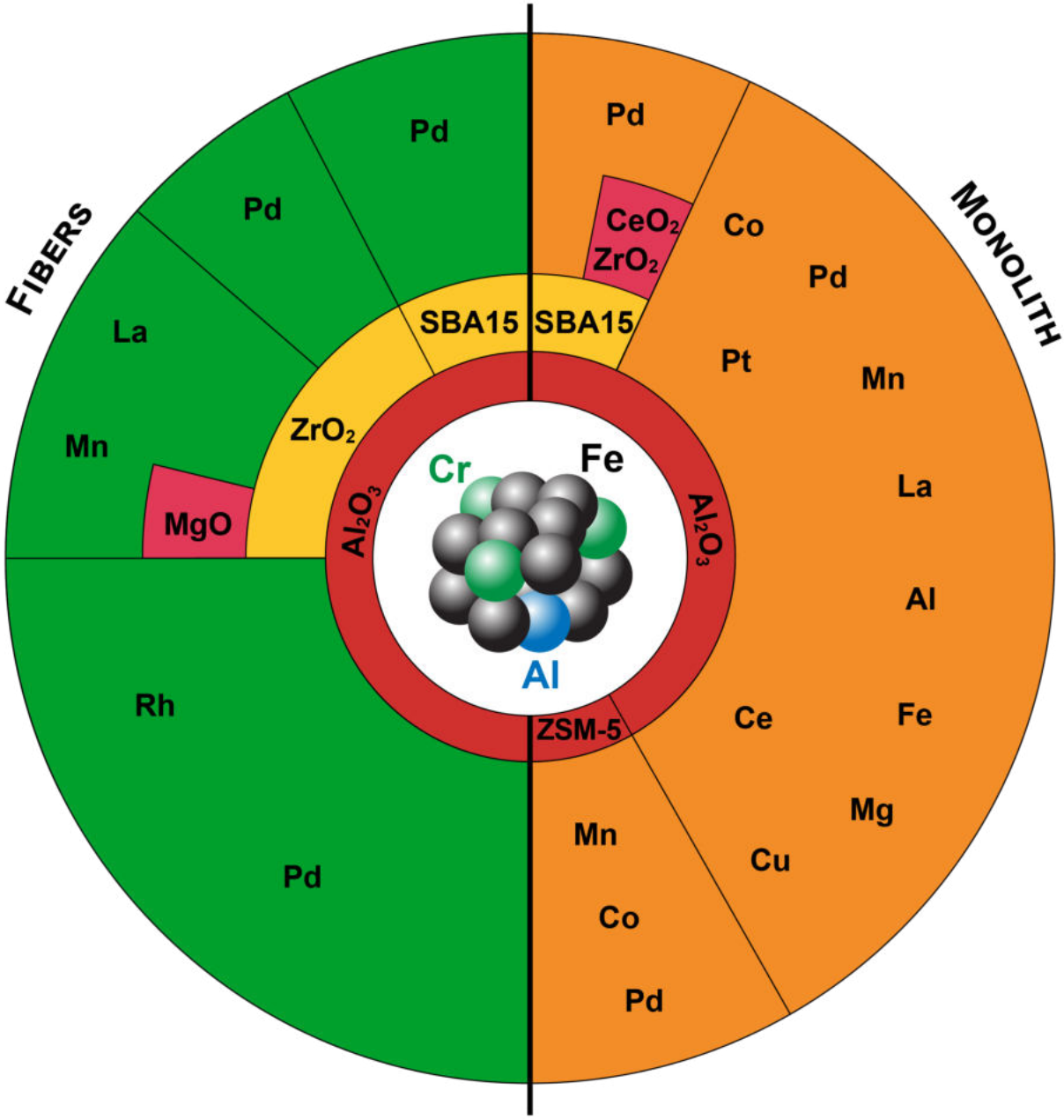

Figure 26: Catalyst structure, formulation and active phase for CH_4 oxidation.

4.2.1 Pd and Pt-based catalysts

Catalytic FeCrAl fibers supporting perovskite/zirconia ($LaMnO_3$-2 ZrO_2) with and without Pd synthesized via in situ SCS with glycerine have a higher specific surface area than sam-

ples prepared using urea.[207] The combustion with these catalytic converters—burners— is more stable, maximizes heat transfer by radiation, and improves natural gas combustion performance.[140,208]

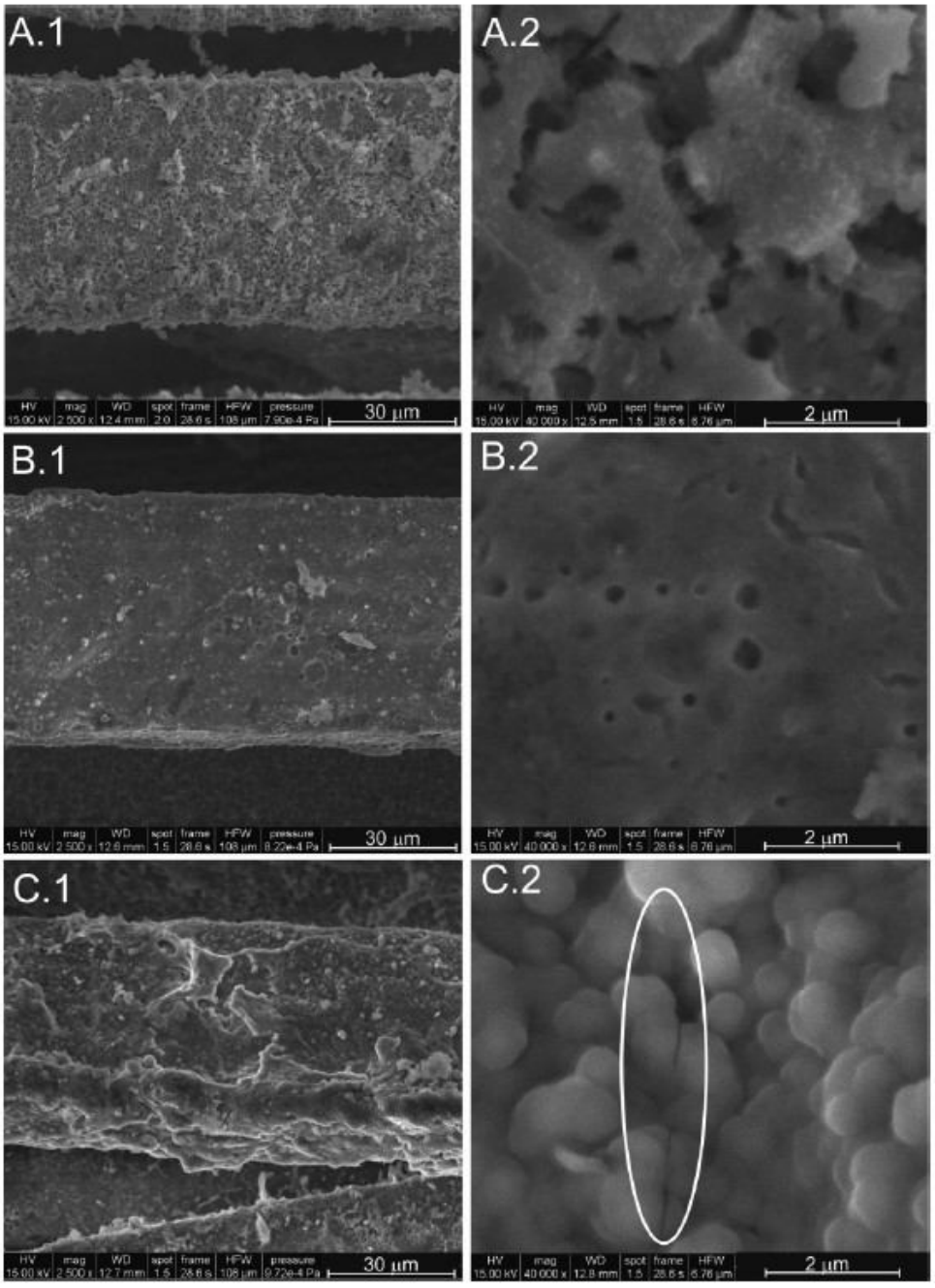

Figure 27: SEM micrographs of fresh (A.1/A.2), 1 week old (B.1/B.2), and 3 week old (C.1/C.2) aged burners at 2500 × magnification (.1 fig) and 40 000 × (.2 fig). Micro-fractures are evident in the oval region of C.2. Adapted with permission from reference.[209] Copyright 2007 American Chemical Society.

Burner aging study demonstrated that after 3-weeks under a flow of 200 ppm SO_2, corresponding to one-year of routine operation, CO and NO emissions remained acceptable:

the burner resisted poisoning and catalytic activity was constant. Cracks (Figure 27) in the coating that formed with time exposed more β-type oxygen desorption sites.[209] Spray pyrolysis disperses catalyst better compared to wash-coating thus NO and CO emissions are between 25 % to 50 % lower.[210]

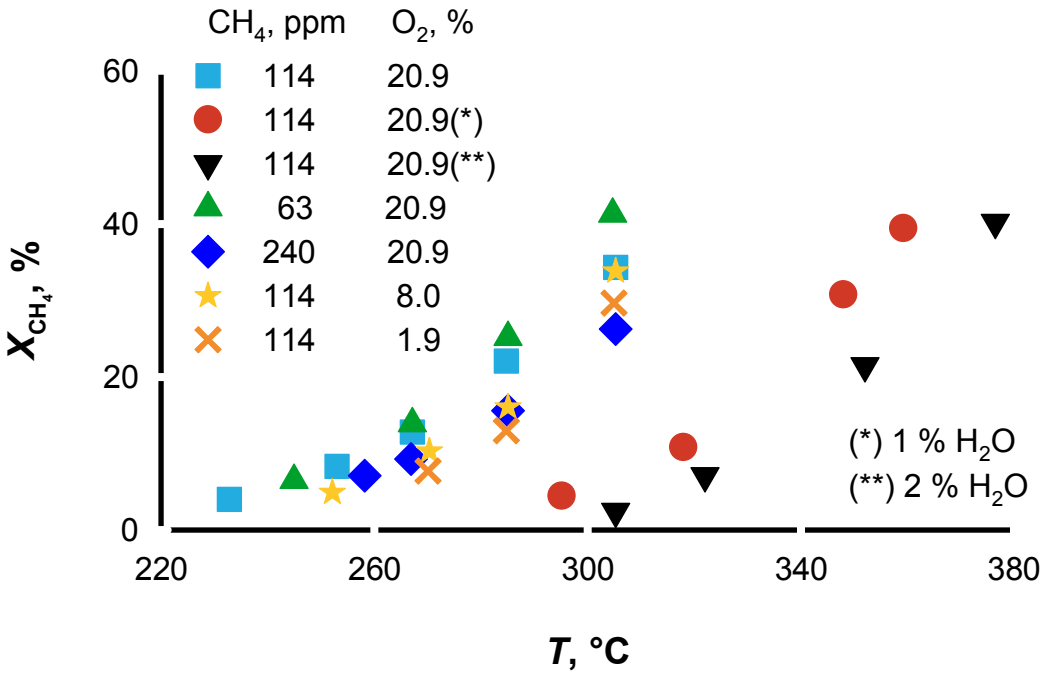

Figure 28: CH_4 conversion vs temperature as a function of co-reactant (O_2 and H_2O) concentration. Adapted with permission from reference.[211] Copyright 2015 Elsevier.

Pd-Co/α-Al_2O_3 catalyst was highly active and stable in CH_4 combustion, because surface Co oxides stored O_2 and stabilize Pd oxides. Adding 1 % (L L^{-1}) water to the gas mixtures delays the light off temperature by 50 °C. CH_4 conversion decreases with increasing inlet concentration, but is relatively insensitive to O_2 concentration (Figure 28).[211]

ZrO_2 improves activity and stability of Pd-based FeCrAl monolithic catalyst. With Pd/ZrO_2/SBA-15/Al_2O_3 on FeCrAl, the methane conversion is complete at 450 °C even after 700 h operation.[212] At low temperature, CH_4 oxidation activity increases with pre-calcination temperature and washcoat loading as the amount of Al_2O_3, promoter for Pd,

changes; Pd/Al_2O_3 activity was higher than Pd/SnO_2.[213]

ZSM-5 with isolated metal ions supported on FeCrAl monoliths promote heterogeneous-homogeneous reactions. The most active metals are Pd, Mn, and Co. Increasing either the temperature or the residence time improves conversion. The final performance depends not only on the catalyst composition, but also on physical properties like surface area and reactor volume. Because of the high heat transfer rates in these monoliths, reactants reach a higher temperature faster, thus, initiating homogeneous reactions.[214] Bimetallic Pd-Rh/γ-Al_2O_3 dip-coated felts with at least 1 % Pd are insensitive to oxidizing or reducing gaseous pretreatments, since they exhibit higher CH_4 conversion than monometallic Rh and Pd.[215] Pd-Pt bimetallic catalysts are also more active than the monometallic catalysts. Impregnated Pd/SBA-15 dipcoated on fibers combust methane entirely below 400 °C; activity is greater in the presence of Ce−Zr oxide.[216] Pt deposited on FeCrAl honeycombs is suitable for CH_4 oxidation. The reaction rate depends mainly on the Pt loading rather than on the mesh density, which is incongruous with the metal ions on ZSM-5 catalyst that promote heterogeneous-homogeneous reactions.[217,218]

4.2.2 La and Ce based catalysts

CO and hydrocarbon emissions are 3 to 5 times lower with catalytic burners based on perovskite-type catalyst ($LaMnO_3$) compared to non catalytic burners operating below 800 kW m^{-2}.[219] Contrary to a La_2O_3 layer, an intermediate layer of Al_2O_3 interacts with the dipcoated LaMn-hexaaluminate catalyst on FeCrAl foil.[124] The conversion is highest (at constant temperature) when the mole fraction of Fe equals that of Mg ($x = 0.5$) in $LaFe_{1-x}Mg_xO_3/Al_2O_3$/FeCrAl catalyst, where Fe and Mg components enhance the thermal stability (Figure 29).

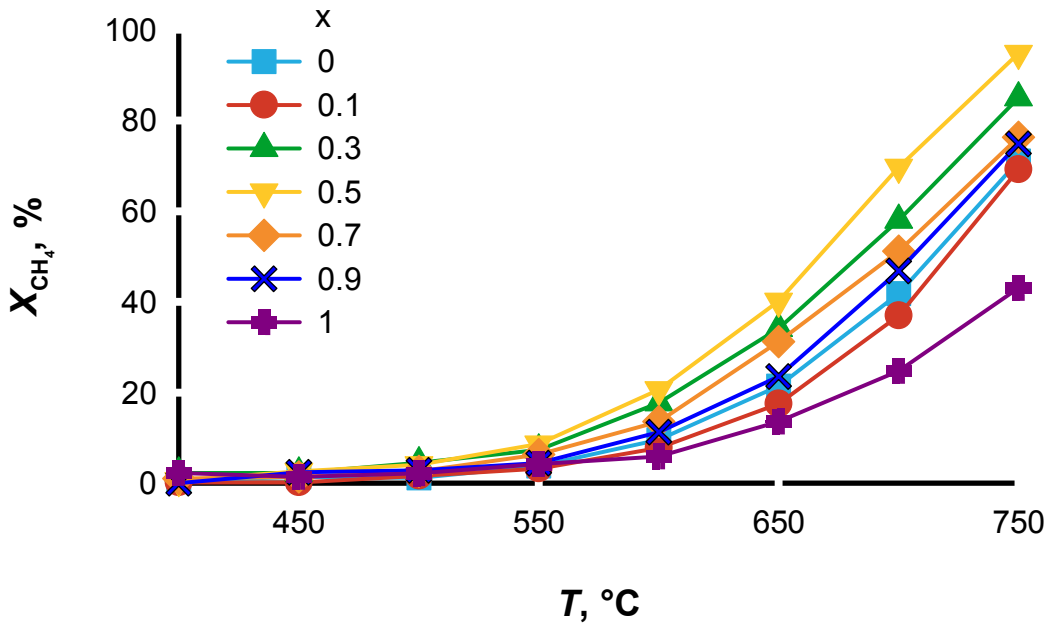

Figure 29: Methane conversion vs temperature over $LaFe_{1-x}Mg_xO_3/Al_2O_3$/FeCrAl catalysts. GHSV = 36 000 mL g^{-1} h^{-1}. Adapted with permission from reference.[220] Copyright 2006 Elsevier.

With this catalyst, CH_4 combustion to CO_2 is complete at 640 °C and 9000 mL g^{-1} h^{-1}.[220] In the context of catalytic micro-combustors using a FeCrAl catalyst support with $LaMnO_3/\gamma$-Al_2O_3 paintbrushed on alloy foils better oxidize CH_4 than Pt/γ-Al_2O_3. Co-feeding CH_4 with H_2 enhances the combustion because H_2 activates CH_4 radicals above 700 °C.[221]

Varying the cerium and lantanium ratio in $Ce_{1-x}La_xO_{2-x/2}/Al_2O_3$/FeCrAl dipcoated monolithic achieves the best activity at $x = 0.3$; at this value, the surface is homogeneous and the particles are smaller than 0.1 µm. The strong interaction among the rare earth solid solutions, the Al_2O_3 washcoats and the FeCrAl support improves the redox properties of the catalysts, and therefore their activity.[222] After replacing La with Cu, the final catalytic system maintains similar behavior.[223]

4.3 VOC oxidation—Volatile organic components

Volatile organic compounds (VOC), besides being the main contributor to the tropospheric ozone levels, are hazardous for human health.[224,225] Thermal and catalytic combustion oxidize VOC, limiting their emissions. Traditional VOC combustion catalysts are noble metals, such as Pt and Pd supported on Al_2O_3 or TiO_2. Supported transition metal oxides offer an alternative, because they are less expensive and more resistant to Cl_2 and HCl than noble metals.[226,227] Not only they are more tolerant towards poisons but they exhibit the same or higher activity than noble metals: MnOx,[228] Mn in combination with Fe,[229] Ni,[229] Cu,[230,231] are examples.

Because of the high volume of exhaust gases to treat linear velocities are high in industrial processes, therefore catalysts geometries must minimize pressure drop. Catalyst supports include ceramic honeycomb monoliths, and metal supports. The latter has the extra advantage of having high mechanical properties, material ductility and electrical resistance. Indeed, the Joule effect makes the temperature of the catalyst more easily controllable, and introduces an additional process design variable that minimize capital and operating costs. In this context, FeCrAl is an active catalyst support for VOC oxidation (Figure 30): Pt, for example, is deposited either on the base FeCrAl (foam and fibre) or on FeCrAl with a CeO_2 layer.[155,170,232]

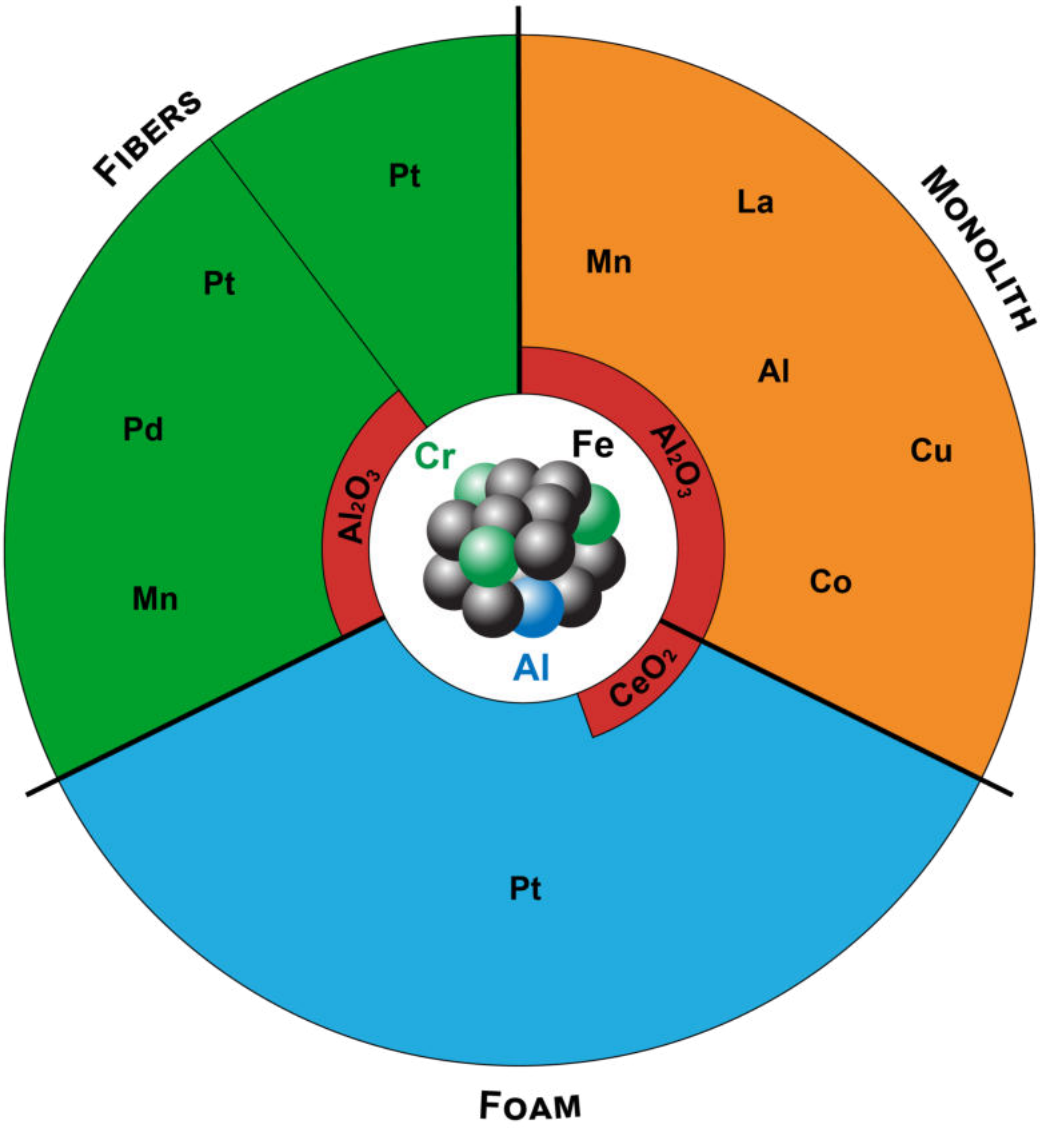

Figure 30: Catalyst structure, formulation and active phase for volatile organic components oxidation.

4.3.1 Pt-based catalysts

Pt electrodeposited cathodically on FeCrAl foams oxidize methanol. The reaction starts at 80 °C at the highest Pt loading ($> 13\,\%$) and at about 140 °C with the lowest metal loading ($< 1\,\%$). Yield of CO was negligible at all conditions during multiple oxidation cycles while even loading of $0.8\,\mathrm{mg\,cm^{-3}}$ approached 100 % yield to CO_2 above 320 °C (Figure 31).

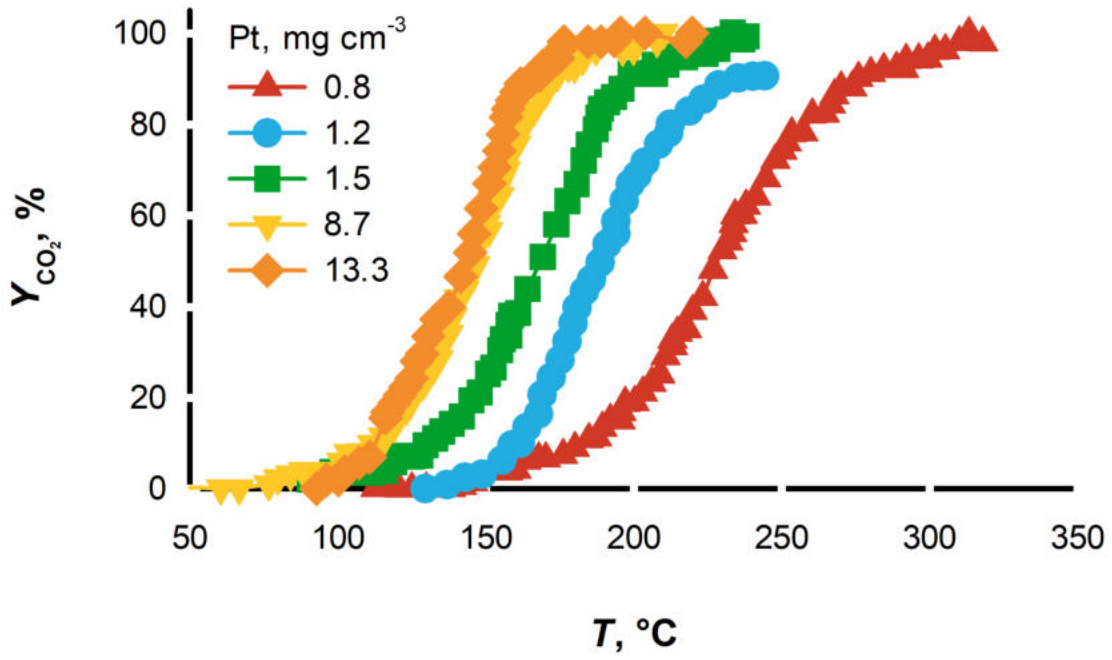

Figure 31: Methanol yield to CO_2 vs reaction temperature over Pt/FeCrAl foam catalysts at increasing Pt loading. Feed conditions: CH_3OH 0.5 % in air, GHSV = 16 500 h^{-1}. Adapted with permission from reference.[155] Copyright 2016 Elsevier.

Cimino et al. reported no correlation between Pt surface area and CO_2 formation rate, characterized by constant apparent activation energy (independing of Pt loading and methanol concentration). It is indeed the FeCrAl support that plays an important role in the oxidation: in particular, the metal oxides next to the noble metal particles activate oxygen, thus, favoring oxygen spillover.[155]

Although the addition of a CeO_2 film onto the Pt-FeCrAl decreases the surface area of the active metal, the activity of the catalyst in methanol oxidation improves, because additional active sites located at the CeO_2–Pt nanoparticle interface are formed. This confirmed previous results that underlined the importance of the interaction support-active phase. Moreover, at the same Pt loading, FeCrAl with CeO_2 produces 10 % more CO_2 at 10 °C lower than Pt-FeCrAl (Figure 32).[168]

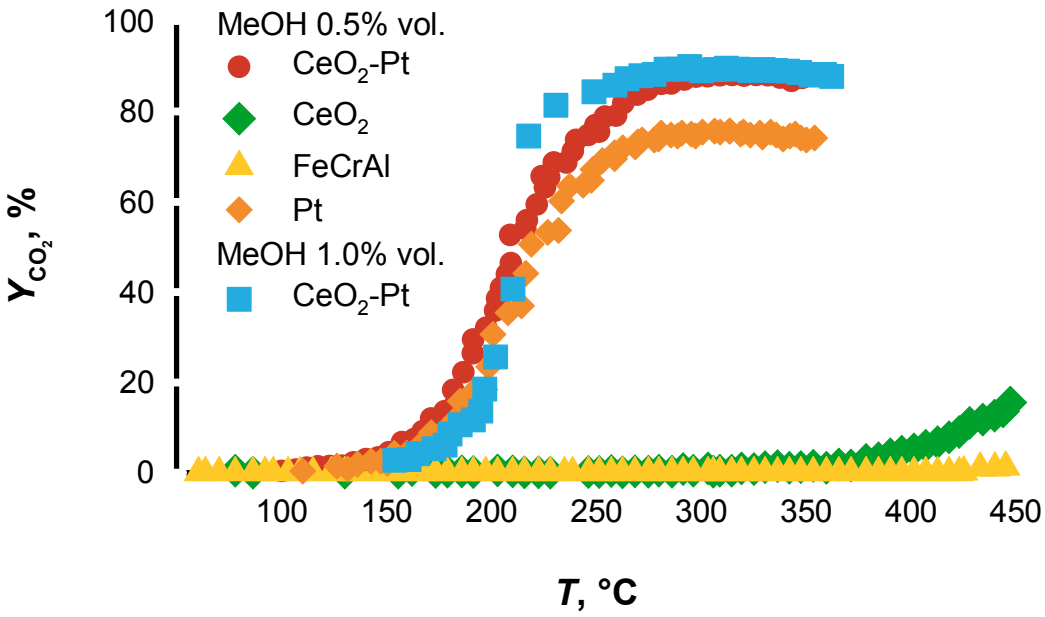

Figure 32: Methanol yield to CO_2 vs reaction temperature over several catalysts. Feed conditions: GHSV = 16 500 h^{-1}, CH_3OH = 0.5 % to 1 % in air. Adapted with permission from reference.[168] Copyright 2017 Elsevier.

Despite the fundamental role of ceria in increasing catalytic performance, the metal support has a much greater influence. This suggests that not only the promotion of the active sites is beneficial to the final catalyst performance but also the structures itself that can also be characterized by different thermal conductivity. Changing the batch or supplier of the metal support maintaining the same alloy composition, apparent density and pores per inch, not only the specific surface can strongly change but also the temperature to achieve the same performance.[155,168]

Electroless plating deposits 0.15 % to 0.20 % ($g\,g^{-1}$) Pt active particles on the wire mesh substrate. The resulting sample after calcination at 450 °C has homogeneously distributed micro particles that enhances the transformation of Pt and PtO and completely oxidizes toluene at 180 °C;[170] simply spraying a solution of Pt precursor on preoxidized metal fibers result in lower activity catalyst that requires between 50 °C to 100 °C to achieve complete

toluene conversion.[232]

4.3.2 Pd-based catalysts

Pd deposited via electroless plating on non-oxidized FeCrAl wire mesh completely oxidizes toluene at temperatures just above 200 °C. The activity comes from 0.3 % to 0.4 % ($g\,g^{-1}$) PdO particles formed during catalyst calcination at 800 °C,[169] and results more active compared to catalyst with Pt.[170,232] Electroplated Pd catalyst was also used as Joule-heated reactors to combust ethylene. The FeCrAl calcined structure usually gives better activity and promotion to the active phase (Figure 33(b)) compared to catalysts deposited on anodized or untreated supports (Figure 33(a)), even though resulting noble metal particles are often bigger. This is attributed to the surface oxides that supply active oxygen species to the neighbor Pd.

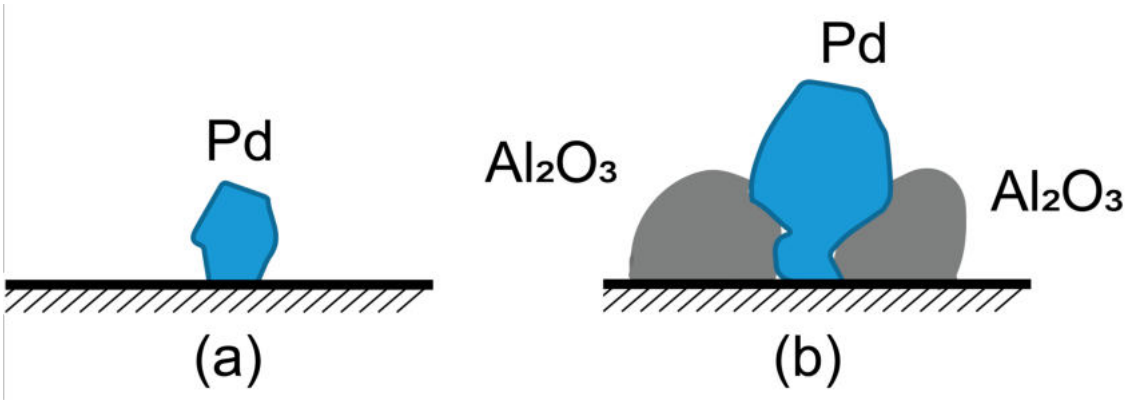

Figure 33: Electroplated palladium particles on virgin (a) and oxidized (b) FeCrAl substrate. Adapted with permission from reference.[233] Copyright 2017 American Chemical Society.

Electroplated catalysts on a calcined surface is the most active combination after comparing the noble metal on an anodized or untreated surface; in this case both intimate contact between Pd and Al_2O_3 and small particles of active species improve supply of oxygen species that facilitates VOC oxidation.[233]

4.3.3 Mn and Cu based catalysts

FeCrAl wires dipcoated with MnO and heated up exploiting their electrical resistance also catalyze the oxidation of toluene. Anodized FeCrAl supports are more active than oxidized ones to increase MnO loading. Precoating with Al_2O_3 further favors active metal oxide loading and dispersion. The mechanical stability increases adding Zr in the Mn precursors.[111] Heating these catalyst above $14\,\mathrm{kW\,m^{-2}}$ oxidizes CO completely and toluene above 90 % (Figure 34). Even though Oshima et al.[111,234] suggested that the electric field affects the chemical equilibrium, in this case, this difference comes from an incongruence between measured and real temperature, given the different heating method.

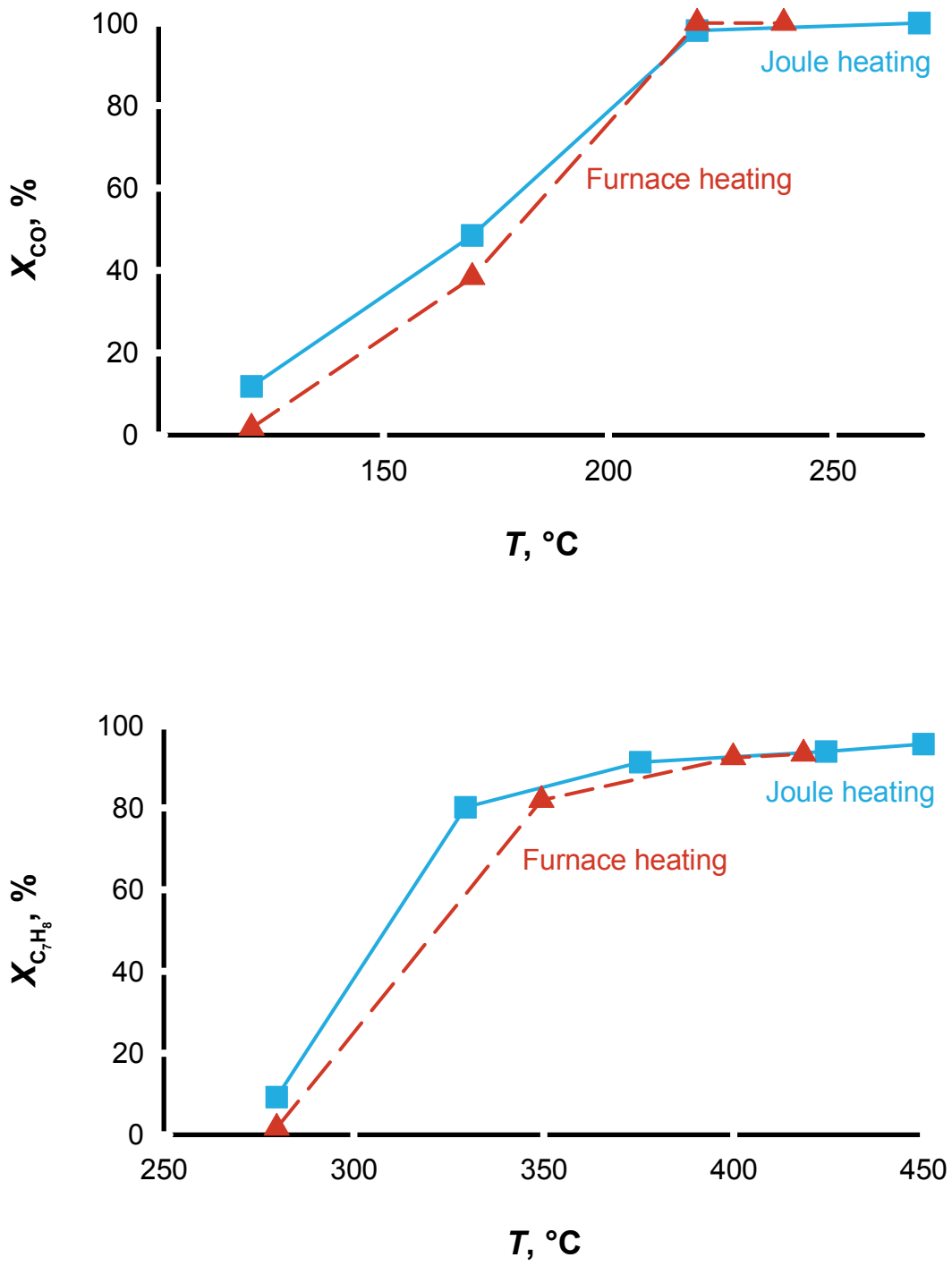

Figure 34: CO and C_7H_8 conversion over Mn supported FeCrAl wire as a function of heating methods. Adapted with permission from reference.[111] Copyright 2017 Elsevier.

FeCrAl monoliths with Mn and MnCu also combust ethyl acetate and toluene. Multiple dipcoating steps increase the amount of Mn and MnCu, thus increasing the catalytic activity but decreasing the adhesion of the active species.[230,235] Powder catalysts, prepared via co-precipitation, with a Mn:Cu ratio of 9:1 have higher conversion compared to FeCrAl structured cataysts.[231] While washocated and impregnated monoliths have similar yield in the oxidation of a variety of VOC, anodized monoliths are more active at the same temperature (Figure 35).

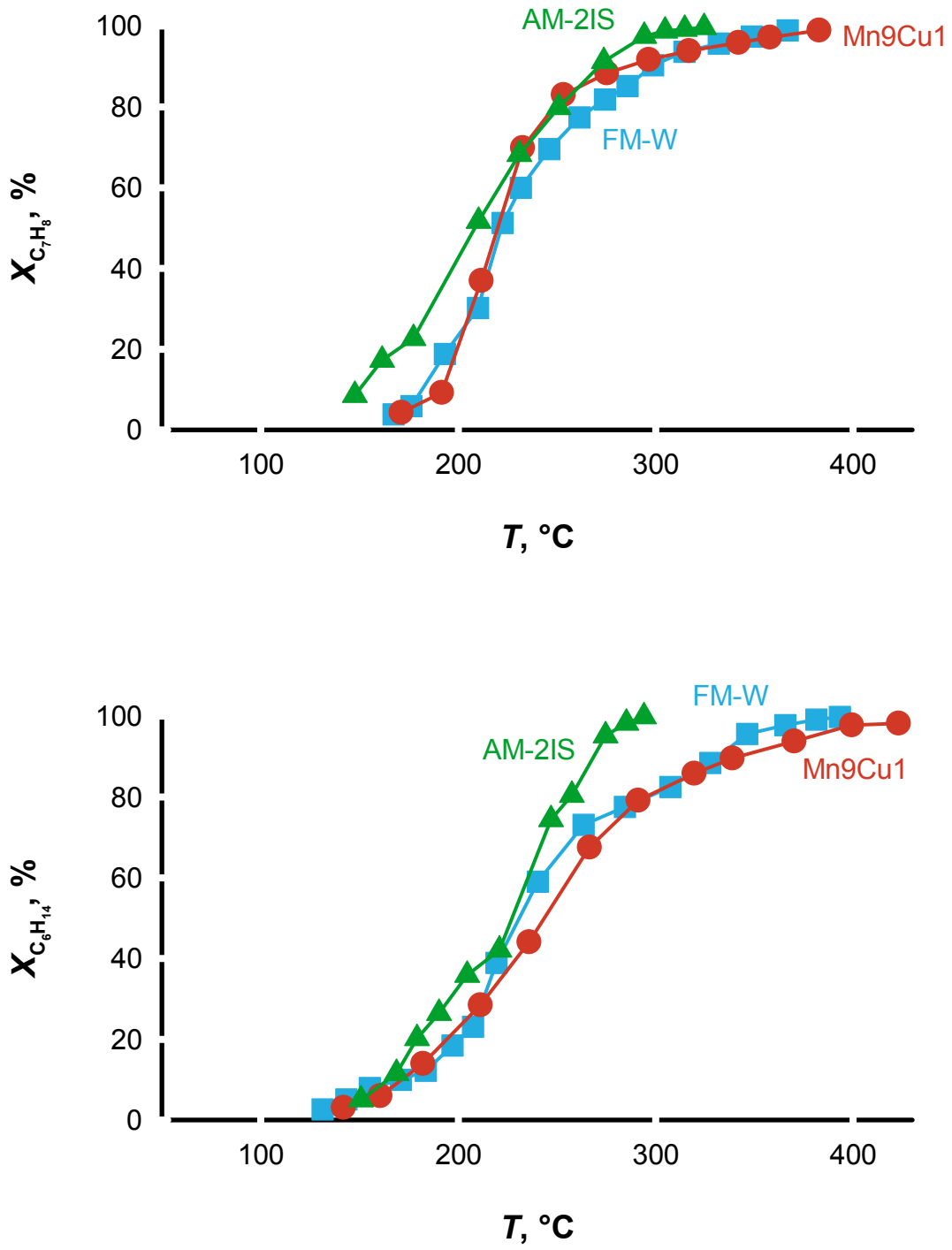

Figure 35: Conversion of toluene (top) and n-hexane vs. reaction temperature on FeCrAl washcoated monolith, impregnated AM-2IS and powder Mn_9Cu_1 catalyst. Adapted with permission from reference.[231] Copyright 2011 Springer Nature.

5 Syngas

Syngas production via steam methane reforming (SMR), auto-thermal reforming (ATR), dry methane reforming (DMR), and catalytic partial oxidation (CPOX) operate above 700 °C, for which the thermal and mechanical properties of FeCrAl are well suited. Methane reacting under extreme conditions destabilizes high temperature resistant metals as Fe−Cr and Ni−Cr alloys.[15] In FeCrAl, the superficial segregated Al_2O_3 isolates the reactive atmosphere and the support, while the thermal conductivity of the bulk material (higher than the majority of the usual ceramic supports) reduces the temperature gradients within the catalytic bed, limiting secondary reactions that decrease selectivity. In the case of CPOX, the heat transfer coefficients of structured bed catalysts is sufficient to dissipate energy and to minimize local hot spots. To keep adiabatic conditions, the gas velocity must not exceed a threshold value to maintain an ignited steady state.[236]

Metal supports with low porosity, induced by thin coating layer, minimize internal mass transfer resistance, one of the governing factor for fast reactions.

5.1 SMR—Steam methane reforming

SMR is the most common chemical process to produce H_2 and is highly endothermic: $CH_4 + H_2O \rightleftharpoons CO + 3\,H_2$ (ΔH_R=205 kJ mol^{-1}). Multi-tubular reactors operate from 700 °C to 1000 °C, 5 bar to 30 bar, and with a steam to carbon ratio (S/C) from 2.5 to 5.0. Industrially, the catalyst consists of Ni supported on cylindrical hollow pellets 1 cm to 3 cm in diameter.[237] The high capital costs, related to the large reactor volume and energy recovery units, discourage applying this technology to small decentralized production facilities. FeCrAl mitigates drawbacks of heat exchange rates in current technology,[238] but this single improvement is insufficient for shut-down economics for existing facilities. Exploiting its high resistance (1.45 Ω mm^2 m^{-1} at 20 °C) and thermal conductivity minimize energy consumption, reactor volumes, start-up time, and replace burners and heat exchange reactors

using the Joule heating effect.[239] All these advantages are more appealing and might push forward current technology retrofit; these have already led to the synthesis of more than 20 different catalysts supported on FeCrAl (Figure 36).

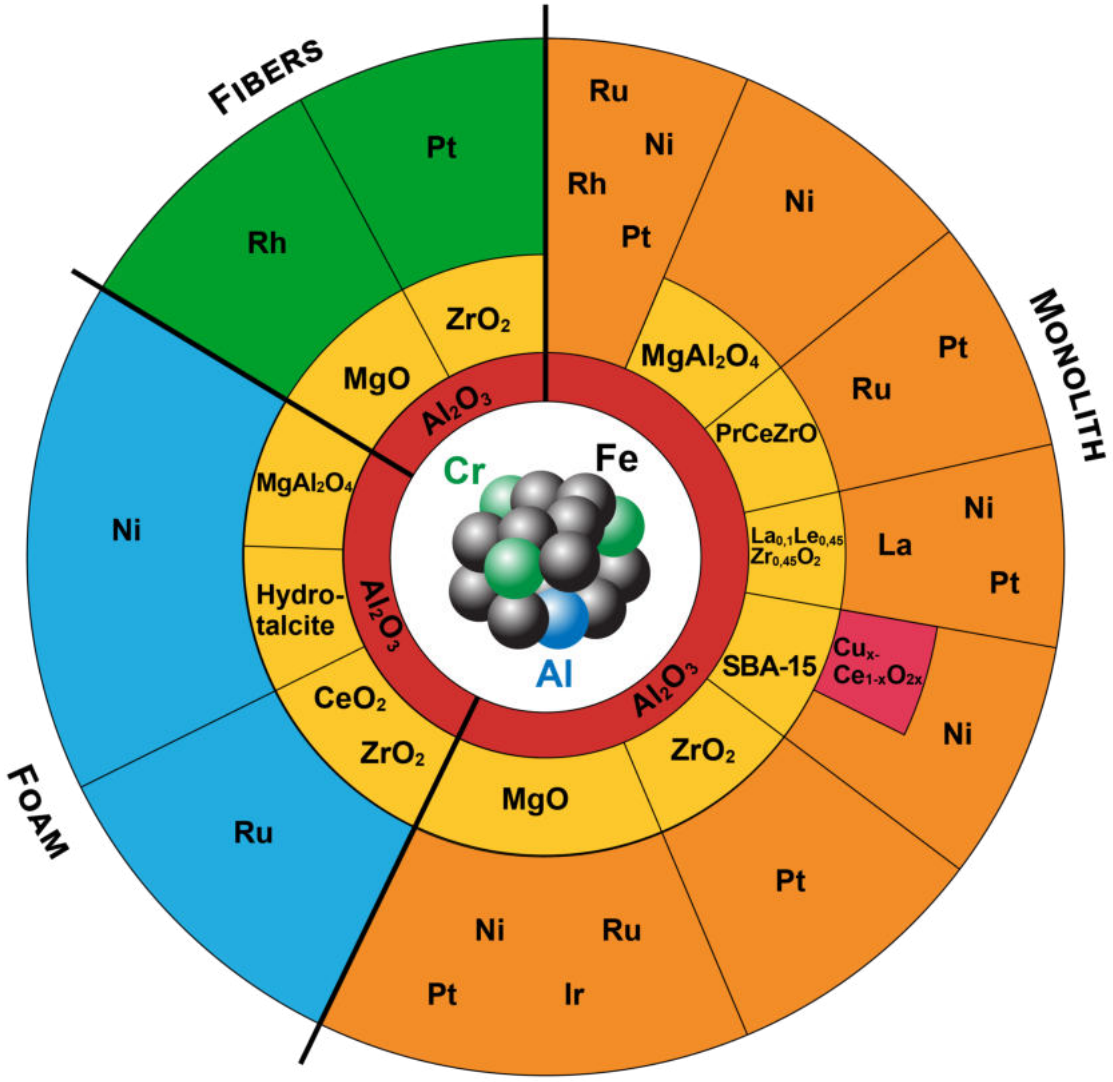

Figure 36: Catalyst structure, formulation and active phase for natural gas steam reforming and water gas shift.

5.1.1 Ni-based catalysts

$Ni/MgAl_2O_4$, a well-known catalyst for SMR, coats the surface of a metal monolith previously preoxidized and electrochemically pretreated. Addition of binders in the milled catalyst

slurry modifies the physico-chemical properties of the catalyst like surface area, degree of reduction, and effective dispersion. These changes decrease the conversion (from 5 % to 10 %) of a FeCrAl structured bed compared to the traditional fixed one that uses the same catalyst.[240] In contrast deposition-precipitation produces a 1 µm thick uniform and highly dispersed nanosheet that increases the availability of surface active metal sites on the FeCrAl monolith (Figure 37), leading to higher activity and stability compared to catalyst pellets.[241]

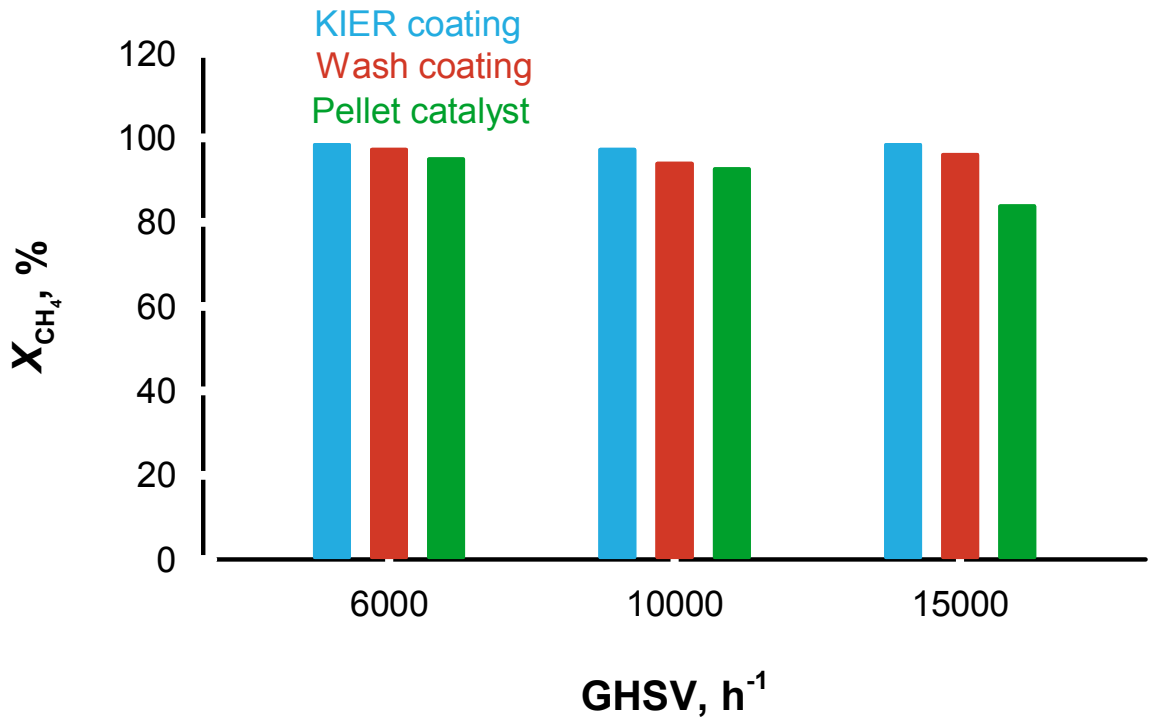

Figure 37: CH_4 conversion vs GHSV for $Ni/MgAl_2O_4$ catalyst. Adapted with permission from reference.[241] Copyright 2016 Elsevier.

Percolation-blowing deposition of $Ni/MgAl_2O_4$ on FeCrAl foams is more reproducible compared to dip-blowing,[242] which is important for industrial applications. Above 450 °C the catalyst operates at 130 000 mL h^{-1} g^{-1} reaching equilibrium performance.[243] Thermally sprayed Al_2O_3 on FeCrAl, afterward impregnated with Ni, is suitable for millisecond SMR micro-channel reactors and is stable for 500 h at a S/C ratio of 3.0 above 700 °C.[244] A metal-

monolith with anodic alumina and Ni promoted Pt catalyst was Joule-heated : the start-up time decreased from 30 min to 30 s (Figure 38).[245]

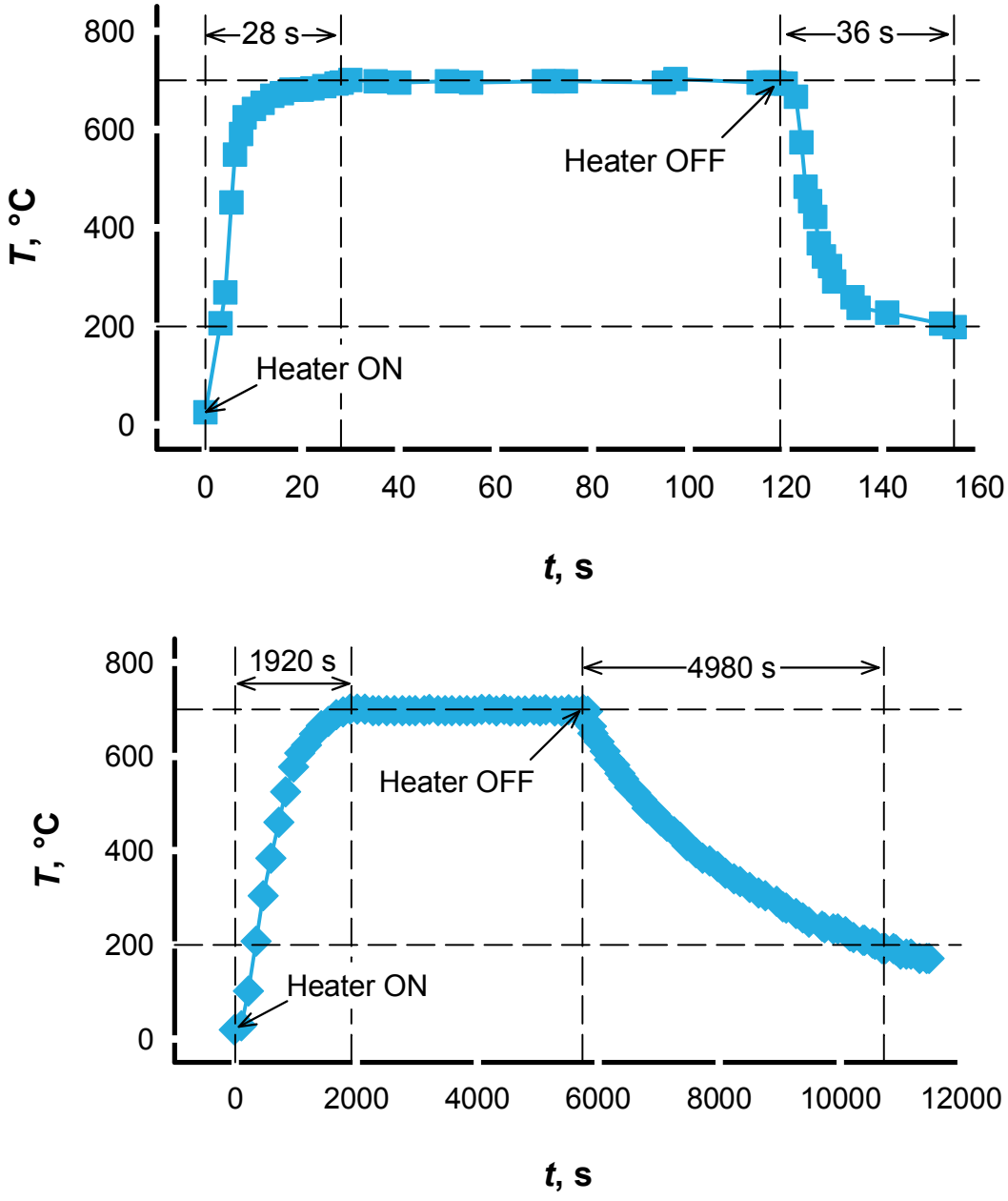

Figure 38: Catalyst temperature profile vs time for electrified support (top) and outside heated (bottom).[245] Copyright 2011 Elsevier.

Ni-Al_2O_3 on microchannel FeCrAl was more active and stable compared to Ni on MgO or CeO_2/Al_2O_3.[246] 10 % $Ni/Ce_{0.5}Zr_{0.5}O_2$/SBA-15 was the most active and stable among the Ni/SBA-15 monolith catalysts. All the CH_4 reacts at 800 °C for 110 h of time-on-stream.[247] Calcination of Ni/Al hydrotalcite-like compounds electrodeposited on FeCrAl foams at −1.2 V, optimum synthesis conditions,[164] vs. SCE for 1000 s produces a thin and strongly adherent film that has higher density of active sites per unit of mass. Ni metal crystallites dispersed on α-Al_2O_3 prove the catalyst layer is stable after reduction and catalytic tests. Coating stability is related to the intermediate Al_2O_3 scale developed from the foam during calcination. Compared with a commercial pelletized Ni catalyst, under industrial conditions, coated foams reacts more CH_4 even though the catalyst loading is lower.[156,248] Methane conversion was also higher over monolith wash-coated Ni compared to powders because of the better heat transfer and catalyst effectiveness factor.[249]

5.1.2 Ru and Pt-based catalysts

Ru FeCrAl monolith, prepared via deposition-precipitation, outperforms commercial Ru/Al_2O_3 at higher GHSV (Figure. 39) even when the active metal content is 14 times lower. These outstanding results come from the high availability of Ru that leads to long-term stability of the structured bed.[250]

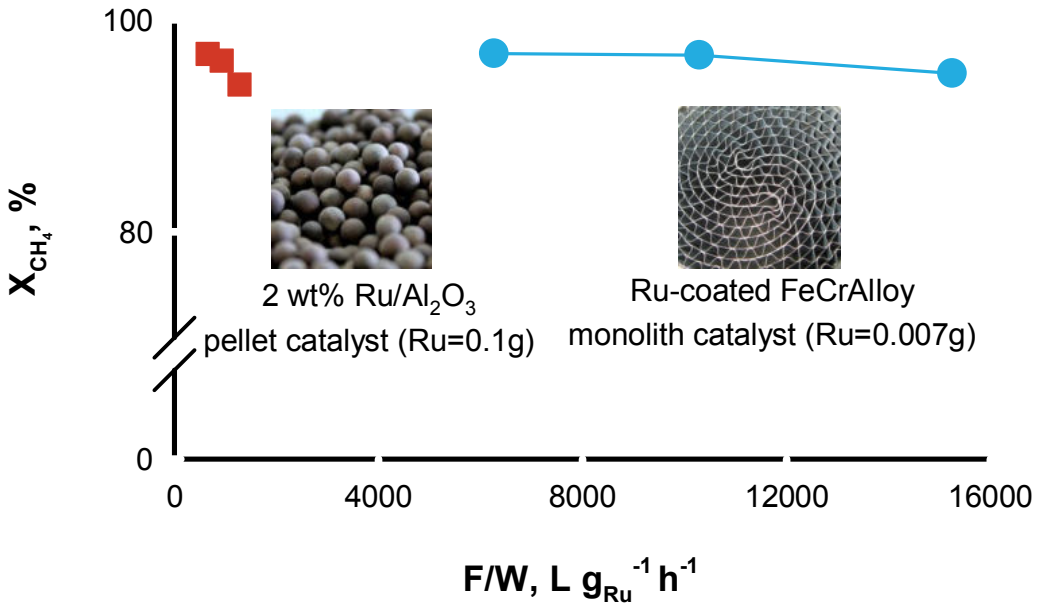

Figure 39: Conversion vs space velocity (flow over weight F/W) over commericial 2 % Ru/Al_2O_3 pellet and Ru-coated FeCrAl monolith in SMR at 700 °C, S/C = 3.0, F/W = 430 L g^{-1} h^{-1} to 15 100 L g^{-1} h^{-1}.[250] Copyright 2017 Elsevier.

Pt-Zr on FeCrAl mesh ignited hydrogen in a microchannel reactor, in which hydrogen provides the start-up fuel. This configuration increases both SMR capacity and energy efficiency without an external energy source from a furnace or burner.[251] Another type of reformer uses metallic heat exchangers coated with catalyst. Compared to conventional reformers, this design minimizes reactor dimensions, heat transfer resistance, and pressure drop.[252] These types of operation are possible because of the high temperature stability and the low heat capacity of the FeCrAl structured catalyst.

5.2 CH_4 CPOX—Catalytic partial oxidation

The partial oxidation of CH_4 to syngas is mildly exothermic $2\,CH_4 + O_2 \rightleftharpoons 2CO + 4H_2$ ($\Delta H_R = -36\,kJ\,mol^{-1}$) and is suitable for Fisher Tropsch (gas to liquid technologies) because it produces syngas with a H_2/CO ratio of two.[253,254] Even if the reaction mechanism and kinetics are widely accepted in the literature, the economics remain unfavourable because

the catalyst deactivates or produces CO_2 at high selectivity while hot spots irreversibly damage the catalyst.[253,255–257] Metal supports minimize hotspots and in the case of FeCrAl the superficial α-Al_2O_3 not only protect the material but also stabilizes the active sites reducing the deactivation rate. Noble metals are more active and less prone to oxidation and carbon deactivation than Ni[258–262] but both have been supported on FeCrAl (Figure 40).

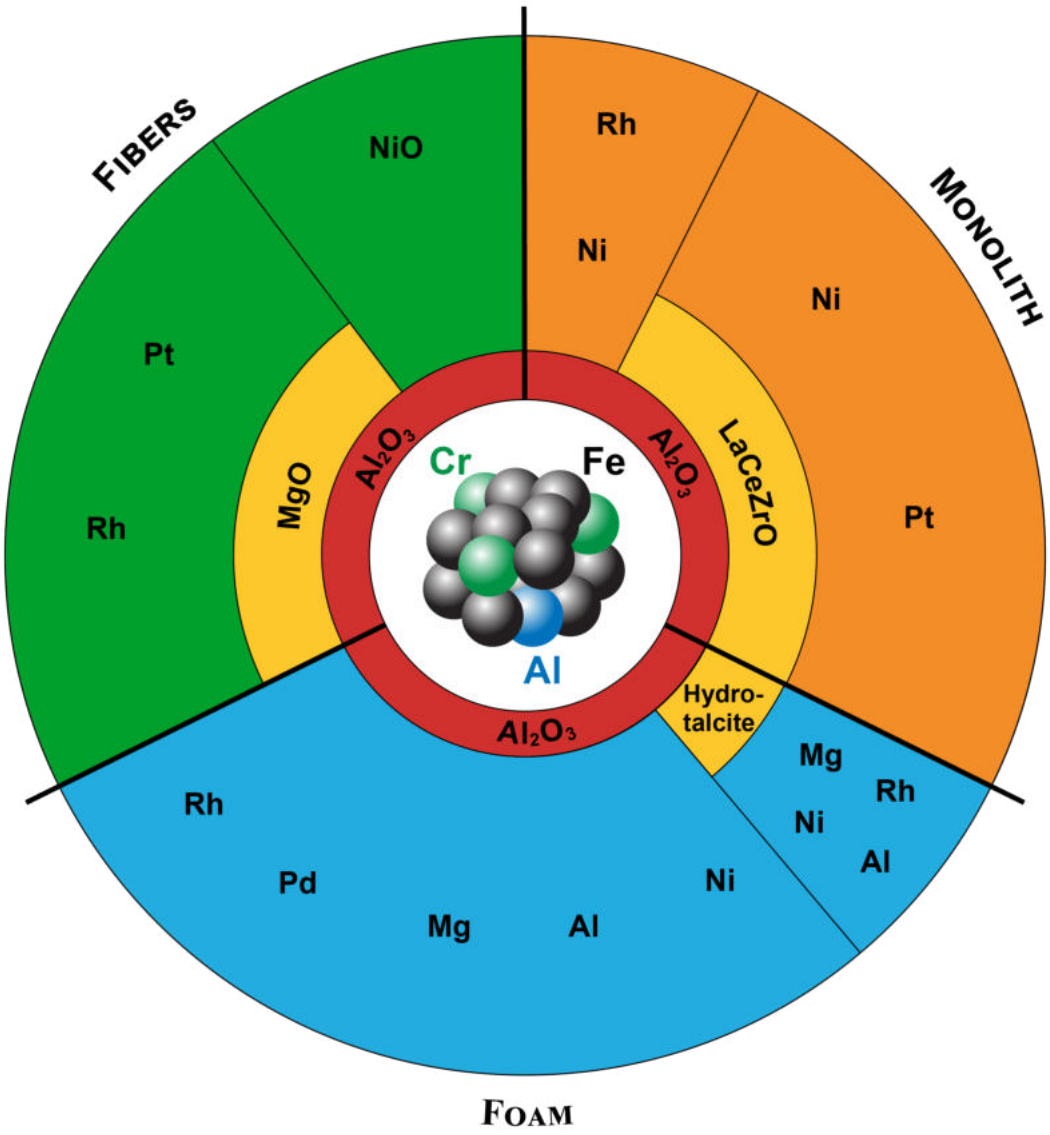

Figure 40: Catalyst structure, formulation and active phase for catalytic partial oxidation of methane.

5.2.1 Rh-based catalysts

Because of their higher surface area (compared to monoliths), electrical conductivity, efficient heat transfer, and resistance to oxidation, FeCrAl foams are excellent supports for methane CPOX.[263] The in situ synthesis of Rh/Mg/Al hydrotalcite-type (HT) compounds on foams by electrodeposition is as an alternative to the conventional washcoating.[162,163,264]

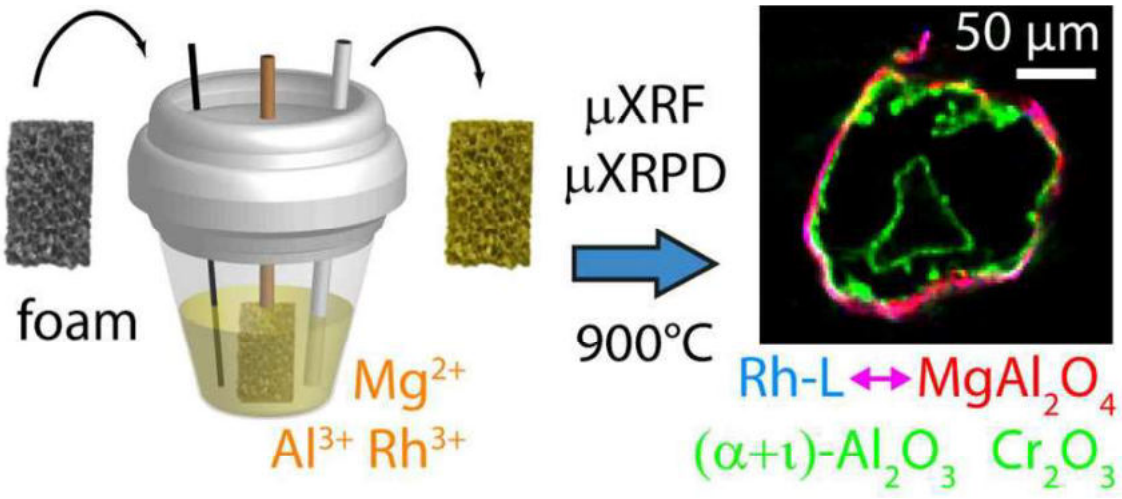

Figure 41: Production method and micrograph of electrosynthesized Rh foam. Adapted with permission from reference.[167] Copyright 2014 American Chemical Society.

These catalysts combine the properties of HT compounds and open cell foams. Thermally stable nano MgO and spinel-type phases contain Rh highly dispersed and stabilized against sintering, with better mass and heat transfer. $MgAl_2O_4$ thin films in the support-coating interface, formed via chemical reaction between Mg^{2+} from the coating and Al^{3+} from the support during calcination, improves catalyst adhesion (Figure 41).[159,167] After 50 h on-stream, the coat is stable and the 2 nm Rh nanoparticles are still well dispersed.[165] Partially substituting Mg^{2+} with Ni^{2+} in the synthesis solution produce an active bimetallic Rh/Ni catalyst with CH_4 conversion and selectivity to syngas higher than 90 %.[165]

Complementary to the electro-base generation method, direct cathodic electrodeposition of Rh on foams produces an active phase that undergoes constant deactivation mainly coming form the growing Al_2O_3 layer. In this case the catalyst stability result lower compared to a

washcoated catalyst sample.[154] Traditional methods impregnate the thermally grown Al_2O_3 on the surface of a microchannel reactor, where dispersed Rh on the porous surface improves H_2 selectivity.[265] Washcoating of a Nicrofer reactor with alumina via a sol-gel technique forms a surface coating with low stability; during operation, Cr species cover the Rh particles and channel surface.[266] Even if hydrocarbons ignition at the entrance of the monolith leads to lower syngas production, higher GHSV limits this phenomenon.[267]

Catalytic modules based on Rh/θ-Al_2O_3/FeCrAl fiber mesh with both radial and axial intermixing (Figure 42), as an alternative to open-cell foams, increase heat transfer. This configuration, coming from a FeCrAl nets, is less expensive and more accessible in the market. Strongly bound θ-Al_2O_3 coating create a porous support for incipient wetness impregnation of Rh. The composite architecture maintains Rh highly dispersed with good adhesion despite operating above 900 °C for 20 h on stream with 4 start-up/shut-down cycles.[268]

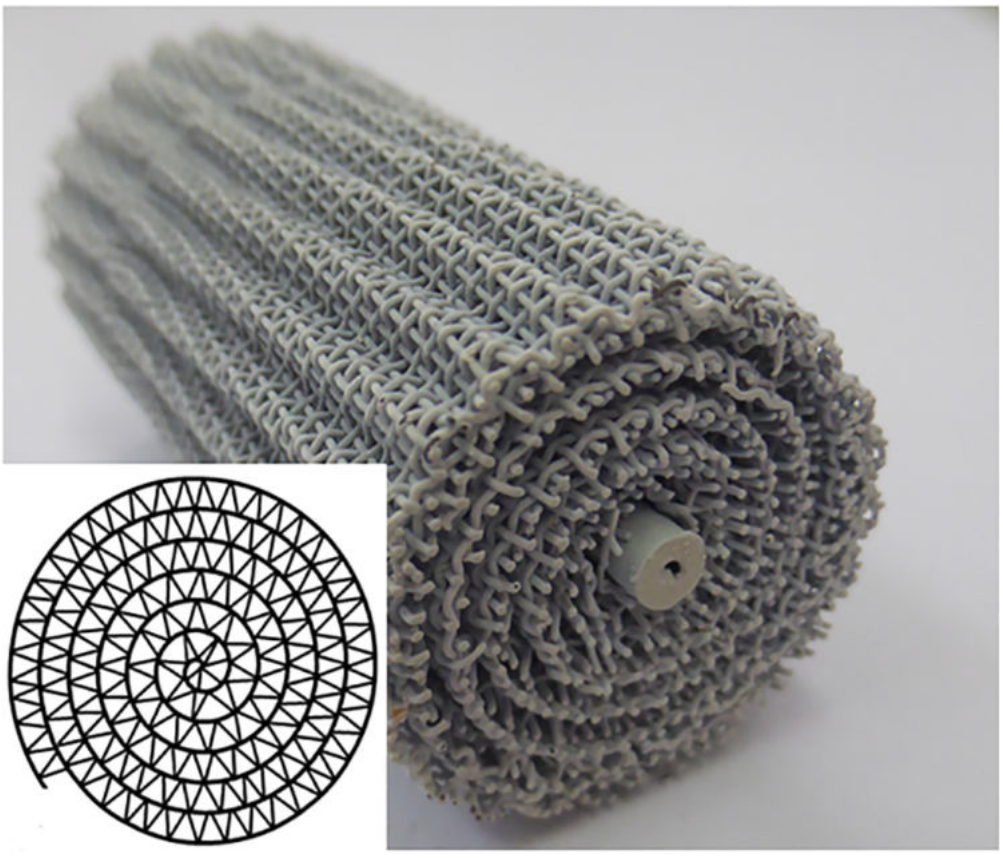

Figure 42: Structured catalyst overview and cross section.[268] Copyright 2019 Elsevier.

Rh impregnated on γ-Al_2O_3 support on FeCrAl foam performed as good as a packed bed in the partial oxidation of dimethyl ether at a catalyst loading 10 times lower for 1200 h.[269]

5.2.2 Pt and Ni-based catalysts

Pt-catalyst deposited on woven fibers partially oxidize CH_4, reaching almost equilibrium performance at 20 bar and 800 °C. Compared to commercial Pt-gauzes, H_2 and CO selectivities were higher.[135] CPOX forms more coke with increasing pressure and deactivates the catalyst. MgO layers, produced via SCS on the alloy fibers, supports a 1 % mass fraction of Pt-Rh that adheres to the support based on an ultrasonic stress test.[141]

Bimetallic Ni-Pt/$La_{0.2}Zr_{0.4}Ce_{0.4}O_x$ partially oxidizes methane in a microchannel reactor containing ten corrugated FeCrAl foil plates. The efficiency of this reactor type is proportional to the number of plates, as both CH_4 conversion and CO selectivity remain constant. All the methane combusts at the inlet and corrodes the plate; complete oxidation in these zones suggests that the oxide layer cracks and exposes Fe. Despite the corrosion, after 40 h on-stream at 840 °C hydrogen yield only dropped by 10 %.[270] Preoxidized FeCrAl fibers supporting Ni-$CeAlO_3$-Al_2O_3 synthesized via hydrothermal growth of LDHs achieving CH_4 conversion higher than 85 % while reacting at 700 °C. Decomposition of NiAl-LDHs stabilizes Ni nanoparticle for more than 350 h on stream, while the presence of $CeAl_2O_3{-}CeO_2$ minimizes carbon.[271]

5.3 DMR—Dry methane reforming

In DMR methane and carbon dioxied react to form carbon monoxide and hydrgen: $CH_4 + CO_2 \rightleftharpoons 2CO + 2H_2$ (ΔH_R=247 kJ mol^{-1}). The high concentration of carbon favors coke and the reaction rate to coke increases with increasing pressure, particularly above 10 bar, which is required to achieve attractive process economics.[272] Even if Pt and Ru are more active and resist coke better, the low cost of base metals like Ni are preferred industrially.[258,273,274] Cold spots (rather than hot spots), reduce conversion and promote coke, while

a highly conductive, permeable 3-D metal support minimizes thermal gradients.[275–277] 3-Aminopropyltriethoxysilane facilitates creating a macro-meso-nano scale structure in a single step, starting from a fiber felt. The resulting Ni on SiO_2/Al_2O_3/FeCrAl contains cross links that are active, selective, and stable even after operating 500 h at 800 °C and a gas hourly space velocity of $5\,L\,g^{-1}\,h^{-1}$.[278]

At these conditions, another promising FeCrAl-fiber-structured nanocomposite, NiO-MgO-Al_2O_3, maintained CH_4 conversion constant at 90 % during the initial 90 h, but decreased to 10 % over the following 180 h.[88] Among the various Ni/SBA-15 catalysts synthesized via wet impregnation and waschoated on FeCrAl monolith, the ones with a Ni loading of 8 % was active and stable at 800 °C for over 1400 h time on stream. The hexagonal mesoporous structure of SBA-15, which minimizes coke formation, together with the benefits coming from the higher thermal conductivity of the support enhance the performance.[279,280]

A laboratory-scale tubular reactor, consisting of two coaxial monolith cylinders, combines two reactions: the heat produced by the catalytic combustion of CH_4 over $LaFe_{0.5}Mg_{0.5}O_3/Al_2O_3$/FeCrAl (inner monolith) moves to the endothermic CO_2-CH_4 reforming over Ni/SBA-15/Al_2O_3/FeCrAl. The conversion of methane and carbon dioxide exceeds 90 % while the energy efficiency reaches 82 %.[281] FeCrAl's ability to be shaped allows creative shapes to create flow paths in reactors to achieve the performance prescribed by process intensification. An electrically heated reactor with $LaNi_{0.95}Ru_{0.05}O_3$ catalyzed CH_4 conversion; conversion increased with temperature but plateaued at 900 °C.[282]

5.4 ATR—Autothermal reforming

While SMR is strongly endothermic and CPOX is mildly exothermic, oxygen is co-fed together with steam so that the ATR operates isothermally and absent of a external heat source or cooling. Like SMR, CPOX, and DMR, ATR requires catalyst supports that operate at high temperature in the presence of H_2O and O_2 rich atmospheres. FeCrAl and traditional ceramic supports are among the few materials that meet these conditions. Methane conver-

sion reaches 88 % over a NiO-Al_2O_3/FeCrAl-fiber catalyst at a H_2/CO selectivity of 90 % at 700 °C. NiO was highly dispersed on Al_2O_3/FeCrAl-fiber prepared via incipient wetness impregnation. Overall the catalyst was stable for more than 30 h, which was 24 h more than a washcoated NiO on FeCrAl-fiber.[283] Rh particles, prepared through sorption-hydrolytic deposition, on $Ce_{0.75}Zr_{0.25}O_{2-\delta}$ mixed with alumina powder show 100 % conversion during the first 6 h on stream that afterward decreases following carbon deposition. When supported on FeCrAl, it achieved 100 % conversion for 12 h without forming coke on the surface.[284] $Ni/Ce_{0.75}Zr_{0.25}O_2$ washcoated on FeCrAl foams autothermally reform iso-octane in stainless steel and quartz microreactors. Quartz and insulated (no contact between reactor walls and catalyst support) reactors reached light off at 150 °C and 100 °C, respectively, lower than the standard assembly configurations, which demonstrates the strong effect of the heat transfer through the reactor walls.[285]

5.5 Methanol steam reforming

The advantages of methanol versus methane as a fuel to produce syngas via steam reformning $CH_3OH + H_2O \rightleftharpoons CO_2 + 3H_2$ (ΔH_R=49 kJ mol^{-1}) relates to logistics and infrastructure capital investment.[286] The major catalyst systems for this process include Cu, Pd/ZnO, Ir and Pd-Zn. A 2.5 % Pd on ZnO prepared via wet impregnation is more active than the same catalyst washcoated on FeCrAl monolith. The catalyst appeared homogeneous and adheres well to the surface, but its activity suffers because of the additional aqueous dissolution and re-precipitation process occurring during washcoating (surface area decreases). Impregnating and washcoating the monolith simultaneously with an aqueous soultion of the ZnO support, colloidal zinc oxide, and palladium nitrate overcome these drawbacks. This all-in-one strategy eliminates also the intermediate calcination step.[287] Performance of aluminum and brass supports were higher than the FeCrAl which was imputed to the formation of cracks or Fe migration that deactivates the active phase but also because of the higher thermal conductivity of the two materials. The surface Al_2O_3 coating dehydrates methanol

to dimethyl ether but none was detected during the tests with the Pd/ZnO coated FeCrAl monolith, which suggests the catalyst homogeneously covered the Al_2O_3.[288]

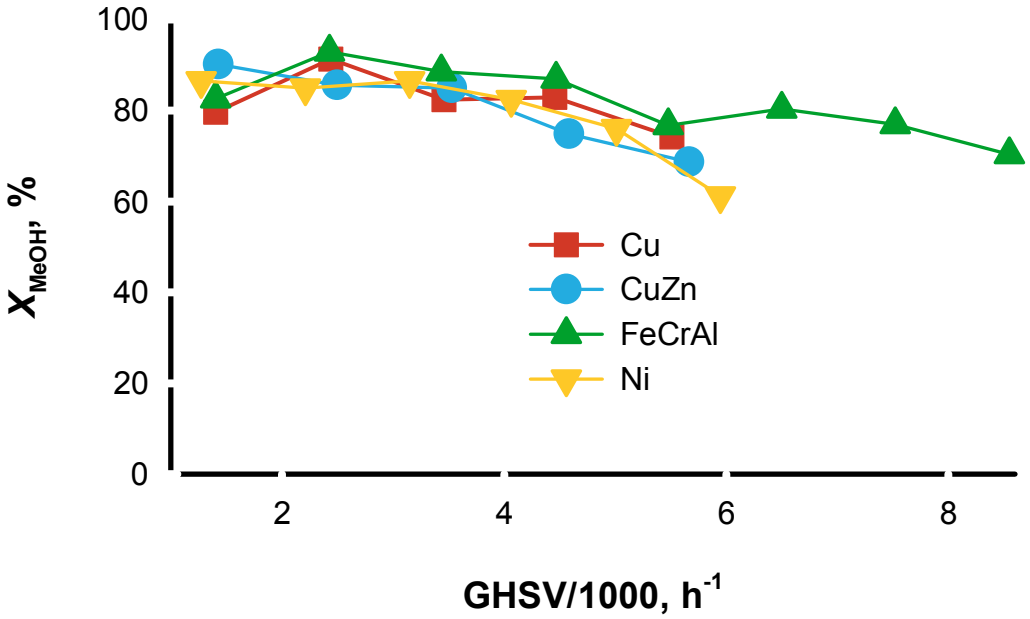

Figure 43: Methanol conversion vs of GHSV on different metal foam.[289] Copyright 2007 Elsevier.

Catalyst poisoning by metal support elements is also reported for Cu/Zn/Al/Zr active phases on foams tested in microcatalytic reformers at 600 °C (Figure 44,43). The calcination temperature during preparation was too low to form a stable and uniform superficial protective alumina coating; however, interactions between active metals and support minimize the WGS, resulting in a higher CO selectivity.[289]

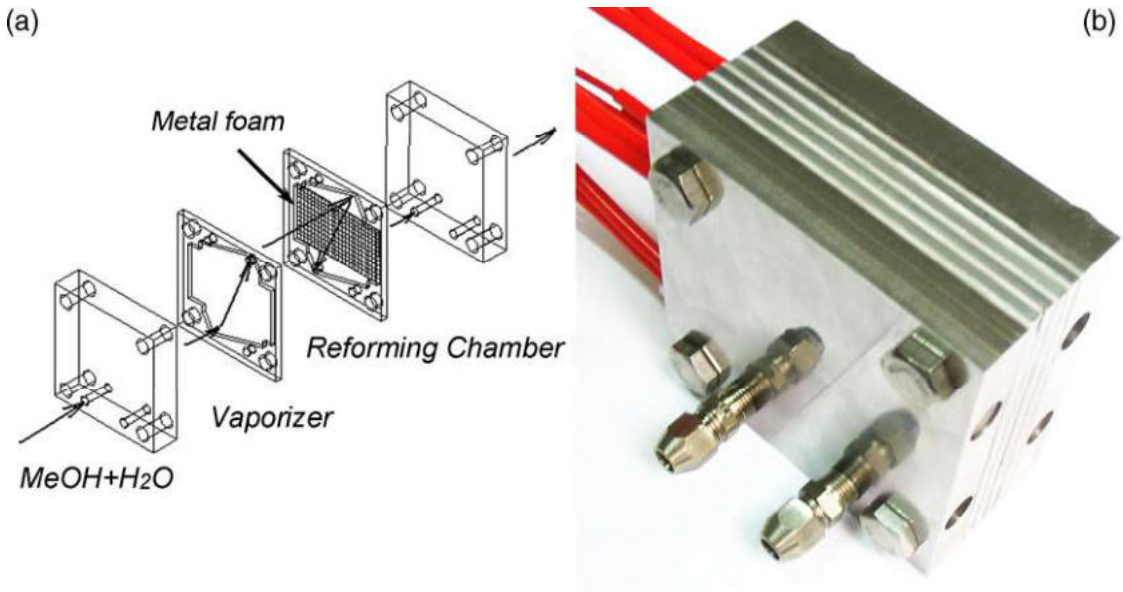

Figure 44: Reactor mechanical drawing: (a) integrated operative reactor (b).[289] Copyright 2007 Elsevier.

Pd/Zn have also activity similar to Cu/Zr.[290] Ir on Al_2O_3 or on $Ce_xZr_{1-x}O_2$ with or without Al_2O_3 are active in the production of H_2 from methanol. Washcoating with boehmite as primer for the combination of these metal oxides as superficial layers well resisted ultrasonic vibration mechanical tests; the final catalyst was active for more than 120 h.[291]

5.6 WGS—Water gas shift reaction

Hydrogen is the desired product in SMR and to increase yield carbon monoxide and water present in the syngas further reacts following the water gas shift reaction (WGS) $CO + H_2O \rightleftharpoons CO_2 + H_2$ ($\Delta H_R = -42\,kJ\,mol^{-1}$).[237] Industry applies Cu promoted Fe−Cr or Cu−Zn at 250 °C to 400 °C.[292] The interests of FeCrAl for this reaction come for the tighter temperature control combined with a lower pressure drop across the catalytic bed. The possibility of electrifying syngas synthesis introduces novel reactor designs with multiple zones and catalysts simultaneously. In this way it is possible to both reform CH_4 and shift CO in the same unit to intensify the process, decreasing capital cost and making it possible to scale down H_2 production avoiding expensive fired furnaces and decreasing the

land footprint.[239,293] Alternate layers of plasma-polymerized precursors form an active layer with Pt and zirconia. During the calcination step, catalyst detaches from the surface and the remaining fraction forms cubic phases and thus requires higher temperatures to activate the WGS.[294] 3 % Ru/TiO_2 and 6 % Ru/CeO_2-ZrO_2 supported on microchannel FeCrAl convert 78 % of the CO_2 in the revers WGS at 365 °C and a GHSV of 30 500 h^{-1}.[295]

5.7 CO PROX—CO preferential oxidation

The increasing demand of H_2 to replace fossil fuel triggers the interest in preferential CO oxidation. In the case of fuel cells for automotives, the upper CO limit, to minimize catalyst deactivation, is 5 ppm.[296] FeCrAl is suitable for this reaction as it is stable at the maximum operating temperatures (400 °C) with a minimal pressure drop. CuO-CeO_2/Al_2O_3 prepared by sol-pyrolysis adheres well to FeCrAl monolith surfaces based on ultrasonic and thermal stress tests. While in this case the catalytic activity is independent of the nature of the support (FeCrAl monolith), the interaction and distribution of the active phase depends on it.[297] Nd and Zr improve the catalytic performance in the selective oxidation of CO−H_2 mixtures. They influence CeO_2 and CuO, decreasing the oxidation of H_2 in favor of CO; the higher thermal properties of FeCrAl decrese temperature gradients limiting the reverse water gas shift reaction.[139] Pt on metal foam is also active in the selective oxidation and the results are similar to those of Pt/Al_2O_3. Fe impurities on the surface creates peculiar features that can be reproduced in the Al_2O_3 powders when Fe is added. Considering the two different materials the metallic foam was more active because of its physical properties (low porosity and low surface area) and of Fe impurities.[298] At 72 000 $cm^3\,g^{-1}\,h^{-1}$ bimetallic Pt-Co impregnated on η-Al_2O_3 on FeCrAl gauze activate CO oxidation at 140 °C, 75 % conversion was achieved at 200 °C.[299]

6 Other applications

Other than for high temperature oxidation (TWC, SMR, CPOX, CO and CH_4 oxidation) FeCrAl structured supports catalyze reactions like oxidative coupling of methane (OCM), Fischer-Tropsch (FT) or mild exothermicity as transesterification and hydrogenation. The excellent mechanical properties, the easy support functionalization, and the benefit of shaping have brought FeCrAl to these lower temperature and non-oxidative applications.' FeCrAl supports improve micro channels reactors, that Velocys® has already exploited in the design of FT production units.[300,301] The wide variety of producible geometries of FeCrAl tune mass and heat transfer increasing yield toward desired products.

6.1 OCM—Oxidative coupling of methane

An alternative to high-temperature processes based on syngas is the oxidative coupling of methane (OCM) ($2\,CH_4 + O_2 \rightleftharpoons C_2H_4 + 2H_2O$, $\Delta H_R = -165\,kJ\,mol^{-1}$).[302,303] Catalyst development stalled because of the poor yields and the research community shifted their focus towards Fischer-Tropsch, with world-scale plants built by Shell and Sasol.[304,305] Recently new studies on OCM are underway.[306]

Na_2WO_4, Mn_2O_3, and PbO catalysts on FeCrAl foil coated with Al_2O_3 and SiO_2 are candidates for the oxidative condensation of methane. SiO_2 is sensitive to calcination conditions and less stable than Al_2O_3 coating, given the chemical affinity.[307] Bulk Mn-Na_2WO_4/SiO_2 catalyst converts 12 % CH_4, this performance was matched by electrophoresis-deposition of the bulk catalyst on SiO_2/FeCrAl monolith. Structured catalyst shows 50 % lower activity compared to bulk catalyst because of the modification induced during electrophoresis deposition.[308] Placing 5 % ($g\,g^{-1}$) Na_2WO_4-2 % Mn/SiO_2 in tandem with Ce/Na_2WO_4/SBA-15/Al_2O_3 as a dual bed reactor increased conversion when a tube fed oxygen at the interface between the two beds. Optimized temperature distribution of this configuration improved C_2H_4 selectivity (2 %) compared to the powder fixed bed.[309]

Joule heated fibers convert methane to acetylene either in the absence of oxygen or at CH_4:O_2 ratios greater than 9.[310] Zirconia or alumina (on FeCrAl) together with silicon carbide catalyzed the reaction. Activation started at 600 °C producing ethane and ethylene. FeCrAl (without any active metal) reached 45 % selectivity at 1200 °C which is 7 times higher compared to the results with carborundum;[311] this is stable but do not contribute to the catalyst activity.

6.2 FT—Fischer Tropsch

Fe and Co are the active catalysts to polymerize CO to hydrocarbons ($n\mathrm{CO}+(2\,n+1)\mathrm{H_2} \longrightarrow \mathrm{C}_n\mathrm{H}_{2n+2} + n\mathrm{H_2O},\ \Delta\mathrm{H_R} = -165\,\mathrm{kJ\,mol^{-1}}$) in the range 200 °C to 350 °C and 10 bar to 25 bar.[312] Slurry reactor technology has displaced Sasol's synthol reactors because of their higher productivity and yield. Recent work, on the other hand, has explored fixed bed reactors with inserts to increase the thermal heat transfer to remove the high amount of heat released during the reaction.[313] FeCrAl and microfibrous structures increase heat transfer from the centre of the bed towards the walls. A new type of engineered catalyst based on multilayer thin film of Al_2O_3 and carbon nanotube arrays over FeCrAl foam showed noteworthy catalytic performance in an associated microchannel reactor (Figure 45). This catalyst enhanced Fischer-Tropsch (FT) synthesis activity by a factor of 4 compared to a catalyst structure without the carbon nanotube arrays. Because of the superior thermal conductivity, carbon nanotubes enhance the heat removal from catalytic active sites during the highly exothermic reaction, the reactor operates at 265 °C without runaway phenomena.[314]

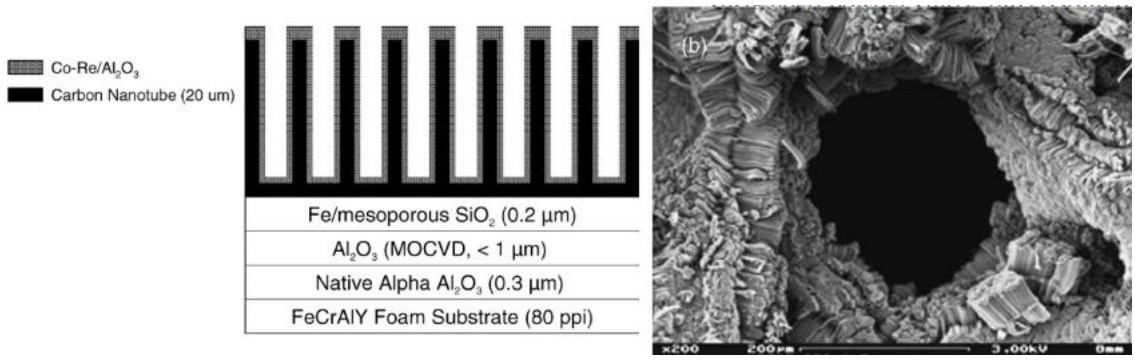

Figure 45: Schematic of engineered catalyst based on multilayer carbon nanotube arrays for Fischer-Tropsch synthesis in a microchannel reactor (left). Micrograph of the prepared foam (right).[314] Copyright 2005 Elsevier.

Activity and selectivity with 20 % ($g\,g^{-1}$) Co/γ-Al_2O_3 catalyst washcoated on monolith operating at 250 °C, 10 bar and H_2/CO=2 were the same as the powder sample.[315] Washcoated Co-Re/Al_2O_3 on monolith catalyzed the FT reaction at 20 bar and 220 °C. Higher average catalyst layer thickness resulted in higher CH_4 and lower C^{5+} selectivities; the local heat removal capacity decreases as the heat transfer in the porous ceramic layer decreases. Overall reactor thermal conductivity, both on a micro and macro scale, must be tuned to remove the heat from the active sites (via coating layer) and to transfer it through the reactor wall (via metal support). In the case of foams, the thermal properties are proportional to cell density and tuning this parameter together with the catalyst activity plays an important role in the reaction yield.[316]

6.3 Biodiesel

Heterogeneous catalysts for biodiesel synthesis and post-treatment potentially decrease operating cost and waste; however, the main challenge is slow mass transfer of the bulky triglycerides and leaching. Anchoring the catalytic active phase on a structured support with tunable pores size addresses both mass transfer and leaching. Ca/Ce oxides on FeCrAl monoliths activate the transesterification of sunflower oil to biodiesel. Metal citrated as precursors and isopropanol as solvent produced the most active catalyst.[317] Transesterifica-

tion with 2 % Mg-Al HT compounds on a similar support reached 62 % to 77 % triglyceride conversion after 10 h in a monolithic stirred reactor at 60 °C. The main challenges for the washcoating are the low surface area coming form the low porosity, and adhesion. Reyero et al. found that a binder is essential to limit the leaching of the active phase: the mass loss of catalyst prepared with a $0.05\,\mathrm{g\,g^{-1}}$ to $0.10\,\mathrm{g\,g^{-1}}$ methanol washcoating slurry was only 4 % after a 30 min ultrasonic stress test.[318] FeCrAl catalyst have yet to achieve commercial activity for biodiesel where commercial technologies convert 95 % of the triglycerides after 2 h. Often, biodiesel derived from unsaturated triglycerides is unstable to oxidation; a mild hydrogenation of the double bonds increases its stability and FeCrAl can be adopted also as a support for hydrogenation catalysts. FeCrAl monolith washcoated with Pd/Al_2O_3 partially hydrogenated sunflower oil at 100 °C and 4 bar. Compared to powder catalysts, the structured ones had lower selectivity to trans-isomers, while the equivalent ceramic monoliths were stable, FeCrAl based catalyst lost 10 % in activity after 3 reaction cycles, because of the active phase leached.[319] Multiple FeCrAl oxidation steps formed Al_2O_3 whiskers (Figure 46); the advantage of this micro structure support is the improved mass transfer and reduced catalyst pore mouth blocking.[320]

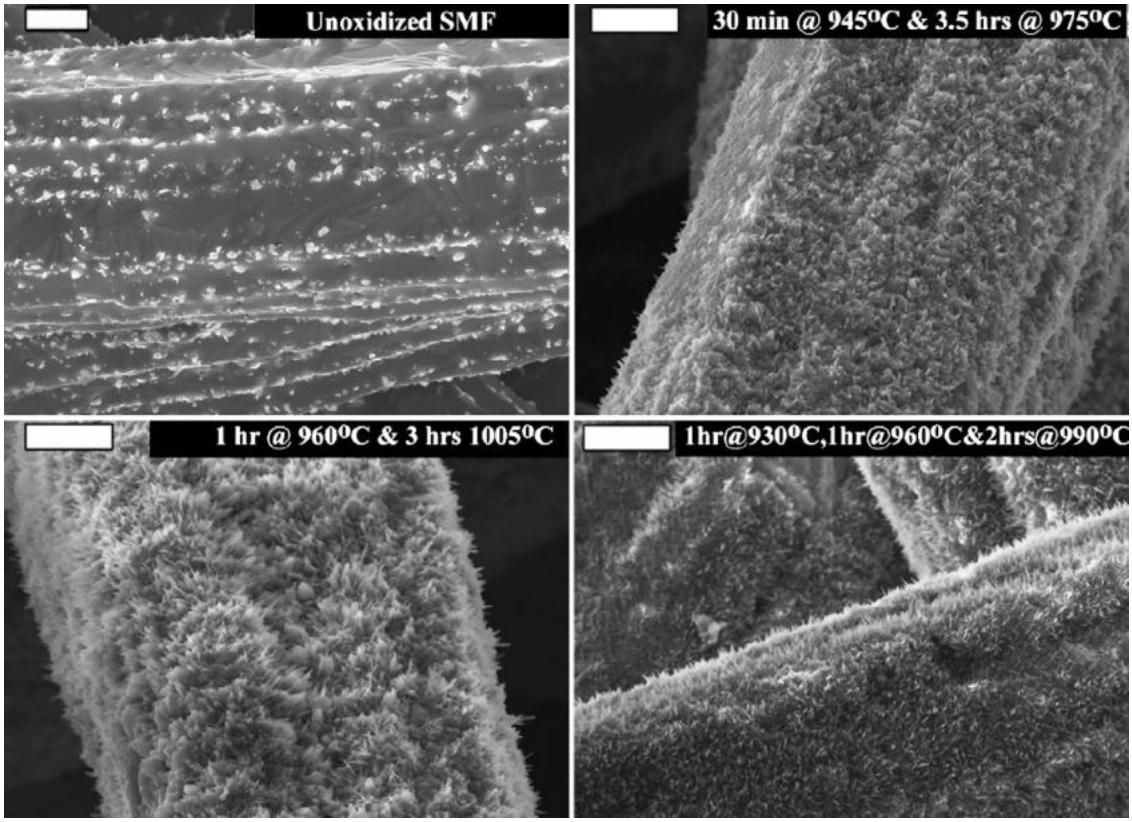

Figure 46: SEM micrograph of sintered micro fibers oxidized at various temperatures.[320] Copyright 2011 Elsevier.

6.4 Miscellaneous

$Cr/SBA\text{-}15/Al_2O_3$ on a FeCrAl monolith oxidatively dehydrogenated ethane with CO_2 for over 1130 h. Ethane conversion and ethylene selectivity were respectively 66.5 % and 99.5 % at 750 °C with a 5 % Cr loading. Cr^{6+} species were the most likely reason the activity was so high.[321] Well adhered catalytic films of zeolites (ZSM-5 and Y) and alumina pre-impregnated with 1 % Pt on metal fibers cracked n-heptane and dehydrogenated methylcyclohexane, respectivel. Yield was comparable to traditional pellet and powder catalyst but these coated structure improved temperature distribution and mass transfer.

Rh in microchannel reactors is active to produce alcohols and C_{2+} oxygenates from biomass-derived syngas. CH_4 formation is suppressed at low temperature, high pressure and low H_2/CO ratio. A hybrid catalyst of CuZnAl and $Rh\text{-}Mn/SiO_2$ showed increasing

activity after redox cycles. Rh-Mn/SiO_2 coated on FeCrAl doubles the catalyst activity considering the moles of CO converted.[322]

Mo and W oxides coated FeCrAl for the thiophene hydrodesulfuration reaction at 400 °C and 1 atm. The slurry of Mo implied higher catalytic activity than the W slurry. Oxidizing atmosphere or concentration of electrolytic solution, long time and high temperature treatment fostered the roughness of the coated layer. In addition to fixing the catalyst, the oxidizing layer contributes to the thiophene conversion.[323]

Gas phase propylene epoxidation on gold catalysts exhibits high selectivity. However, propylene conversion was low and the catalyst deactivated rapidly. These issues led to the design of new microchannel reactors, allowing catalyst regeneration thanks to a fast electric heating. Exploiting FeCrAl resistance, Au/TiO_2 dip-coated on alloy served as catalyst for the reaction.[324] Application of FeCrAl materials has also been reported in the methanation of CO as this metal fibers and monolith offer additional benefits like higher thermal conductivity and mechanical resistance compared to other ceramic supports.[325–327] Washcoating a FeCrAl monolith after preoxidation at 900 °C with RuO_2/Al_2O_3 produced a more active structure compared to the primary particles. The preparation of the slurry and the calcination of the structured catalyst after washcoating modified the active phase. Conversion was higher than 93 °C and the optimal temperature of the metal supported catalyst was shifted to a lower temperature compared to RuO_2/Al_2O_3.[325]

7 Future applications

One of the most promising applications of FeCrAl supported catalysts is the possibility of exploiting the electrical resistance of the support.[328,329] This will make it possible to switch from fuel combustion as a heat source to renewable electricity in the chemical industry.[330] Only recently SMR electrification has been reported in the scientific literature,[239,331] while a similar technology has been reported in the patent literature.[293] The high mass and heat

transferring properties of FeCrAl structures, combined with the in-situ generation of heat, would reduce land and carbon footprint of the chemical industry. The remaining problems limiting these applications are:

- unsatisfactory stability and adhesion of the catalyst coatings with the bulk metal support that limits operating lifetime;
- low electrical resistance of the macroscopic structure given the considerable cross section that requires prohibitive currents at low potential to achieve required wattage per volume.

Different high resistivity and high temperature materials such as SiC and tungsten could also be used but in this case their ceramic-behaving mechanical properties limit their application and transformation into macroscopic structures.[332] Achieving a more environmentally friendly chemical industry through electrification will require tighter collaboration between chemical engineering, catalysis, surface science, metallurgy and electrical engineering

8 Conclusions

FeCrAl as a catalytic support has a tremendous potential for energetic reactions operating in challenging environments not only because of its exceptional thermal characteristics and superior mechanical properties but also because it is flexible and can be formed into many shapes. 3-D printing represents an opportunity to optimize reactor configuration and flow patterns to minimize mass transfer resistance and maximize heat transfer area; FeCrAl offers similar flexibility but with the advantage of economies of scale in the manufacturing process. Pressure drop across FeCrAl structured supports are orders of magnitude lower than in packed beds. Exploiting Joule heating in SMR minimizes reactor volume and catalyst mass and would decrease the annual world wide CO_2 emission by 1 %.[239]

Mobile micro-gas-to-liquids units that convert flared natural gas to fuel and chemicals exploit

FeCrAl features to partially oxidize methane to syngas at 1000 °C and milli-second residence times.

The potential of FeCrAl relates to it ability to operate at high temperature—Three-Way-Catalysts and syngas production, for example—but also for Fischer-Tropsch synthesis, transesterification, and hydrogenation. The bulk of the published literature is still mainly focused on the metallurgical aspects of the material and uptake in the chemical field is lagging. Austenitic FeNiCr covered with Al combines mechanical and oxidation resistance features,[333] but requires an additional step in the production process that increases further the cost of this high temperature alloy; adhesion between Al_2O_3 coating and bulk metal also requires additional improvement. FeCrAl has already been applied to more than 10 chemical processes and improved yield while reducing the physical footprint. The possibility of washcoating and even more of synthesizing in situ zeolite, hydrotalcites, bentonites and metal oxides will further enhance the application of this material in the chemical industry and in the development on new catalysts and processes.

Operating at higher temperature increases reaction rates and by controlling heat transfer and mass transfer, yield improves. Introducing structure to reactor design reduces spatial randomness and these features correspond to the principles of process intensification to reduce the equipment scale by improving efficiency while meeting the goals of sustainability.

9 Biographies

Gianluca Pauletto received his M.Sc. in Chemical and Process Engineering at University of Padua in 2016. During his studies, he had international experiences in United Kingdom, Russia, Swizerland and Germany before completing his thesis at IQS (Barcelona, Spain) on the switch of a pharmaceutical process from batch to continuous. He is currently completing his PhD working on CPOX of methane both on catalysis and demonstration plant development under the co-supervision of Prof G. S. Patience (Polytechnique of Montreal) and

Prof J. A. Lercher (Technical University of Munich) while collaborating with other research groups in Canada, Italy, Germany and United States (Prof J. Miller, Purdue University and APS Argonne).

Angelo Vaccari graduated in 1972 in Industrial Chemistry with honors at ALMA MATER STUDIORUM – University of Bologna, were he was Assistant Professor, Associated Professor, from 2002 Full Professor of Industrial Chemistry and from 2006 to 2018 Head of the Department. Awards: 1993 Italian Federation of Chemical Industries; 1996 Italian Catalysis Group; 2004 Professor HC of the Universitad del Litoral (Arg); 2010 Gold medal "P. Pino" of the Italian Industrial Division; 2011 Chemical Engineering Club; 2018 Silver Plate "G. Fauser" of the of Italian Catalysis Group. He is author of 280 papers, 275 Congress Communications and 20 Patents (16 EU or WO), with H index = 44. Active in the R&D of new catalytic processes of economic and environmental relevance, he has been Task and/or Team Leader of 7 EU Projects, Coordinator of 2 National Projects, and Team Leader of many National and International Projects in collaboration with Research Institutions or Companies. He is member of the Editorial board of Applied Clay Science and was Guest-Editor of 4 Special Issues of Applied Clay Science, 4 of Catalysis Today and of the book "Natural Conversion V", Studies in Surface Science and Catalysis, Vol. 119.

Gianpiero Groppi graduated in Chemical Engineering at Politecnico di Milano in 1989 and took a PhD in Industrial Chemistry in 1994. Since 2005 he has been full Professor of Chemical Technology at Politecnico di Milano. His main research interests are in the field of heterogeneous catalysis and chemical reaction engineering, with focus on catalysis for energy and environmental processes and on structured catalysts and reactors. He co-authored about 160 publications on ISI journals with more than 5600 citations (H-Index=45). He is co-inventor of 9 international patents. He has been a member of the organizing committee of scientific committee of the International Conference on Structured Catalysts and Reactors

(ICOSCAR) since 2013. From 2003 to 2009 he was a member of the Editorial Board of Catalysis Today.

Lauriane Bricaud is a student in Ecole des Mines de Saint Etienne, France. She will graduate from both engineering and master degree in February 2020. Her major is chemical engineering. She completed an internship in Polytechnique Montreal in summer 2018 working on catalysts, under the supervision of G. Pauletto and Prof G. S. Patience. She spent 2019 Spring semester in NCTU (Taiwan), to study about energy conversion and storage. In september 2019, she started an second internship in the Energy Systems Engineering Lab of KAIST, South Korea. She is currently studying the transformation process of CO2 into formic acid, including the economical and environnemental analysis.

Patricia Benito received her MsC and PhD in Chemistry at the University of Salamanca (Spain) and after that she moved to the University of Bologna (Italy) where she is currently Associate Professor of Industrial Chemistry. She is co-author of more than 75 articles (hindex = 23). Her research interest focus on gas and liquid phase catalytic processes for the conversion of fossil and biomass feedstocks and CO_2. In particular, she has consolidated expertise in structured catalysts based on FeCrAl open-cell metallic foams prepared by electrodeposition.

Daria C. Boffito is Assistant Professor in Chemical Engineering at Polytechnique Montréal since 2016, whereby she is the head of the Process Intensification and Heterogenous Catalysis (EPIC) research group. She holds the Canada Research Chair in Intensified Mechano-Chemical Processes for Sustainable Biomass Conversion. She received Canadian and International prizes, including the NSERC Banting post-doctoral fellowship, the PBEEE FRQNT scholarship, GreenTalents2012 (German govt.), and The Australia Awards Endeavour Research Fellowship (2011, Australian govt.). She completed a PhD in Industrial Chemistry at the University of Milan in 2013 . Besides biomass conversion, her research interests include

sonochemistry, heterogeneous catalyst design, photocatalysis, drug delivery, and water treatment. Prof. Boffito is also active in the field of scientific communication. She co-authored one book on how to redact scientific papers, posters and presentations. Prof. Boffito collaborates with Canadian companies in the field of oil and gas, material synthesis and biomass conversion.

Johannes Lercher is Professor of Chemistry and member of the Catalysis Research Institute at the Technische Universität München as well as Director of the Institute for Integrated Catalysis at the Pacific Northwest National Laboratory, Richland, USA. During 1993-1998 he was Professor of Chemical Technology at the University of Twente, Netherlands. In 1998 he was appointed as Professor of Chemistry at the Technische Universität München. Since 2011 he is also the Director of the Institute of Integrated Catalysis and Battelle Fellow at the Pacific Northwest National Laboratory. Johannes Lercher is Editor-in-Chief of the Journal of Catalysis, the premier journal in the field of catalysis, and is member of the Editorial board of several catalysis journals. He has served as President of the International Zeolite Association (2001 - 2004) and as President of the European Federation of Catalysis Societies (2013 - 2017). In 2015, he was elected to the European Academy of Sciences, 2017 to US National Academy of Engineering, and 2019 to the US National Academy of Inventors. Prof. Lercher's research addresses fundamental aspects of catalysts and catalyzed reactions that enable catalysis to lower the carbon footprint via radically new approaches to synthesize energy carriers and chemical intermediates.

Gregory Patience holds a Canada Research Chair in high temperature, high pressure heterogeneous catalysis and is professor of Chemical Engineering at Polytechnique Montreal. He published two books – Experimental Methods and Instrumentation for Chemical Engineers and Communicate Science Papers, Presentations and Poster Effectively – filed 14 patents and published 160 scientific articles. Together with process development, his research fo-

cuses on catalysis and gas-solids fluidization applied to biodiesel from waste fat and oils, (2) producing carboxylic acid from glucose, xylose and lignin, (3) converting waste natural gas to Fischer- Tropsch fuels, (4) deriving value added chemicals from glycerol, and (5) synthesizing carbon coated $LiFePO_4$ for batteries. Prof. Patience started his career at DuPont in 1990 after completing his PhD at Polytechnique Montreal. He helped develop fluidized bed catalyst in Delaware and joined the commercial team in 1996 in Asturias, Spain. In 2000, he moved to Lycra® and managed the Fibres Technology Laboratory in Geneva and was the Technology lead for new business development.

10 Acknowledgments

This research was undertaken, in part, thanks to funding from the Canada Research Chairs Program and Canada Foundation for Innovation. We gratefully acknowledge Prof Stefano Trasatti, University of Milan, for the helpful discussion on high temperature stability. We express special thanks to Mathilde Medil, Seda Yilmaz and Marco Giuseppe Pauletto for their participation in the preparation of the graphic material.

11 Abbreviations

ψ	elemental stoichiometric coefficient
σ_{B}	Stefan-Boltzmann constant
τ	tortuosity
ε	void fraction
b	constant varies from 0.63 to 0.65
C_{r}	constant equal to 2.65
d_{c}	foam cell diameter

d_{f}	diameter fiber
$d_{\mathrm{s,av}}$	average strut diameter
d_{h}	hydraulic diameter
d_{sauter}	Sauter mean diameter
E_{r}	Rosseland extinction coefficient
h	heat transfer rate coefficient
K_{r}	constant equal to 16.67, 14.5 or 8
K_{r}	radial dispersion coefficient
$k_{\mathrm{eff,ax}}$	axial effective conductivity
$k_{\mathrm{eff,cond}}$	effective conduction
$k_{\mathrm{eff,conv}}$	effective convection
$k_{\mathrm{eff,rad}}$	effective radiation
k_{eff}	effective conductivity
k_{g}	intrinsic gas conductivity
k_{m}	mass transfer rate coefficient
k_{parallel}	in-series conductivity
k_{s}	intrinsic solid conductivity
k_{serial}	in-parallel conductivity
N_{Nu}	Nusselt number
N_{Pe}	Peclet number
N_{Pr}	Prandtl number
N_{Re}	Reynolds number
N_{Sc}	Schmidt number
N_{Sh}	Sherwood number

S_{V}	surface to volume ratio
s_{A}	specific surface area
T	temperature
x	characteristic length
z	axial coordinate
A	air
ATR	auto-thermal reforming
BET	Brunauer–Emmett–Teller surface area
C	carbon
CFD	computational fluid dynamics
CPOX	catalytic partial oxidation
DC	direct current
DMR	dry methane reforming
EDS	energy dispersive X-ray spectroscopy
F	flow
F	fuel
FT	Fisher Tropsch
GHSV	gas hourly space velocity
GTL	gas-to-liquid
HA	hexaaluminate
HT	hydrotalcite-type
KIER	Korea Institute of Energy Research
LDHs	layered double hydroxides
NSR	NOx storage-reduction

OCM	Oxidative coupling of methane
PI	process intensification
PROX	preferential CO oxidation
PVA	polyvinyl alcohol
RF	radio frequency
S	steam
SCE	saturated calomel electrode
SCR	selective catalytic reduction
SCS	solution combustion synthesis
SEM	scanning electron microscope
SMR	steam methane reforming
TEM	transmission electron microscope
TWC	three way catalysts
VOC	volatile organic compounds
W	weight
WGS	water gas shift
WHSV	weight hourly space velocity
XPS	X-ray photoelectron spectroscopy
XRD	X-ray diffraction

References

(1) C. Boffito, D.; Van Gerven, T. *Process Intensification and Catalysis*; 2018.

(2) Toulhoat, H. *Heterogeneous Catalysis: Use of Density Functional Theory*; 2010; pp 1–7.

(3) T. Mika, L.; Cséfalvay, E.; Nemeth, A. Catalytic Conversion of Carbohydrates to

Initial Platform Chemicals: Chemistry and Sustainability. *Chem. Rev.* **2017**, *118*, 505–613.

(4) Sudarsanam, P.; Zhong, R.; Van den Bosch, S.; Coman, S.; I Parvulescu, V.; Sels, B. Functionalised Heterogeneous Catalysts for Sustainable Biomass Valorisation. *Chem. Soc. Rev.* **2018**, *47*, 8349–8402.

(5) Descorme, C.; Gallezot, P.; Geantet, C.; George, C. Heterogeneous Catalysis: a Key Tool toward Sustainability. *ChemCatChem* **2012**, *4*, 1897–1906.

(6) Jaber, M.; Mahboub, D.; Wright, J.; Bo, D. C.; Dubois, J.-l.; Patience, G. S. Cs , V , Cu Keggin-type Catalysts Partially Oxidize 2-methyl-1, 3-propanediol to Methacrylic Acid. *Appl. Catal. A* **2018**, *554*, 105–116.

(7) Lotfi, S.; Boffito, D. C.; Patience, G. S. Gas-Phase Partial Oxidation of Lignin to Carboxylic Acids over Vanadium Pyrophosphate and Aluminum – Vanadium – Molybdenum. *ChemSusChem* **2015**, *8*, 3424–3432.

(8) García-Bordejé, E.; Liu, Y.; Su, D. S.; Pham-Huu, C. Hierarchically Structured Reactors Containing Nanocarbons for Intensification of Chemical Reactions. *J. Mater. Chem. A* **2017**, *5*, 22408–22441.

(9) Davis, M. Ordered Porous Materials for Emerging Applications. *Nature* **2002**, *417*, 813–821.

(10) Perego, C.; Millini, R. Porous Materials in Catalysis: Challenges for Mesoporous Materials. *Chem. Soc. Rev.* **2012**, *42*, 3956–3976.

(11) Gascon, J.; van Ommen, J. R.; Moulijn, J. A.; Kapteijn, F. Structuring Catalyst and Reactor – an Inviting Avenue to Process Intensification. *Catal. Sci. Technol.* **2015**, *5*, 807–817.

(12) Van Gerven, T.; Stankiewicz, A. Structure, Energy, Synergy, Time-The Fundamentals of Process Intensification. *Ind. Eng. Chem. Res.* **2009**, *48*, 2465–2474.

(13) Forzatti, P.; Groppi, G.; Cristiani, C. *Handbook of Heterogeneous Catalysis*; 2008; Chapter 11.6, pp 2411–2426.

(14) Weng, J.; Lu, X.; Gao, P.-X. Nano-Array Integrated Structured Catalysts: A New Paradigm upon Conventional Wash-Coated Monolithic Catalysts? *Catalysts* **2017**, *7*, 253–280.

(15) Cairns, J. A.; Nelson, R. S.; Acres, G. K. The Evolution of Fecralloy® Steel-based Catalysts. *Int. J. Mater. Eng. Applicat.* **1979**, *1*, 162–166.

(16) Namkung, J.; C Kim, M.; W Park, W. Fabrication of Fe–Cr–Al Base Alloy Strips by Melt Dragging and their Oxidation Resistance at Elevated Temperature. *J. Mater. Process. Technol.* **2001**, *115*, 391–395.

(17) Koo, B. U.; Yi, Y.; Lee, M.; Kim, B. K. Effects of Particle Size and Forming Pressure on Pore Properties of Fe-Cr-Al Porous Metal by Pressureless Sintering. *Met. Mater. Int.* **2017**, *23*, 336–340.

(18) Zhang, D. The Ductility Below the Ductile-to-brittle Transition Temperature of the FeCrAlloy. *J. Alloys Compd.* **2009**, *479*, 47–49.

(19) Giani, L.; Groppi, G.; Tronconi, E. Heat Transfer Characterization of Metallic Foams. *Ind. Eng. Chem. Res.* **2005**, *44*, 9078–9085.

(20) Bianchi, E.; Heidig, T.; Visconti, C. G.; Groppi, G.; Freund, H.; Tronconi, E. An Appraisal of the Heat Transfer properties of Metallic Open-cell Foams for Strongly Exo-/endo-thermic Catalytic Processes in Tubular Reactors. *Chem. Eng. J.* **2012**, *198–199*, 512–528.

(21) Bianchi, E.; Heidig, T.; Visconti, C. G.; Groppi, G.; Freund, H.; Tronconi, E. Heat Transfer Properties of Metal Foam Supports for Structured Catalysts: Wall Heat Transfer Coefficient. *Catal. Today* **2013**, *216*, 121–134.

(22) Aghaei, P.; Visconti, C. G.; Groppi, G.; Tronconi, E. Development of a heat Transport Model for Open-cell Metal Foams with High Cell Densities. *Chem. Eng. J.* **2017**, *321*, 432–446.

(23) Lofberg, A.; Essakhi, A.; Paul, S.; Swesi, Y.; Zanota, M. L.; Meille, V.; Pitault, I.; Supiot, P.; Mutel, B.; Le Courtois, V.; et al., Use of Catalytic Oxidation and Dehydrogenation of Hydrocarbons Reactions to Highlight Improvement of Heat Transfer in Catalytic Metallic Foams. *Chem. Eng. J.* **2011**, *176-177*, 49–56.

(24) Caplovicova, M.; Caplovic, L.; Buc, D.; Vinduska, P.; Janik, J. Carbon Nanostructures Grown on Fe-Cr-Al alloy. *J. Electr. Eng.* **2010**, *61*, 373–377.

(25) Altin, O.; Eser, S. Analysis of Carboneceous Deposits from Thermal Stressing of a JP-8 Fuel on Superalloy Foils in a Flow Reactor. *Ind. Eng. Chem. Res.* **2001**, *40*, 589–595.

(26) Bauman, Y.; Vedyagin, A.; Mishakov, I. Carbon Erosion of FeCrAl Bulk Alloy by Chlorinated Hydrocarbons. *Prot. Met. Phys. Chem. Surf.* **2016**, *52*, 309–315.

(27) Coke Formation and Metal Dusting of Electroplated Ni_3Al-CeO_2-based Coatings in CO-H_2-H_2O. *Corros. Sci.* **2007**, *49*, 4134–4153.

(28) Chesnokov, V. V.; Buyanov, R. A. The Formation of Carbon Filaments upon Decomposition of Hydrocarbons Catalysed by Iron Subgroup Metals and their Alloys. *Russ. Chem. Rev.* **2000**, *69*, 623–638.

(29) Borisov, V. A.; Sigaeva, S. S.; Tsyrul'nikov, P. G.; Trenikhin, M. V.; Leont'eva, N. N.;

Slepterev, A. A.; Kan, V. E.; Biryukov, M. Y. Carbon Deposits on a Resistive FeCrAl Catalyst for the Suboxidative Pyrolysis of Methane. *Kinet. Catal.* **2014**, *55*, 319–326.

(30) Longson, T.; Maddocks, J.; Kashani, A. Morphological Impact on Thermal Interface Resistance of Self Catalyzing Fecralloy MWNT TIMs. 2015.

(31) Liu, H.; Chen, W. Carburization Behavior of Electrodeposited Ni_3Al-CeO_2-base Coatings on Fe-Ni-Cr Alloys. *Oxid. Met.* **2007**, *67*, 129–152.

(32) Frías, D. M.; Nousir, S.; Barrio, I.; Montes, M.; Martínez T, L. M.; Centeno, M. A.; Odriozola, J. A. Nucleation and Growth of Manganese Oxides on Metallic Surfaces as a Tool to Prepare Metallic Monoliths. *Appl. Catal. A* **2007**, *325*, 205–212.

(33) Vázquez-Gómez, L.; Cattarin, S.; Comisso, N.; Guerriero, P.; Musiani, M.; Verlato, E. Spontaneous Deposition of Pd onto Fe-Cr-Al Alloys. *Electrochim. Acta* **2012**, *68*, 114–122.

(34) Cao, X.; Vassen, R.; Stoever, D. Ceramic Materials for Thermal Barrier Coatings. *J. Eur. Ceram. Soc.* **2004**, *24*, 1–10.

(35) Jönsson, B.; Berglund, R.; Magnusson, J.; Henning, P.; Hättestrand, M. High Temperature Properties of a New Powder Metallurgical FeCrAl Alloy. *Mater. Sci. Forum* **2004**, *464*, 455–462.

(36) Czyrska-Filemonowicz, A.; Clemens, D.; Quadakkers, W. The Effect of High Temperature Exposure on the Structure and Oxidation Behaviour of Mechanically Alloyed Ferritic ODS Alloys. *J. Mater. Process. Technol.* **1995**, *53*, 93–100.

(37) Jönsson, B.; Lu, Q.; Chandrasekaran, D.; Berglund, R.; Rave, F. Oxidation and Creep Limited Lifetime of Kanthal APMT®, a Dispersion Strengthened FeCrAlMo Alloy Designed for Strength and Oxidation Resistance at High Temperatures. *Oxid. Met.* **2012**, *79*, 29–39.

(38) Analytics, C. Web of Science Core Collection, accessed on 10 October 2018, http://apps.webofknowledge.com. 2018.

(39) Ballhaus, C.; Berry, R. F.; Green, D. H. High-Pressure Experimental Calibration of the Olivine-Ortho-Pyroxene-Spinel Oxygen Geobarometer—Implications for the Oxidation-State of the Upper Mantle. *Contrib. to Mineral. Petrol.* **1991**, *207*, 27–40.

(40) Pint, B. A. Experimental Observations in Support of the Dynamic-Segregation Theory to Explain the Reactive-Element Effect. *Chem. Rev.* **1996**, *45*, 1–37.

(41) McCafferty, E.; Wightman, J. P. Determination of the Concentration of Surface Hydroxyl Groups on Metal Oxide Films by a Quantitative XPS Method. *Surf. Interface Anal.* **1998**, *26*, 549–564.

(42) van Eck, N. J.; Waltman, L. Software Survey: VOSviewer, a Computer Program for Bibliometric Mapping. *Scientometrics* **2010**, *84*, 523–538.

(43) Mizuno, N.; Misono, M. Heterogeneous Catalysis. *Chem. Rev.* **1998**, *98*, 199–218.

(44) Chen, X.; Mao, S. S. Titanium Dioxide Nanomaterials: Synthesis, Properties, Modifications, and Applications. *Chem. Rev.* **2007**, *107*, 2891–2959.

(45) Paier, J.; Penschke, C.; Sauer, J. Oxygen Defects and Surface Chemistry of Ceria: Quantum Chemical Studies Compared to Experiment. *Chem. Rev.* **2013**, *113*, 3949–3985.

(46) Munnik, P.; de Jongh, P. E.; de Jong, K. P. Recent Developments in the Synthesis of Supported Catalysts. *Chem. Rev.* **2015**, *115*, 6687–6718.

(47) Montini, T.; Melchionna, M.; Monai, M.; Fornasiero, P. Fundamentals and Catalytic Applications of CeO_2-Based Materials. *Chem. Rev.* **2016**, *116*, 5987–6041.

(48) Liu, L.; Corma, A. Metal Catalysts for Heterogeneous Catalysis: From Single Atoms to Nanoclusters and Nanoparticles. *Chem. Rev.* **2018**, *118*, 4981–5079.

(49) Heck, R. M.; Gulati, S.; Farrauto, R. J. The application of Monoliths for Gas Phase Catalytic Reactions. *Chem. Eng. J.* **2001**, *82*, 149–156.

(50) Twigg, M. V.; Richardson, J. T. Fundamentals and Applications of Structured Ceramic Foam Catalysts. *Ind. Eng. Chem. Res.* **2007**, *46*, 4166–4177.

(51) Brück, R.; Diewald, R.; Hirth, P.; Kaiser, F.-W. Design Criteria for Metallic Substrates for Catalytic Converters. SAE Technical Paper. 1995.

(52) Marsh, P.; Acke, F.; Konieczny, R.; Brück, R.; Hirth, P. Application Guideline to Define a Catalyst Layout for Maximum Catalytic Efficiency. SAE Technical Paper. 2001.

(53) Christian Hulteberg. `https://www.catalysis.se`, accessed Apr.25, 2020.

(54) Groppi, G.; Tronconi, E.; Bozzano, G.; Dente, M. Experimental and Theoretical Study of Gas/solid Mass Transfer in Metallic Filters as Supports for Micro-structured Catalysts. *Chem. Eng. Sci.* **2010**, *65*, 392–397.

(55) Reichelt, E.; Heddrich, M. P.; Jahn, M.; Michaelis, A. Fiber Based Structured Materials for Catalytic Applications. *Appl. Catal. A* **2014**, *476*, 78–90.

(56) Lu, T. J.; Stone, J. A.; Ashby, M. F. Heat Transfer in Open-cell Metal Foams. *Acta Mater.* **1998**, *46*, 3619–3635.

(57) Huu, T. T.; Lacroix, M.; Huu, C. P.; Schweich, D.; Edouard, D. Towards a more Realistic Modeling of Solid Foam: Use of the Pentagonal Dodecahedron Geometry. *Chem. Eng. Sci.* **2009**, *64*, 5131–5142.

(58) Inayat, A.; Freund, H.; Zeiser, T.; Schwieger, W. Determining the Specific Surface Area of Ceramic Foams: the Tetrakaidecahedra Model Revisited. *Chem. Eng. Sci.* **2011**, *66*, 1179–1188.

(59) Gibson, L. J.; Ashby, M. F. *Cellular Solids, Structures and Properties*; Pergamon Press: Oxford, 1988; pp 915–925.

(60) Ambrosetti, M.; Bracconi, M.; Groppi, G.; Tronconi, E. Analytical Geometrical Model of Open Cell Foams with Detailed Description of Strut-node Intersection. *Chem. Ing. Tech.* **2017**, *89*, 915–925.

(61) Hawthorn, R. D. After Burner Catalysts: Effect of Heat and Mass Transfer between Gas and Catalyst Surface. *AIChE Symp. Ser.* **1974**, *70*, 428–438.

(62) Tronconi, E.; Forzatti, P. Adequacy of Lumped Parameter Models for SCR Rreactors with Monolith Structure. *AIChE J.* **1992**, *38*, 201–210.

(63) Bhattacharya, M.; Harold, M. P.; Balakotaiah, V. Mass-Transfer Coefficients in Wash-coated Monoliths. *AIChE J.* **2004**, *50*, 2939–2955.

(64) Downey, M.; Müller-Haas, K.; Park, T.; Diewald, R.; Radovanovic, R. Structured Foil Catalysts: A Road Map to Highly Effective, Compact Aftertreatment Systems. SAE Technical Paper. 2007.

(65) Richardson, J. T.; Remue, D.; Hung, J. K. Properties of Ceramic Foam Catalyst Supports: Mass and Heat Transfer. *Appl. Catal. A* **2003**, *250*, 319–329.

(66) Garrido, G. I.; Patcas, F. C.; Lang, S.; Kraushaar-Czarnetzki, B. Mass Transfer and Pressure Drop in Ceramic Foams: a Description for Different Pore Sizes and Porosities. *Chem. Eng. Sci.* **2008**, *63*, 5202–5217.

(67) Giani, L.; Groppi, G.; Tronconi, E. Mass-transfer Characterization of Metallic Foams as Supports for Structured Catalysts. *Ind. Eng. Chem. Res.* **2005**, *44*, 4993–5002.

(68) Bracconi, M.; Ambrosetti, M.; Maestri, M.; Groppi, G.; Tronconi, E. A Fundamental Investigation of Gas/solid Mass Transfer in Open-cell Foams Using a Combined Experimental and CFD Approach. *Chem. Eng. J.* **2018**, *352*, 558–571.

(69) Reichelt, E.; Jahn, M. Generalized Correlations for Mass Transfer and Pressure Drop in Fiber-based Catalyst Supports. *Chem. Eng. J.* **2017**, *325*, 655 – 664.

(70) Groppi, G.; Tronconi, E. Continuous vs. Discrete Models of Nonadiabatic Monolith Catalysts. *AIChE J.* **1996**, *42*, 2382–2387.

(71) Field, K. G.; Snead, M.; Yamamoto, Y.; Terrani, K. A. *Handbook on the Material Properties of FeCrAl Alloys for Nuclear Power Production Applications*; 2015.

(72) CHARACTERISTICS of KYOCERA FINE CERAMICS. `https://global.kyocera.com/prdct/fc/list/material/alumina/alumina.html`, accessed Apr.25, 2020.

(73) Visconti, C. G.; Groppi, G.; Tronconi, E. Accurate Prediction of the Effective Radial Conductivity of Highly Conductive Honeycomb Monoliths with Square Channels. *Chem. Eng. J.* **2013**, *223*, 224–230.

(74) Bhattacharya, A.; Calmidi, V.; Mahajan, R. Thermophysical Properties of High Porosity Metal Foams. *Int. J. Heat Mass Transf.* **2002**, *45*, 1017–1031.

(75) Edouard, D.; Huu, T. T.; Huu, C. P.; Luck, F.; Schweich, D. The Effective Thermal Properties of Solid Foam Beds: Experimental and Estimated Temperature Profiles. *Int. J. Heat Mass Transf.* **2010**, *53*, 3807–3816.

(76) Wallenstein, M.; Kind, M.; Dietrich, B. Radial Two-phase Thermal Conductivity and Wall Heat Transfer Coefficient of Ceramic Sponges–experimental Results and Correlation. *Int. J. Heat Mass Transf.* **2014**, *79*, 486–495.

(77) Bracconi, M.; Ambrosetti, M.; Maestri, M.; Groppi, G.; Tronconi, E. A Fundamental Analysis of the Influence of the Geometrical Properties on the Effective Thermal Conductivity of Open-cell Foams. *Chem. Eng. Process.* **2018**, *129*, 181–189.

(78) Lemlich, R. A Theory for the Limiting Conductivity of Polyhedral Foam at Low Density. *J. Colloid Interface Sci.* **1978**, *64*, 107–110.

(79) Calmidi, V. V.; Mahajan, R. L. Forced Convection in High Porosity Metal Foams. *J. Heat Transfer* **2000**, *122*, 557–565.

(80) Groppi, G.; Tronconi, E. Honeycomb Supports with High Thermal Conductivity for Gas/solid Chemical Processes. *Catal. Today* **2005**, *105*, 297–304.

(81) Nijhuis, T. A.; Beers, A. E. W.; Vergunst, T.; Hoek, I.; Kapteijn, F.; Moulijn, J. A. Preparation of monolithic catalysts. *Catal. Rev.* **2001**, *43*, 345–380.

(82) Avila, P.; Montes, M.; Miró, E. E. Monolithic Reactors for Environmental Applications: a Review on Preparation Technologies. *Chem. Eng. J.* **2005**, *109*, 11–36.

(83) Meille, V. Review on Methods to Deposit Catalysts on Structured Surfaces. *Appl. Catal. A* **2006**, *315*, 1–17.

(84) Mehla, S.; Das, J.; Jampaiah, D.; Periasamy, S.; Nafady, A.; Bhargava, S. K. Recent Advances in Preparation Methods for Catalytic Thin Films and Coatings. *Catal. Sci. Technol.* **2019**, *9*, 3582–3602.

(85) Gaigneaux, E., Devillers, M., Hermans, S., Jacobs, P., Martens, J., Ruiz, P., Eds. *Scientific Bases for the Preparation of Heterogeneous Catalysts*; Studies in Surface Science and Catalysis; 2010; Vol. 175; pp 25–33.

(86) Montebelli, A.; Visconti, C. G.; Groppi, G.; Tronconi, E.; Cristiani, C.; Ferreira, C.; Kohler, S. Methods for the Catalytic Activation of Metallic Structured Substrates. *Catal. Sci. Technol.* **2014**, *4*, 2846–2870.

(87) Laguna, O.; Domínguez, M.; Centeno, M.; Odriozola, J. In *New Materials for Catalytic Applications*; Parvulescu, V. I., Kemnitz, E., Eds.; 2016; pp 81–120.

(88) Chai, R.; Fan, S.; Zhang, Z.; Chen, P.; Zhao, G.; Liu, Y.; Lu, Y. Free-Standing NiO-MgO-Al_2O_3 Nanosheets Derived from Layered Double Hydroxides Grown onto FeCrAl-Fiber as Structured Catalysts for Dry Reforming of Methane. *ACS Sustain. Chem. Eng.* **2017**, *5*, 4517–4522.

(89) Oxidative Decomposition of o-dichlorobenzene over V_2O_5/TiO_2 Catalyst Washcoated onto Wire-mesh Honeycombs. *Appl. Catal. A* **2002**, *237*, 81–89.

(90) Cai, S. H.; Rashkeev, S. N.; Pantelides, S. T.; Sohlberg, K. Phase transformation mechanism between γ- and θ-alumina. *Phys. Rev. B Condens. Matter Mater. Phys.* **2003**, *67*.

(91) Martínez Tejada, L. M.; Domínguez, M. I.; Sanz, O.; Centeno, M. A.; Odriozola, J. A. Au/CeO_2 Metallic Monolith Catalysts: Influence of the Metallic Substrate. *Gold Bulletin* **2013**, *46*, 221–231.

(92) Laguna, O.; Domínguez, M.; Centeno, M.; Odriozola, J. Forced Deactivation and Postmortem Characterization of a Metallic Microchannel Reactor Employed for the Preferential Oxidation of CO (PROX). *Chem. Eng. J.* **2016**, *302*, 650–662.

(93) Kaltner, W.; Veprek-Heijman, M.; Jentys, A.; Lercher, J. A. Effect of Chromium Migration from Metallic Supports on the Activity of Diesel Exhaust Catalysts. *Appl. Catal. B* **2009**, *89*, 123–127.

(94) Rallan, C.; Al-Rubaye, R.; Garforth, A. Generation of Catalytic Films of Alumina and Zeolites on FeCralloy Rods. *Chem. Eng. Trans.* **2015**, *43*, 907–912.

(95) Rallan, C.; Garforth, A. Growth of Hierarchically Structured High-surface Area Alumina on FeCralloy® Rods. *Chin. J. Chem. Eng.* **2014**, *22*, 861–868.

(96) Tran, T. P.; Guo, Y.; Zhou, L.; Kameyama, H. Anodic Alumina Catalyst Support with High Heat-resistance for Hydrocarbon Steam Reformers. *J. Chem. Eng. Japan* **2007**, *40*, 1229–1234.

(97) Kim, D. H.; Yu, B. Y.; Cha, P. R.; Yoon, W. Y.; Byun, J. Y.; Kim, S. H. A Study on FeCrAl Foam as Effective Catalyst Support under Thermal and Mechanical Stresses. *Surf. Coat. Technol.* **2012**, *209*, 169–176.

(98) Zhang, D.; Zhang, L.; Liang, B.; Li, Y. Effect of Acid Treatment on the High-temperature Surface Oxidation Behavior of FeCrAlloy Foil Used for Methane Combustion Catalyst Support. *Ind. Eng. Chem. Res.* **2009**, *48*, 5117–5122.

(99) Wu, D.; Zhang, Y.; Li, Y. Mechanical Stability of Monolithic Catalysts: Improving Washcoat Adhesion by FeCrAl Alloy Substrate Treatment. *J. Ind. Eng. Chem.* **2017**, *56*, 175–184.

(100) Quadakkers, W. J.; Naumenko, D.; Wessel, E.; Kochubey, V. Growth Rates of Alumina Scales on Fe–Cr–Al Alloys. *Oxid. Met.* **2004**, *61*, 17–37.

(101) Chadli, H.; Retima, M.; Khenioui, Y. Kinetics of Oxidation of Fe-Cr-Al Alloy Characterization by Electrochemical Spectroscopy of Impedance in a 3% Medium NaCl. *Phys. Procedia* **2009**, *2*, 1015–1020.

(102) Nicholls, J. R.; Bennett, M. J.; Newton, R. A Life Prediction Model for the Chemical Failure of FeCrAl Alloys: Preliminary Assessment of Model Extension to Lower Temperatures. *Mater. at High Temp.* **2003**, *20*, 429–438.

(103) Reszka, K.; Morgiel, J.; Reszka, J. Structure and Properties of an Alumina/amorphous-alumina/platinum Catalytic System Deposited on FeCrAl Steel. *J. Microsc.* **2006**, *224*, 46–48.

(104) Białas, A.; Osuch, W.; Łasocha, W.; Najbar, M. The Influence of the Cr-Al Foil Texture on Morphology of Adhesive Al_2O_3 Layers in Monolithic Environmental Catalysts. *Catal. Today* **2008**, *137*, 489–492.

(105) Engkvist, J.; Canovic, S.; Liu, F.; Götlind, H.; Svensson, J. E.; Johansson, L. G.; Olsson, M.; Halvarsson, M. Oxidation of FeCrAl Foils at 500 °C to 900 °C in Dry O_2 and O_2 with 40% H_2O. *Mater. at High Temp.* **2009**, *26*, 199–210.

(106) Bennett, M. J.; Nicholls, J. R.; Simms, N. J.; Naumenko, D.; Quadakkers, W. J.; Kochubey, V.; Fordham, R.; Bachorczyk, R.; Goossens, D.; Hattendorf, H.; Smith, A. B.; Britton, D. Lifetime Extension of FeCrAl Alloys in Air: Potential Roles of an Enhanced Al-reservoir and Surface Pre-treatment. *Mater. Corros.* **2005**, *56*, 854–866.

(107) Fukuda, K.; Takao, K.; Hoshi, T.; Usui, Y.; Furukimi, O. Improvement of High Temperature Oxidation Resistance of Rare Earth Metal-added Fe-20%Cr-5%Al Alloys by Pre-annealing Treatment. *Mater. at High Temp.* **2003**, *20*, 319–326.

(108) Reszka, K.; Szczypiński, M.; Pomorska, M. Influence of Substrate Local Heating on Morphology of Al and Al_2O_3 Nanofilms. *Acta Phys. Pol.* **2011**, *120*, 177–180.

(109) Reszka, K.; Rakoczy, J.; Zurek, Z.; Czyzniewski, A.; Gilewicz, A.; Homa, M. Catalytic Properties of Al_2O_3 Deposited by Ion Sputtering Using DC and RF Sources. *Vacuum* **2005**, *78*, 149–155.

(110) Wu, X.; Weng, D.; Zhao, S.; Chen, W. Influence of an Aluminized Intermediate Layer on the Adhesion of a γ-Al_2O_3 Washcoat on FeCrAl. *Surf. Coat. Technol.* **2005**, *190*, 434–439.

(111) Li, J.; Lu, X.; Wu, F.; Qin, S.; You, Z. Metallic-substrate-supported Manganese Oxide as Joule-heat-ignition Catalytic Reactor for Removal of Carbon Monoxide and Toluene in Air. *Chem. Eng. J.* **2017**, *328*, 1058–1065.

(112) Li, J.; Lu, X.; Wu, F.; Cheng, W.; Zhang, W.; Qin, S.; Wang, Z.; You, Z. Electroplated Palladium Catalysts on FeCrAlloy for Joule-Heat-Ignited Catalytic Elimination of Ethylene in Air. *Ind. Eng. Chem. Res.* **2017**, *56*, 12520–12528.

(113) Valentini, M.; Groppi, G.; Cristiani, C.; Levi, M.; Tronconi, E.; Forzatti, P. The Deposition of γ-Al_2O_3 Layers on Ceramic and Metallic Supports for the Preparation of Structured Catalysts. *Catal. Today* **2001**, *69*, 307–314.

(114) Zhao, S.; Zhang, J.; Weng, D.; Wu, X. A Method to Form Well-adhered γ-Al_2O_3 Layers on FeCrAl Metallic Supports. *Surf. Coat. Technol.* **2003**, *167*, 97–105.

(115) Serres, T.; Dreibine, L.; Schuurman, Y. Synthesis of Enamel-protected Catalysts for Microchannel Reactors: Application to Methane Oxidative Coupling. *Chem. Eng. J.* **2012**, *213*, 31–40.

(116) Smeacetto, F.; Chrysanthou, A.; Salvo, M.; Moskalewicz, T.; Bytner, F. D.; Ajitdoss, L.; Ferraris, M. Thermal Cycling and Ageing of a Glass-ceramic Sealant for Planar SOFCs. *Int. J. Hydrog. Energy* **2011**, *36*, 11895–11903.

(117) Wright, R. E.; Wolff, H. I. Refractory Problems in Production of Hydrogen by Pyrolisis of Natural Gas. *J. Am. Ceram. Soc.* **1948**, *31*, 31–38.

(118) Herbell, T. P.; Hull, D. R.; Garg, A. Hot Hydrogen Exposure Degradation of the Strength of Mullite. *J. Am. Ceram. Soc.* **1998**, *81*, 910–916.

(119) Domínguez, M.; Pérez, A.; Centeno, M.; Odriozola, J. Metallic structured catalysts: Influence of the Substrate on the Catalytic Activity. *Appl. Catal. A* **2014**, *478*, 45–57.

(120) Jia, J.; Zhou, J.; Zhang, J.; Yuan, Z.; Wang, S. The Influence of Preparative Parameters on the Adhesion of Alumina Washcoats Deposited on Metallic Supports. *Appl. Surf. Sci.* **2007**, *253*, 9099–9104.

(121) Wu, X.; Weng, D.; Xu, L.; Li, H. Structure and Performance of α-alumina Washcoat Deposited by Plasma Spraying. *Surf. Coat. Technol.* **2001**, *145*, 226–232.

(122) Jia, L.; Shen, M.; Wang, J. Preparation and Characterization of Dip-coated γ-alumina Based Ceramic Materials on FeCrAl Foils. *Surf. Coat. Technol.* **2007**, *201*, 7159–7165.

(123) Shen, M.-q.; Jia, L.-w.; Zhou, W.-l.; Wang, J. U. N.; Huang, Y. Influence of $Ce_{0.68}Zr_{0.32}O_2$ Solid Solution on Depositing γ-alumina Washcoat on FeCrAl Foils. *Bull. Mater. Sci.* **2006**, *29*, 73–76.

(124) Zhang, L.; Li, T.; Zhang, M.; Li, Y. Effect of Intermediate Layer on the Activity and Adhesion Stability of Metal Monolith Supported LaMn-hexaaluminate Catalyst for Methane Combustion. *J. Rare Earths* **2011**, *29*, 758–762.

(125) Fei, W.; Kuiry, S. C.; Sohn, Y.; Seal, S. Sol Gel Alumina Coating On Fe–Cr–Al–Y Fibre Media for Catalytic Converters. *Surf. Eng.* **2003**, *19*, 189–194.

(126) Ozawa, M.; Araki, K.-i. Effect of La Modification on Stability of Coating Alumina Layer on FeCrAl Alloy Substrate. *Surf. Coat. Technol.* **2015**, *271*, 80–86.

(127) Chen, D.; Zhang, L. H.; Li, H. Z.; Liu, Y. A Simple Method for Growing Hexaaluminate on the Surface of FeCrAl Alloy. *Appl. Surf. Sci.* **2014**, *301*, 280–288.

(128) Chen, D.; Zhang, L.; Liu, Y. Vertical and in-situ Growth of Hexaaluminate Embedded in Alumina Intermediate Layer with High Stability. *RSC Adv.* **2013**, *3*, 2534–2537.

(129) Yang, H. S.; Jang, D. H.; Lee, K. J. Aluminum Oxide Formation on Fecral atalyst Support by Electro-chemical Coating. *Arch. Metall. Mater.* **2015**, *60*, 1503–1506.

(130) Pérez, H.; Navarro, P.; Montes, M. Deposition of SBA-15 Layers on Fecralloy Monoliths by Washcoating. *Chem. Eng. J.* **2010**, *158*, 325–332.

(131) Bobadilla, L.; Muñoz-Murillo, A.; Laguna, O.; Centeno, M.; Odriozola, J. Does Shaping Catalysts Modify Active Phase Sites? A Comprehensive in situ FTIR Sectroscopic

Study on the Performance of a Model Ru/Al_2O_3 Catalyst for the CO Methanation. *Chem. Eng. J.* **2019**, *357*, 248–257.

(132) Pérez, H.; Navarro, P.; Montes, M. Deposition of SBA-15 Layers on Fecralloy Monoliths by Washcoating. *Chem. Eng. J.* **2010**, *158*, 325–332.

(133) Giani, L.; Cristiani, C.; Groppi, G.; Tronconi, E. Washcoating Method for Pd/γ-Al_2O_3 Deposition on Metallic Foams. *Appl. Catal. B* **2006**, *62*, 121–131.

(134) Ambrosetti, M.; Balzarotti, R.; Cristiani, C.; Groppi, G.; Tronconi, E. The Influence of the Washcoat Deposition Process on High Pore Density Open Cell Foams Activation for CO Catalytic Combustion. *Catalysts* **2018**, *8*, 510.

(135) Neagoe, C.; Boffito, D. C.; Ma, Z.; Trevisanut, C.; Patience, G. S. Pt on Fecralloy Catalyses Methane Partial Oxidation to Syngas at High Pressure. *Catal. Today* **2016**, *270*, 43–50.

(136) Specchia, S.; Ercolino, G.; Karimi, S.; Italiano, C.; Vita, A. Solution Combustion Synthesis for Preparation of Structured Catalysts: a Mini-review on Process Intensification for Energy Applications and Pollution Control. *Int. J. self Propag. high Temp. Synth.* **2017**, *26*, 166–186.

(137) Thoda, O.; Xanthopoulou, G.; Vekinis, G.; Chroneos, A. Review of Recent Studies on Solution Combustion Synthesis of Nanostructured Catalysts. *Adv. Eng. Mater.* **2018**, *20*, 1800047.

(138) Zeng, S.; Su, H.; Liu, Y.; Wang, Y.; Wang, D. CuO-CeO_2/Al_2O_3/FeCrAl Monolithic Catalysts Prepared by in situ Combustion Synthesis Method for Preferential Oxidation of Carbon Monoxide. *J. Rare Earths* **2011**, *29*, 69–73.

(139) Zeng, S. H.; Liu, Y. Nd- or Zr-modified CuO-CeO_2/Al_2O_3/FeCrAl Monolithic Cat-

alysts for Preferential Oxidation of Carbon Monoxide in Hydrogen-rich Gases. *Appl. Surf. Sci.* **2008**, *254*, 4879–4885.

(140) Specchia, S.; Galletti, C.; Specchia, V. In *Scientific Bases for the Preparation of Heterogeneous Catalysts*; Gaigneaux, E., Devillers, M., Hermans, S., Jacobs, P., Martens, J., Ruiz, P., Eds.; Stud. Surf. Sci. Catal.; 2010; Vol. 175; pp 59 – 67.

(141) Ma, Z.; Ouzilleau, P.; Trevisanut, C.; Neagoe, C.; Lotfi, S.; Boffito, D. C.; Patience, G. S. Partial Oxidation of Methane to Syngas over Pt/Rh/MgO Catalyst Supported on FeCralloy Woven Fiber. *Can. J. Chem. Eng.* **2016**, *94*, 642–649.

(142) Eleta, A.; Navarro, P.; Costa, L.; Montes, M. Deposition of Zeolitic Coatings onto Fecralloy Microchannels: Washcoating vs. in situ Growing. *Microporous and Mesoporous Mater.* **2009**, *123*, 113–122.

(143) Rebrov, E.; Mies, M.; Croon, de, M.; Schouten, J. In *Ordered porous solids : recent advances and prospects*; Valtchev, V., Mintova, S., Tsapatsis, M., Eds.; Elsevier, 2009; pp 311–334.

(144) Pérez, N. C.; Miró, E. E.; Zamaro, J. M. Cu, Ce/mordenite Coatings on FeCrAl-alloy Corrugated Foils Employed as Catalytic Microreactors for CO Oxidation. *Catal. Today* **2013**, *213*, 183–191.

(145) Rallan, C.; Alrubaye, R.; Garforth, A. Generation of Catalytic Films of Alumina and Zeolites on FeCralloy Rods. *Chem. Eng. Trans.* **2015**, *43*.

(146) Ochonska, J.; Rogulska, A.; Jodowski, P. J.; Iwaniszyn, M.; Michalik, M.; Lasocha, W.; Kolodziej, A.; Lojewska, J. Prospective Catalytic Structured Converters for NH_3-SCR of NOx from Biogas Stationary Engines: in situ Template-free Synthesis of ZSM-5 Cu Exchanged Catalysts on Steel Carriers. *Top. Catal.* **2013**, *56*, 56–61.

(147) Włoch, E.; Łukaszczyk, A.; Zurek, Z.; Sulikowski, B. Synthesis of Ferrierite Coatings on the FeCrAl Substrate. *Catal. Today* **2006**, *114*, 231–236.

(148) Zamaro, J. M.; Ulla, M. A.; Miró, E. E. ZSM5 Growth on a FeCrAl Steel Support. Coating Characteristics upon the Catalytic Behavior in the NOx SCR. *Microporous Mesoporous Mater.* **2008**, *115*, 113–122.

(149) Kryca, J.; Jodłowski, P.; Iwaniszyn, M.; Gil, B.; Sitarz, M.; Kołodziej, A.; Łojewska, T.; Łojewska, J. Cu SSZ-13 Zeolite Catalyst on Metallic Foam Support for SCR of NOx with Ammonia: Catalyst Layering and Characterisation of Active Sites. *Catal. Today* **2016**, *268*, 142–149.

(150) Kryca, J.; Iwaniszyn, M.; Piatek, M.; Jodlowski, P. J.; Jedrzejczyk, R.; Pedrys, R.; Wrobel, A.; Lojewska, J.; Kolodziej, A. Structured Foam Reactor with CuSSZ-13 Catalyst for SCR of NOx with Ammonia. *Top. Catal.* **2016**, *59*, 887–894.

(151) Chai, R.; Zhao, G.; Zhang, Z.; Chen, P.; Liu, Y.; Lu, Y. High Sintering-/coke-resistance Ni@SiO_2/Al_2O_3/FeCrAl-fiber Catalyst for Dry Reforming of Methane: One-step, Macro-to-nano Organization via Cross-linking Molecules. *Catal. Sci. Technol.* **2017**, *7*, 5500–5504.

(152) Vázquez-Gómez, L.; Cattarin, S.; Comisso, N.; Guerriero, P.; Musiani, M.; Verlato, E. Spontaneous Deposition of Pd onto Fe–Cr–Al Alloys. *Electrochim. Acta* **2012**, *68*, 114–122.

(153) Cimino, S.; Gerbasi, R.; Lisi, L.; Mancino, G.; Musiani, M.; Vázquez-Gómez, L.; Verlato, E. Oxidation of CO and CH_4 on Pd-Fecralloy Foam Catalysts Prepared by Spontaneous Deposition. *Chem. Eng. J.* **2013**, *230*, 422–431.

(154) Verlato, E.; Barison, S.; Cimino, S.; Dergal, F.; Lisi, L.; Mancino, G.; Musiani, M.; Vázquez-Gómez, L. Catalytic Partial Ooxidation of Methane over Nanosized Rh Supported on Fecralloy Foams. *Int. J. Hydrog. Energy* **2014**, *39*, 11473–11485.

(155) Cimino, S.; Gambirasi, A.; Lisi, L.; Mancino, G.; Musiani, M.; Vázquez-Gómez, L.; Verlato, E. Catalytic Combustion of Methanol on Pt-Fecralloy Foams Prepared by Electrodeposition. *Chem. Eng. J.* **2016**, *285*, 276–285.

(156) Basile, F.; Benito, P.; Bugani, S.; De Nolf, W.; Fornasari, G.; Janssens, K.; Morselli, L.; Scavetta, E.; Tonelli, D.; Vaccari, A. Combined use of Synchrotron-radiation-based Imaging Techniques for the Characterization of Structured Catalysts. *Adv. Funct. Mater.* **2010**, *20*, 4117–4126.

(157) Ho, P. H.; de Nolf, W.; Ospitali, F.; Gondolini, A.; Fornasari, G.; Scavetta, E.; Tonelli, D.; Vaccari, A.; Benito, P. Coprecipitated-like Hydrotalcite-derived Coatings on Open-cell Metallic Foams by Electrodeposition: Rh Nanoparticles on Oxide Layers Stable under Harsh Reaction Conditions. *Appl. Catal. B* **2018**, *560*, 12–20.

(158) Ho, P. H.; Ambrosetti, M.; Groppi, G.; Tronconi, E.; Jaroszewicz, J.; Ospitali, F.; Rodríguez-Castellón, E.; Fornasari, G.; Vaccari, A.; Benito, P. One-step Electrodeposition of Pd–CeO_2 on High Pore Density Foams for Environmental Catalytic Processes. *Catal. Sci. Technol.* **2018**, *8*, 4678–4689.

(159) Ho, P. H.; Monti, M.; Scavetta, E.; Tonelli, D.; Bernardi, E.; Nobili, L.; Fornasari, G.; Vaccari, A.; Benito, P. Reactions Involved in the Electrodeposition of Hydrotalcite-type Compounds on FeCrAlloy Foams and Flates. *Electrochim. Acta* **2016**, *222*, 1335–1344.

(160) Ho, P. H.; Jabłońska, M.; Palkovits, R.; Rodríguez-Castellón, E.; Ospitali, F.; Fornasari, G.; Vaccari, A.; Benito, P. N_2O Catalytic Decomposition on Electrodeposited Rh-based Open-cell Metallic Foams. *Chem. Eng. J.* **2020**, *379*, 122259.

(161) Benito, P.; Monti, M.; Bersani, I.; Basile, F.; Fornasari, G.; Scavetta, E.; Tonelli, D.; Vaccari, A. Coating of FeCrAlloy Foam with Rh Catalysts: Optimization of Elec-

trosynthesis Parameters and Ccatalyst Composition. *Catal. Today* **2012**, *197*, 162–169.

(162) Benito, P.; Monti, M.; De Nolf, W.; Nuyts, G.; Janssen, G.; Fornasari, G.; Scavetta, E.; Basile, F.; Janssens, K.; Ospitali, F.; et al., Improvement in the Coating Homogeneity in Electrosynthesized Rh Structured Catalysts for the Partial Oxidation of Methane. *Catal. Today* **2015**, *246*, 154–164.

(163) Basile, F.; Benito, P.; Fornasari, G.; Monti, M.; Scavetta, E.; Tonelli, D.; Vaccari, A. Novel Rh-based Structured Catalysts for the Catalytic Partial Oxidation of Methane. *Catal. Today* **2010**, *157*, 183 – 190.

(164) Basile, F.; Benito, P.; Fornasari, G.; Rosetti, V.; Scavetta, E.; Tonelli, D.; Vaccari, A. Electrochemical Synthesis of Novel Structured Catalysts for H_2 Production. *Appl. Catal. B* **2009**, *91*, 563–572.

(165) Benito, P.; Nuyts, G.; Monti, M.; De Nolf, W.; Fornasari, G.; Janssens, K.; Scavetta, E.; Vaccari, A. Stable Rh Particles in Hydrotalcite-derived Catalysts Coated on FeCrAlloy Foams by Electrosynthesis. *Appl. Catal. B* **2015**, *179*, 321–332.

(166) Ho, P. H.; Ambrosetti, M.; Groppi, G.; Tronconi, E.; Fornasari, G.; Vaccari, A.; Benito, P. Electrodeposition of CeO_2 and Pd-CeO_2 on Small Pore Size Metallic Foams: Selection of Deposition Parameters. *Catal. Today* **2019**, *334*, 37–47.

(167) Benito, P.; De Nolf, W.; Nuyts, G.; Monti, M.; Fornasari, G.; Basile, F.; Janssens, K.; Ospitali, F.; Scavetta, E.; Tonelli, D.; et al., Role of Coating-metallic Support Interaction in the Properties of Electrosynthesized Rh-based Structured Catalysts. *ACS Catal.* **2014**, *4*, 3779–3790.

(168) Verlato, E.; Barison, S.; Cimino, S.; Lisi, L.; Mancino, G.; Musiani, M.; Paolucci, F. Electrochemical Preparation of Nanostructured CeO_2-Pt Catalysts on Fe-Cr-Al Alloy

Foams for the Low-temperature Combustion of Methanol. *Chem. Eng. J.* **2017**, *317*, 551–560.

(169) Li, Y.; Li, Y.; Yu, Q.; Yu, L. The Catalytic Oxidation of Toluene over Pd-based FeCrAl Wire Mesh Monolithic Catalysts Prepared by Electroless Plating Method. *Catal. Commun.* **2012**, *29*, 127–131.

(170) Li, Y.; Fan, Y.; Jian, J.; Yu, L.; Cheng, G.; Zhou, J.; Sun, M. Pt-based Structured Catalysts on Metallic Supports Synthesized by Electroless Plating Deposition for Toluene Complete Oxidation. *Catal. Today* **2017**, *281*, 542–548.

(171) Lambert, C.; Theis, J.; Cavataio, G. *Chapter 16: LNT Catalysis at Ford Motor Company - A Case History*; 2018; pp 467–489.

(172) Johnson, T. Vehicular Emissions in Review. *SAE Int. J. Engines* **2016**, *9*, 1258–1275.

(173) Lee, J.; Theis, J. R.; Kyriakidou, E. A. Vehicle Emissions Trapping Materials: Successes, Challenges, and the Path Forward. *Appl. Catal. B* **2019**, *243*, 397–414.

(174) Andersen, O.; Waag, U.; Schneider, L.; Stephani, G.; Kieback, B. Novel Metallic Hollow Sphere Structures. *Adv. Eng. Mater.* **2000**, *2*, 192–195.

(175) Govender, S.; Friedrich, H. Monoliths: A Review of the Basics, Preparation Methods and Their Relevance to Oxidation. *Catalysts* **2017**, *7*, 62–91.

(176) Leone, E. A.; Rabinkin, A.; Sarna, B. Microstructure of Thin-gauge Austenitic and Ferritic Stainless Steel Joints Brazed Using Metglas Amorphous Foil. *J. Adv. Mater.* **2006**, *38*, 28–39.

(177) Qi, G.; Zhang, Y.; Chen, A.; Yu, Y. Potassium-Activated Wire Mesh: A Stable Monolithic Catalyst for Diesel Soot Combustion. *Chem. Eng. Technol.* **2017**, *40*, 50–55.

(178) Martínez T, L. M.; Domínguez, M. I.; Sanabria, N.; Hernández, W. Y.; Moreno, S.; Molina, R.; Odriozola, J. A.; Centeno, M. A. Deposition of Al-Fe Pillared Bentonites

and Gold Supported Al-Fe Pillared Bentonites on Metallic Monoliths for Catalytic Oxidation Reactions. *Appl. Catal. A* **2009**, *364*, 166–173.

(179) Centeno, M. A.; Carrizosa, I.; Odriozola, J. A. In situ Drifts Study of the SCR Reaction of NO with NH_3 in the Presence of O_2 over Lanthanide Doped V_2O_5/Al_2O_3 Catalysts. *Appl. Catal. B* **1998**, *19*, 67–73.

(180) Smirnov, M. Y.; Kalinkin, A. V.; Nazimov, D. A.; Bukhtiyarov, V. I.; Vovk, E. I.; Ozensoy, E. An XPS Study of the Interaction of Model Ba/TiO_2 and Ba/ZrO_2 NSR Catalysts with NO_2. *Journal of Structural Chemistry* **2014**, *55*, 757–763.

(181) Johnson, T.; Joshi, A. *Chapter 1: Review of deNOx Technology for Mobile Applications*; 2018; pp 1–35.

(182) Takahashi, N.; Shinjoh, H.; Suzuki, T. The New Concept 3-way Catalyst for Automotive Lean-burn Engine: NOx Storage and Reduction Catalyst. *Catal. Today* **1996**, *27*, 63–69.

(183) Centi, G.; Arena, G. E.; Perathoner, S. Nanostructured Catalysts for NOx Storage – Reduction and N_2O Decomposition. *J. Catal.* **2003**, *216*, 443–454.

(184) Fornasiero, P.; Montini, T.; Graziani, M.; Zilio, S.; Succi, M. Development of Functionalized Fe-Al-Cr Alloy Fibers as Innovative Catalytic Oxidation Devices. *Catal. Today* **2008**, *137*, 475–482.

(185) Smirnov, M. Y.; Kalinkin, A. V.; Nazimov, D. A.; Toktarev, A. V.; Bukhtiyarov, V. I. Model Sulfur-resistant NSR Catalysts: an XPS Study of the Interaction of BaO/TiO_2-ZrO_2 and Pt-BaO/TiO_2-ZrO_2 with NO_2. *Kinetics and Catalysis* **2015**, *56*, 540–548.

(186) Cooper, B. J.; Beecham, J. A Study of Platinum Group Metals in Three-Way Autocatalysts. *Platin. Met. Rev.* **2013**, 281–288.

(187) Wang, J.; Chen, H.; Hu, Z.; Yao, M.; Li, Y. A Review on the Pd-Based Three-Way Catalyst. *Catal. Rev.* **2015**, *57*, 79–144.

(188) Lukiyanchuk, I. V.; Rudnev, V. S.; Serov, M. M.; Krit, B. L.; Lukiyanchuk, G. D.; Nedozorov, P. M. Effect of Copper Coating on Fibers Made of Aluminum Alloy, Titanium, and FeCrAl Alloy on Surface Morphology and Activity in CO Oxidation. *Appl. Surf. Sci.* **2018**, *436*, 1–10.

(189) Block, M.; Clark, N.; Wayne, S.; Nine, R.; Miller, W. An Investigation into the Emissions Reduction Performance of an SCR System Over Two Years' In-Use Heavy-Duty Vehicle Operation. 2005; pp 1–25.

(190) Marklund, S.; Andersson, R.; Tysklind, M.; Rappe, C.; Egebäck, K.-E.; Björkman, E.; Grigoriadis, V. Emissions of PCDDs and PCDFs in gasoline and diesel fueled cars. *Chemosphere* **1990**, *20*, 553–561.

(191) Zhao, F.; Ji, S.; Wu, P.; Li, Z.; Li, C. Catalytic Oxidation of CO over $Cu_xCe_{1-x}O_{2-x}$/SBA-15/FeCrAl Monolithic Catalysts. *Catal. Today* **2009**, *147*, 215–219.

(192) Ochonska-Kryca, J.; Iwaniszyn, M.; Piatek, M.; Jodlowski, P. J.; Thomas, J.; Kolodziej, A.; Lojewska, J. Mass Transport and Kinetics in Structured Steel Foam Reactor with Cu-ZSM-5 Catalyst for SCR of NOx with Ammonia. *Catal. Today* **2013**, *216*, 135–141.

(193) Zamaro, J. M.; Ulla, M. A.; Miró, E. E. Growth of Mordenite on Monoliths by Secondary Synthesis. Effects of the Substrate on the Coating Structure and Catalytic Activity. *Appl. Catal. A* **2006**, *314*, 101–113.

(194) Leman, A.; Afiqah, J.; Rahman, F.; Feriyanto, D.; Zakaria, S.; Rahmad, R. Catalytic Converter Developed By Washcoat Of γ-Alumina On Nickel Oxide (Nio) Catalyst

In FeCrAl Substrate For Exhaust Emission Control: A Review. *MATEC Web Conf.* **2016**, *78*.

(195) Feriyanto, D.; Leman, A. M.; Baba, I.; Rahman, F.; Jajuli, F. A. Diffusion and Bonding Mechanism of Protective γ-Al_2O_3 on FeCrAl Foil for Metallic Three-Way Catalytic Converter. *MATEC Web Conf.* **2017**, *02019*.

(196) Leman, A.; Feriyanto, D.; Farhana, N.; Rahmat, R.; Bakar, B.; Baba, I. Oxidation Resistance Analysis Of Metallic (FeCrAl Foil) Catalytic Converter Developed By Ultrasonic Approach. *MATEC Web Conf.* **2016**, *78*.

(197) Setiawan, A.; Kennedy, E. M.; Stockenhuber, M. Development of Combustion Technology for Methane Emitted from Coal-Mine Ventilation Air Systems. *Energy Technol.* **2017**, 521–538.

(198) Yang, Z.; Yang, P.; Zhang, L.; Ran, J.; Guo, M.; Yan, Y. Research Progress in Fluidized Combustion Technology for Low-concentration Coalbed Methane. *Nat. Gas Ind.* **2015**, *35*, 98–104.

(199) Prasad, R.; Kennedy, L. A.; Ruckenstein, E. Catalytic Combustion. *Catalysis Rev.* **1984**, *26*, 1–58.

(200) Zwinkels, M. F. M.; Järås, S. G.; Menon, P. G.; Griffin, T. A.; Zwinkels, M. F. M.; Järås, S. G.; Menon, P. G.; Griffin, T. A. Catalytic Materials for High-Temperature Combustion. *Catalysis Rev.* **2006**, *4940*, 319–358.

(201) Hayes, R. E.; Kolaczkowski, S. T. *Introduction to Catalytic Combustion*; Amsterdam: Gordon and Breach Science Publishers, 1997.

(202) Chen, J.; Arandiyan, H.; Gao, X.; Li, J. Recent Advances in Catalysts for Methane Combustion. *Catal. Surv. from Asia* **2015**, *19*, 140–171.

(203) Choudhary, T. V.; Banerjee, S.; Choudhary, V. R. Catalysts for Combustion of Methane and Lower Alkanes. *Appl. Catal. A* **2002**, *234*, 1–23.

(204) Yang, J.; Guo, Y. Nanostructured Perovskite Oxides as Promising Substitutes of Noble Metals Catalysts for Catalytic Combustion of Methane. *Chin. Chem. Lett.* **2018**, *29*, 252–260.

(205) Gélin, P.; Primet, M. Complete Oxidation of Methane at Low Temperature Over Noble Metal Based Catalysts: a Review. *Appl. Catal. B* **2002**, *39*, 1–37.

(206) Cybulski, A.; Moulijn, J. *Structured Catalysts and Reactors*; Chemical Industries; Boca Raton: CRC Press, 2005.

(207) Civera, A.; Pavese, M.; Saracco, G.; Specchia, V. Combustion Synthesis of Perovskite-type Catalysts for Natural Gas Combustion. *Catal. Today* **2003**, *83*, 199–211.

(208) Specchia, S.; Civera, A.; Saracco, G. In situ Combustion Synthesis of Perovskite Catalysts for Efficient and Clean Methane Premixed Metal Burners. *Chem. Eng. Sci.* **2004**, *59*, 5091–5098.

(209) Specchia, S.; Ahumada Irribarra, M. A.; Palmisano, P.; Saracco, G.; Specchia, V. Aging of Premixed Metal Fiber Burners for Natural Gas Combustion Catalyzed with Pa/$LaMnO_3$ 2ZrO_2. *Ind. Eng. Chem. Res.* **2007**, *46*, 6666–6673.

(210) Ugues, D.; Specchia, S.; Saracco, G. Optimal Microstructural Design of a Catalytic Premixed FeCrAlloy Fiber Burner for Methane Combustion. *Ind. Eng. Chem. Res.* **2004**, *43*, 1990–1998.

(211) Stefanov, P.; Todorova, S.; Naydenov, A.; Tzaneva, B.; Kolev, H.; Atanasova, G.; Stoyanova, D.; Karakirova, Y.; Aleksieva, K. On the Development of Active and Stable Pd-Co/γ-Al_2O_3 Catalyst for Complete Oxidation of Methane. *Chem. Eng. J.* **2015**, *266*, 329–338.

(212) Yin, F.; Ji, S.; Wu, P.; Zhao, F.; Liu, H.; Li, C. Preparation of Pd-based metal monolithic catalysts and a study of their performance in the catalytic combustion of methane. *ChemSusChem* **2008**, *1*, 311–319.

(213) Kikuchi, R.; Maeda, S.; Sasaki, K.; Wennerström, S.; Ozawa, Y.; Eguchi, K. Catalytic Activity of Oxide-supported Pd Catalysts on a Honeycomb for Low-temperature Methane Oxidation. *Appl. Catal. A* **2003**, *239*, 169–179.

(214) Slovetskaya, K. I.; Kustov, L. M. High-temperature Methane Oxidation over Metallic Monolith-supported Zeolite Catalysts Containing Mn, Co, and Pd Ions. *Russ. Chem. Bull.* **2003**, *52*, 1933–1939.

(215) Maione, A.; André, F.; Ruiz, P. The Effect of Rh Addition on Pd/γ-Al_2O_3 Catalysts Deposited on FeCrAlloy Fibers for Total Combustion of Methane. *Appl. Catal. A* **2007**, *333*, 1–10.

(216) Fan, X.; Wang, F.; Zhu, T.; He, H. Effects of Ce on Catalytic Combustion of Methane over Pd-Pt/Al_2O_3 Catalyst. *J. Environ. Sci.* **2012**, *24*, 507–511.

(217) Uda, T.; Tanaka, M.; Munakata, K. Characteristics of Honeycomb Catalysts for Oxidation of Tritiated Hydrogen and Methane Gases. *Fusion Eng. Des.* **2008**, *83*, 1715–1720.

(218) Uda, T.; Sugiyama, T.; Asakura, Y.; Munakata, K.; Tanaka, M. Development of High Performance Catalyst for Oxidation of Tritiated Hydrogen and Methane Gases. *Fusion Sci. Technol.* **2005**, *48*, 480–483.

(219) Cerri, I.; Saracco, G.; Geobaldo, F.; Specchia, V. Development of a Methane Premixed Catalytic Burner for Household Applications. *Ind. Eng. Chem. Res.* **2000**, *39*, 24–33.

(220) Yin, F.; Ji, S.; Chen, B.; Zhao, L.; Liu, H.; Li, C. Preparation and Characterization

of $LaFe_{1-x}Mg_xO_3/Al_2O_3$/FeCrAl: Catalytic properties in Methane Combustion. *Appl. Catal. B* **2006**, *66*, 265–273.

(221) Scarpa, A.; Barbato, P. S.; Landi, G.; Pirone, R.; Russo, G. Combustion of Methane-hydrogen Mixtures on Catalytic Tablets. *Chem. Eng. J.* **2009**, *154*, 315–324.

(222) Yin, F.; Ji, S.; Chen, B.; Zhou, Z.; Liu, H.; Li, C. Catalytic Combustion of Methane over $Ce_{1-x}La_xO_{2-x/2}/Al_2O_3$/FeCrAl Catalysts. *Appl. Catal. A* **2006**, *310*, 164–173.

(223) Yin, F.; Ji, S.; Chen, N.; Zhang, M.; Zhao, L.; Li, C.; Liu, H. $Ce_{1-x}Cu_xO_{2-x}/Al_2O_3$/FeCrAl Catalysts for Catalytic Combustion of Methane. *Catal. Today* **2005**, *105*, 372–377.

(224) Stucchi, M.; Galli, F.; Bianchi, C. L.; Pirola, C.; Boffito, D. C.; Biasioli, F.; Capucci, V. Simultaneous Photodegradation of VOC Mixture by TiO_2 Powders. *Chemosphere* **2018**, *193*, 198–206.

(225) McDonald, B. C.; de Gouw, J. A.; Gilman, J. B.; Jathar, S. H.; Akherati, A.; Cappa, C. D.; Jimenez, J. L.; Lee-Taylor, J.; Hayes, P. L.; McKeen, S. A.; et al., Volatile Chemical Products Emerging as Largest Petrochemical Source of Urban Organic Emissions. *Science* **2018**, *359*, 760–764.

(226) Everaert, K.; Baeyens, J. Catalytic Combustion of Volatile Organic Compounds. *J. Hazard. Mater.* **2004**, *109*, 113–139.

(227) Li, W. B.; Wang, J. X.; Gong, H. Catalytic Combustion of VOCs on non-noble Metal Catalysts. *Catal. Today* **2009**, *148*, 81–87.

(228) Lahousse, C.; Bernier, A.; Grange, P.; Delmon, B.; Papaefthimiou, P.; Ioannides, T.; Verykios, X. Evaluation of γ -MnO_2 as a VOC Removal Catalyst : Comparison with a Noble Metal Catalyst. *J. Catal.* **1998**, *225*, 214–225.

(229) Morales, R.; Barbero, B. P.; Cadu, L. E. Combustion of Volatile Organic Compounds on Manganese Iron or Nickel Mixed Oxide Catalysts. *Appl. Catal. B* **2007**, *74*, 1–10.

(230) Barbero, B. P.; Costa-Almeida, L.; Sanz, O.; Morales, M. R.; Cadus, L. E.; Montes, M. Washcoating of Metallic Monoliths with a MnCu Catalyst for Catalytic Combustion of Volatile Organic Compounds. *Chem. Eng. J.* **2008**, *139*, 430–435.

(231) Morales, M. R.; Barbero, B. P.; Cadús, L. E. MnCu Catalyst Deposited on Metallic Monoliths for Total Oxidation of Volatile Organic Compounds. *Catal. Letters* **2011**, *141*, 1598–1607.

(232) Li, H.; Wang, Y.; Chen, X.; Liu, S.; Zhou, Y.; Zhu, Q.; Chen, Y.; Lu, H. Preparation of Metallic Monolithic Pt/FeCrAl Fiber Catalyst by Suspension Sspraying for VOCs Combustion. *RSC Adv.* **2018**, *8*, 14806–14811.

(233) Li, J.; Lu, X.; Wu, F.; Cheng, W.; Zhang, W.; Qin, S.; Wang, Z.; You, Z. Electroplated Palladium Catalysts on FeCrAlloy for Joule-Heat-Ignited Catalytic Elimination of Ethylene in Air. *Ind. Eng. Chem. Res.* **2017**, *56*, 12520–12528.

(234) Oshima, K.; Shinagawa, T.; Nogami, Y.; Manabe, R.; Ogo, S.; Sekine, Y. Low temperature catalytic reverse water gas shift reaction assisted by an electric field. *Catal. Today* **2014**, *232*, 27–32.

(235) Peluso, M. A.; Costa-Almeida, L.; Sanz, O.; Sambeth, J. E.; Thomas, H. J.; Montes, M. Washcoating of MnOx on FeCrAlloy Monoliths. *Lat. Am. Appl. Res.* **2013**, *43*, 301–306.

(236) Maestri, M.; Beretta, A.; Groppi, G.; Tronconi, E.; Forzatti, P. Comparison Among Structured and Packed-bed Reactors for the Catalytic Partial Oxidation of CH_4 at Short Contact Times. *Catal. Today* **2005**, *105*, 709–717.

(237) Rostrup-Nielsen, J. R.; Sehested, J.; Nørskov, J. K. *Hydrogen and Synthesis Gas by Steam- and CO_2 Reforming*; Advances in Catalysis; Academic Press, 2002; Vol. 47; pp 65–139.

(238) Sadykov, V.; Sobyanin, V.; Mezentseva, N.; Alikina, G.; Vostrikov, Z.; Fedorova, Y.; Pelipenko, V.; Usoltsev, V.; Tikhov, S.; Salanov, A.; et al., Transformation of CH_4 and Liquid Fuels into Syngas on Monolithic Catalysts. *Fuel* **2010**, *89*, 1230–1240.

(239) Wismann, S. T.; Engbæk, J. S.; Vendelbo, S. B.; Bendixen, F. B.; Eriksen, W. L.; Aasberg-Petersen, K.; Frandsen, C.; Chorkendorff, I.; Mortensen, P. M. Electrified Methane Reforming: a Compact Approach to Greener Industrial Hydrogen Production. *Science* **2019**, *364*, 756–759.

(240) Katheria, S.; Deo, G.; Kunzru, D. Washcoating of $Ni/MgAl_2O_4$ Catalyst on FeCralloy Monoliths for Steam Reforming of Methane. *Energy Fuels* **2017**, *31*, 3143–3153.

(241) Koo, K. Y.; Eom, H. J.; Jung, U. H.; Yoon, W. L. Ni Nanosheet-coated Monolith Catalyst with High Performance for Hydrogen Production via Natural Gas Steam Reforming. *Appl. Catal. A* **2016**, *525*, 103–109.

(242) Cristiani, C.; Visconti, C. G.; Latorrata, S.; Bianchi, E.; Tronconi, E.; Groppi, G.; Pollesel, P. In *Scientific Bases for the Preparation of Heterogeneous Catalysts*; Gaigneaux, E., Devillers, M., Hermans, S., Jacobs, P., Martens, J., Ruiz, P., Eds.; Studies in Surface Science and Catalysis; 2010; Vol. 175; pp 653–656.

(243) Cristiani, C.; Finocchio, E.; Latorrata, S.; Visconti, C. G.; Bianchi, E.; Tronconi, E.; Groppi, G.; Pollesel, P. Activation of Metallic Open-cell Foams via Washcoat Deposition of $Ni/MgAl_2O_4$ Catalysts for Steam Reforming Reaction. *Catal. Today* **2012**, *197*, 256–264.

(244) Cheng, Y.; Zhai, X.; Cheng, Y.; Zhang, Z.; Jin, Y. Steam Reforming of Methane over Ni Catalyst in Micro-channel Reactor. *Int. J. Hydrog. Energy* **2011**, *36*, 7105–7113.

(245) Guo, Y.; Zhou, L.; Kameyama, H. Thermal and hydrothermal stability of a metal monolithic anodic alumina support for steam reforming of methane. *Chem. Eng. J.* **2011**, *168*, 341–350.

(246) De Miguel, N.; Manzanedo, J.; Thormann, J.; Pfeifer, P.; Arias, P. L. Ni Catalyst Coating on Fecralloy Microchanneled Foils and Testing for Methane Steam Reforming. *Chem. Eng. Technol.* **2010**, *33*, 155–166.

(247) Wu, P.; Li, X.; Ji, S.; Lang, B.; Habimana, F.; Li, C. Steam Reforming of Methane to Hydrogen over Ni-based Metal Monolith Catalysts. *Catal. Today* **2009**, *146*, 82–86.

(248) Basile, F.; Benito, P.; Del Gallo, P.; Fornasari, G.; Gary, D.; Rosetti, V.; Scavetta, E.; Tonelli, D.; Vaccari, A. Highly Conductive Ni Steam Reforming Catalysts Prepared by Electrodeposition. *ChemComm* **2008**, 2917–2919.

(249) Ryu, J. H.; Lee, K. Y.; La, H.; Kim, H. J.; Yang, J. I.; Jung, H. Ni Catalyst Wash-coated on Metal Monolith with Enhanced Heat-transfer Capability for Steam Reforming. *J. Power Sources* **2007**, *171*, 499–505.

(250) Koo, K. Y.; Eom, H. J.; Kwon, S. C.; Jung, U. H.; Yoon, W. L. Ru-coated Metal Monolith Catalyst Prepared by Novel Coating Method for Hydrogen Production via Natural Gas Steam Reforming. *Catal. Today* **2017**, *293-294*, 129–135.

(251) Ryi, S. K.; Park, J. S.; Cho, S. H.; Kim, S. H. Fast Start-up of Microchannel Fuel Processor Integrated with an Igniter for Hydrogen Hombustion. *J. Power Sources* **2006**, *161*, 1234–1240.

(252) Shi, Y.; Pelt, J. V.; Cross, J.; Pollica, D.; Brien, C. O.; Leshchiner, M. Catalysis Studies for H_2 Production by Metallic Heat Exchanger-Coated Catalysts. *Sci. World J.* **2008**, *12*, 511–522.

(253) Christian Enger, B.; Lødeng, R.; Holmen, A. A Review of Catalytic Partial Oxidation of Methane to Synthesis Gas with Emphasis on Reaction Mechanisms over Transition Metal Catalysts. *Appl. Catal. A* **2008**, *346*, 1–27.

(254) Ghoneim, S.; Elsalamony, R.; EL-Temtamy, S. Review on Innovative Catalytic Reforming of Natural Gas to Syngas. *W. J. Eng. Tech.* **2016**, *04*, 116–139.

(255) Chin, Y.-H. C.; Iglesia, E. Elementary Steps, the Role of Chemisorbed Oxygen, and the Effects of Cluster Size in Catalytic CH_4–O_2 Reactions on Palladium. *J. Phys. Chem. C* **2011**, *115*, 17845–17855.

(256) Chin, Y.-H. C.; Buda, C.; Neurock, M.; Iglesia, E. Selectivity of Chemisorbed Oxygen in C–H Bond Activation and CO Oxidation and Kinetic Consequences for CH_4-O_2 Catalysis on Pt and Rh Clusters. *J. Catal.* **2011**, *283*, 10–24.

(257) Chin, Y.-H.; Buda, C.; Neurock, M.; Iglesia, E. Reactivity of Chemisorbed Oxygen Atoms and Their Catalytic Consequences during CH_4–O_2 Catalysis on Supported Pt Clusters. *J. Am. Chem. Soc.* **2011**, *133*, 15958–15978.

(258) Lou, Y.; Steib, M.; Zhang, Q.; Tiefenbacher, K.; Horváth, A.; Jentys, A.; Liu, Y.; Lercher, J. A. Design of Stable Ni/ZrO_2 Catalysts for Dry Reforming of Methane. *J. Catal.* **2017**, *356*, 147–156.

(259) Urasaki, K.; Kado, S.; Kiryu, A.; Imagawa, K.-i.; Tomishige, K.; Horn, R.; Korup, O.; Suehiro, Y. Synthesis gas Production by Catalytic Partial Oxidation of Natural Gas Using Ceramic Foam Catalyst. *Appl. Catal. A* **2018**, *299*, 219–228.

(260) Qin, L.; Guo, M.; Liu, Y.; Cheng, Z.; Fan, J. A.; Fan, L.-S. Enhanced Methane Conversion in Chemical Looping Partial Oxidation Systems Using a Copper Doping Modification. *Appl. Catal. B* **2018**, *235*, 143–149.

(261) Wang, F.; Li, W.-z.; Lin, J.-d.; Chen, Z.-q.; Wang, Y. Crucial Support Effect on the Durability of $Pt/MgAl_2O_4$ for Partial Oxidation of Methane to Syngas. *Appl. Catal. B* **2018**, *231*, 292–298.

(262) Singha, R. K.; Shukla, A.; Yadav, A.; Konathala, L. N. S.; Bal, R. Effect of Metal-support Interaction on Activity and Stability of Ni-CeO_2 Catalyst for Partial Oxidation of Methane. *Appl. Catal. B* **2017**, *202*, 473–488.

(263) Musiani, M.; Cattarin, S.; Cimino, S.; Comisso, N.; Mattarozzi, L.; Vázquez-Gómez, L.; Verlato, E. Preparation of 3D Electrocatalysts and Catalysts for Gas-phase Reactions, Through Electrodeposition or Galvanic Displacement. *J. Appl. Electrochem.* **2015**, *45*, 715–725.

(264) Basile, F.; Benito, P.; Fornasari, G.; Monti, M.; Scavetta, E.; Tonelli, D.; Vaccari, A. *Studies in Surface Science and Catalysis*; 2010; Vol. 175; pp 51–58.

(265) Aartun, I.; Gjervan, T.; Venvik, H.; Görke, O.; Pfeifer, P.; Fathi, M.; Holmen, A.; Schubert, K. Catalytic Conversion of Propane to Hydrogen in Microstructured Rreactors. *Chem. Eng. J.* **2004**, *101*, 93–99.

(266) Enger, B. C.; Walmsley, J.; Bjørgum, E.; Lødeng, R.; Pfeifer, P.; Schubert, K.; Holmen, A.; Venvik, H. J. Performance and SEM Characterization of Rh Impregnated Microchannel Reactors in the Catalytic Partial Oxidation of Methane and Propane. *Chem. Eng. J.* **2008**, *144*, 489–501.

(267) Aartun, I.; Venvik, H. J.; Holmen, A.; Pfeifer, P.; Görke, O.; Schubert, K. Temperature Profiles and Residence Time Effects During Catalytic Partial Oxidation and Oxidative Steam Reforming of Propane in Metallic Microchannel Reactors. *Catal. Today* **2005**, *110*, 98–107.

(268) Rogozhnikov, V.; Snytnikov, P.; Salanov, A.; Kulikov, A.; Ruban, N.; Potemkin, D.;

Sobyanin, V.; Kharton, V. Rh/θ-Al_2O_3/FeCrAlloy Wire Mesh Composite Catalyst for Partial Oxidation of Natural Gas. *Mater. Lett.* **2019**, *236*, 316–319.

(269) Kim, D. H.; Kim, S. H.; Byun, J. Y. A Microreactor with Metallic Catalyst Support for Hydrogen Production by Partial Oxidation of Dimethyl Ether. *Chem. Eng. J.* **2015**, *280*, 468–474.

(270) Makarshin, L. L.; Sadykov, V. A.; Andreev, D. V.; Gribovskii, A. G.; Privezentsev, V. V.; Parmon, V. N. Syngas Production by Partial Oxidation of Methane in a Microchannel Reactor Over a Ni-Pt/$La_{0.2}Zr_{0.4}Ce_{0.4}$Ox Catalyst. *Fuel Process. Technol.* **2015**, *131*, 21–28.

(271) Zhao, G.; Chai, R.; Zhang, Z.; Sun, W.; Liu, Y.; Lu, Y. High-performance Ni-$CeAlO_3$-Al_2O_3/FeCrAl-fiber Catalyst for Catalytic Oxy-methane Reforming to Syngas. *Fuel* **2019**, *258*, 116102.

(272) Schulz, L. A.; Kahle, L. C.; Delgado, K. H.; Schunk, S. A.; Jentys, A.; Deutschmann, O.; Lercher, J. A. On the Coke Deposition in Dry Reforming of Methane at Elevated Pressures. *Appl. Catal. A* **2015**, *504*, 599–607.

(273) Lercher, J.; Bitter, J.; Hally, W.; Niessen, W.; Seshan, K. In *11th International Congress On Catalysis - 40th Anniversary*; Hightower, J. W., Delgass, W. N., Iglesia, E., Bell, A. T., Eds.; Studies in Surface Science and Catalysis; 1996; Vol. 101; pp 463–472.

(274) Aziz, M.; Setiabudi, H.; Teh, L.; Annuar, N.; Jalil, A. A Review of Heterogeneous Catalysts for Syngas Production via Dry Reforming. *J. Taiwan Inst. Chem. Eng.* **2019**, *101*, 139–158.

(275) Zhang, J.; Li, F. Coke-resistant Ni@SiO_2 Catalyst for Dry Reforming of Methane. *Appl. Catal. B* **2015**, *176-177*, 513–521.

(276) Cao, A.; Lu, R.; Veser, G. Stabilizing Metal Nanoparticles for Heterogeneous Catalysis. *Phys. Chem. Chem. Phys.* **2010**, *12*, 13499–13510.

(277) Peng, H.; Zhang, X.; Zhang, L.; Rao, C.; Lian, J.; Liu, W.; Ying, J.; Zhang, G.; Wang, Z.; Zhang, N.; et al., One Pot Facile Fabrication of Multiple-Nickel Confined in Microporous Silica with Multiple-core@shell Structure as a Highly Efficient Catalyst for Methane Dry Reforming. *ChemCatChem* **2017**, 127–136.

(278) Chai, R.; Zhao, G.; Zhang, Z.; Chen, P.; Liu, Y.; Lu, Y. High Sintering-/coke-resistance Ni@SiO_2/Al_2O_3/FeCrAl-fiber Catalyst for Dry Reforming of Methane: One-step, Macro-to-nano Organization via Cross-linking Molecules. *Catal. Sci. Technol.* **2017**, *7*, 5500–5504.

(279) Wang, K.; Li, X.; Ji, S.; Huang, B.; Li, C. Preparation of Ni-based Metal Monolithic Catalysts and a Study of their Performance in Methane Reforming with CO_2. *ChemSusChem* **2008**, *1*, 527–533.

(280) Wang, K.; Li, X.; Ji, S.; Sun, S.; Ding, D.; Li, C. In *Natural Gas Conversion VIII*; Noronha, F. B., Schmal, M., Sousa-Aguiar, E. F., Eds.; Studies in Surface Science and Catalysis; 2007; Vol. 167; pp 367–372.

(281) Yin, F.; Ji, S.; Mei, H.; Zhou, Z.; Li, C. Coupling of Highly Exothermic and Endothermic Reactions in a Metallic Monolith Catalyst Reactor: a Preliminary Experimental Study. *Chem. Eng. J.* **2009**, *155*, 285–291.

(282) Rieks, M.; Bellinghausen, R.; Kockmann, N.; Mleczko, L. Experimental Study of Methane Dry Reforming in an Electrically Heated Reactor. *Int. J. Hydrog. Energy* **2015**, *40*, 15940–15951.

(283) Chai, R.; Chen, P.; Zhang, Z.; Zhao, G.; Liu, Y.; Lu, Y. Thin-felt NiO-Al_2O_3/FeCrAl-fiber Catalyst for High-throughput Catalytic oxy-methane Reforming to Syngas. *Catal. Commun.* **2017**, *101*, 48–50.

(284) Shoynkhorova, T. B.; Rogozhnikov, V. N.; Simonov, P. A.; Snytnikov, P. V.; Salanov, A. N.; Kulikov, A. V.; Gerasimov, E. Y.; Belyaev, V. D.; Potemkin, D. I.; Sobyanin, V. A. Highly Dispersed $Rh/Ce_{0.75}Zr_{0.25}O_{2-\delta}$-$\eta$-$Al_2O_3$ /FeCrAl wire Mesh Catalyst for Autothermal n-Hexadecane Reforming. *Mater. Lett.* **2018**, *214*, 290–292.

(285) Tadd, A. R.; Gould, B. D.; Schwank, J. W. Packed Bed Versus Microreactor Performance in Autothermal Reforming of Isooctane. *Catal. Today* **2005**, *110*, 68–75.

(286) Palo, D. R.; Dagle, R. A.; Holladay, J. D. Methanol Steam Reforming for Hydrogen Production. *Chem. Rev.* **2007**, *107*, 3992–4021.

(287) Echave, F. J.; Sanz, O.; Montes, M. Washcoating of Microchannel Reactors with PdZnO Catalyst for Cethanol Steam Reforming. *Appl. Catal. A* **2014**, *474*, 159–167.

(288) Echave, F. J.; Sanz, O.; Velasco, I.; Odriozola, J. A.; Montes, M. Effect of the Alloy on Micro-structured Reactors for Methanol Steam Reforming. *Catal. Today* **2013**, *213*, 145–154.

(289) Yu, H.; Chen, H.; Pan, M.; Tang, Y.; Zeng, K.; Peng, F.; Wang, H. Effect of the Metal Foam Materials on the Performance of Pethanol Steam Micro-reformer for Fuel Cells. *Appl. Catal. A* **2007**, *327*, 106–113.

(290) Wang, X.; Jia, J.; Mu, X.; Pan, L.; Wang, S. Methanol Steam Reforming over Metal Wall-Coated $PdZn/Al_2O_3$/FeCrAl Catalyst for Hydrogen Production. *Chinese J. Catal.* **2008**, *29*, 99–101.

(291) Jia, J.; Zhou, J.; Zhang, C.; Yuan, Z.; Wang, S.; Cao, L.; Wang, S. Preparation and Characterization of Ir-based Catalysts on Metallic Supports for High-temperature Steam Reforming of Methanol. *Appl. Catal. A* **2008**, *341*, 1–7.

(292) Holladay, J.; Hu, J.; King, D.; Wang, Y. An Overview of Hydrogen Production Technologies. *Catal. Today* **2009**, *139*, 244–260.

(293) Basini, L.; Guarinoni, A.; Lainati, A. Process for the Production of Synthesis Gas and Hydrogen Tarting From Liquid or Gaseous Hydrocarbons. 2012; US Patent 2013/0028815 A1.

(294) Dhar, R.; Pedrow, P. D.; Liddell, K. C.; Ming, Q.; Moeller, T. M.; Osman, M. A. Synthesis of Pt/ZrO_2 Catalyst on Fecralloy Substrates Using Composite Plasma-polymerized films. *IEEE Trans. Plasma. Sci.* **2005**, *33*, 2035–2045.

(295) Hu, J.; Brooks, K. P.; Holladay, J. D.; Howe, D. T.; Simon, T. M. Catalyst Development for Microchannel Reactors for Martian in situ Propellant Production. *Catal. Today* **2007**, *125*, 103–110.

(296) Korotkikh, O.; Farrauto, R. Selective Catalytic Oxidation of CO in H_2: Fuel Cell Applications. *Catal. Today* **2000**, *62*, 249–254.

(297) Zeng, S. H.; Liu, Y.; Wang, Y. Q. CuO-CeO_2/Al_2O_3/FeCrAl Monolithic Catalysts Prepared by Sol-pyrolysis Mmethod for Preferential Oxidation of Carbon Monoxide. *Catal. Letters* **2007**, *117*, 119–125.

(298) Sirijaruphan, A.; Goodwin, J. G.; Rice, R. W.; Wei, D.; Butcher, K. R.; Roberts, G. W.; Spivey, J. J. Metal Foam Supported Pt Catalysts for the Selective Oxidation of CO in Hydrogen. *Appl. Catal. A* **2005**, *281*, 1–9.

(299) Potemkin, D.; Filatov, E.; Zadesenets, A.; Rogozhnikov, V.; Gerasimov, E.; Snytnikov, P.; Korenev, S.; Sobyanin, V. Bimetallic Pt-Co/η-Al_2O_3/FeCrAl Wire Mesh Composite Catalyst Prepared via Double Complex Salt $[Pt(NH_3)_4][Co(C_2O_4)_2(H_2O)_2]$-$2H_2O$ Decomposition. *Mater. Lett.* **2019**, *236*, 109–111.

(300) Lerou, J. J.; Tonkovich, A. L.; Silva, L.; Perry, S.; McDaniel, J. Microchannel Reactor Architecture Enables Greener Processes. *Chem. Eng. Sci.* **2010**, *65*, 380–385.

(301) LeViness, S.; Deshmukh, S. R.; Richard, L. A.; Robota, H. J. Velocys Fischer–Tropsch Synthesis Technology—New Advances on State-of-the-Art. *Top. Catal.* **2014**, *57*, 518–525.

(302) Galadima, A.; Muraza, O. Revisiting the Oxidative Coupling of Methane to Ethylene in the Golden Period of Shale Gas: a Review. *J. Ind. Eng. Chem.* **2016**, *37*, 1–13.

(303) Lunsford, J. H. The Catalytic Oxidative Coupling of Methane. *Angew. Chem. Int. Ed.* **1995**, *34*, 970–980.

(304) Hoek, A.; Kersten, L. *The Shell Middle Distillate Synthesis Process: Technology, Products and Perspective*; 2004; Vol. 147; pp 25–30.

(305) Sichinga, J.; Buchanan, A. *Unlocking the Potential Wealth of Coal Introducing Sasol's Unique Coal-To-Liquids Technology*; 2005.

(306) Weinberger, S.; Scher, E.; Iyer, R. Natural Gas to Ethylene in one step Siluria Technologies OCM (Oxidative Coupling of Methane). *12AIChE - 2012 AIChE Spring Meeting and 8th Global Congress on Process Safety, Conference Proceedings* **2012**,

(307) Kustov, L. M.; Tkachenko, O. P. Spectral Study of Catalysts for the Oxidative Condensation of Methane. *Russ. J. Phys. Chem. A* **2013**, *87*, 2005–2012.

(308) Greish, A. A.; Glukhov, L. M.; Finashina, E. D.; Kustov, L. M.; Sung, J. S.; Choo, K. Y.; Kim, T. H. Comparison of Activities of Bulk and Monolith Mn-Na_2WO_4/SiO_2 Catalysts in Oxidative Coupling of Methane. *Mendeleev Commun.* **2009**, *19*, 337–339.

(309) Wang, W.; Zhang, Z.; Ji, S. Particle/metal-based Monolithic Catalysts Dual-bed Reactor with Beds-interspace Ssupplementary Oxygen: Construction and Performance for Oxidative Coupling of Methane. *J. Nat. Gas Chem.* **2012**, *21*, 400–406.

(310) Sigaeva, S. S.; Likholobov, V. A.; Tsyrul'nikov, P. G. Pyrolysis of Methane on a Heat-treated FeCrAl Coil Heated with Electric Current. *Kinet. Catal.* **2013**, *54*, 199–206.

(311) Sigaeva, S.; Temerev, V.; Kuznetsova, N.; Tsyrul'nikov, P. Pyrolysis of Methane on Ooxide Catalysts Supported by Resistive Fechral and Carborundum. *Catal. Ind.* **2017**, *9*, 181–188.

(312) Speight, J. G. In *Gasification of Unconventional Feedstocks*; Speight, J. G., Ed.; Gulf Professional Publishing: Boston, 2014; pp 118–134.

(313) Frost, L.; Elangovan, E.; Hartvigsen, J. Production of Synthetic Fuels By High-Temperature Co-Electrolysis of Carbon Dioxide And Steam With Fischer-Tropsch Synthesis. *Can. J. Chem. Eng.* **2016**, *94*, 636–641.

(314) Chin, Y. H.; Hu, J.; Cao, C.; Gao, Y.; Wang, Y. Preparation of a Novel Sstructured Catalyst Based on Aligned Carbon Nanotube Arrays for a Microchannel Fischer-Tropsch Synthesis Reactor. *Catal. Today* **2005**, *110*, 47–52.

(315) Almeida, L.; González, O.; Sanz, O.; Paul, A.; Centeno, M.; Odriozola, J.; Montes, M. In *Natural Gas Conversion VIII*; Noronha, F. B., Schmal, M., Sousa-Aguiar, E. F., Eds.; Studies in Surface Science and Catalysis; 2007; Vol. 167; pp 79–84.

(316) Merino, D.; Sanz, O.; Montes, M. Effect of the Thermal Conductivity and Catalyst Layer Thickness on the Fischer-Tropsch Synthesis Selectivity Using Structured Catalysts. *Chem. Eng. J.* **2017**, *327*, 1033–1042.

(317) Reyero, I.; Moral, A.; Bimbela, F.; Radosevic, J.; Sanz, O.; Montes, M.; Gandía, L. M. Metallic Monolithic Catalysts Based on Calcium and Cerium for the Production of Biodiesel. *Fuel* **2016**, *182*, 668–676.

(318) Reyero, I.; Velasco, I.; Sanz, O.; Montes, M.; Arzamendi, G.; Gandía, L. M. Structured

Catalysts Based on Mg-Al Hydrotalcite for the Synthesis of Biodiesel. *Catal. Today* **2013**, *216*, 211–219.

(319) Sánchez M.,; F., J.; González Bello, O. J.; Montes, M.; Tonetto, G. M.; Damiani, D. E. Pd/Al_2O_3-cordierite and Pd/Al_2O_3-Fecralloy Monolithic Catalysts for the Hydrogenation of Sunflower Oil. *Catal. Commun.* **2009**, *10*, 1446–1449.

(320) Samad, J. E.; Nychka, J. A.; Semagina, N. V. Structured Catalysts via Multiple Stage Thermal Oxidation Synthesis of FeCrAl Alloy Sintered Microfibers. *Chem. Eng. J.* **2011**, *168*, 470–476.

(321) Shi, X.; Ji, S.; Wang, K.; Li, C. Oxidative Dehydrogenation of Ethane with CO_2 over Novel Cr / SBA-15 / Al_2O_3 / FeCrAl Monolithic Catalysts. *Energy Fuels* **2008**, *22*, 3631–3638.

(322) Hu, J.; Wang, Y.; Cao, C.; Elliott, D. C.; Stevens, D. J.; White, J. F. Conversion of Biomass-derived Syngas to Alcohols and C2 Oxygenates Using Supported Rh Catalysts in a Microchannel Reactor. *Catal. Today* **2007**, *120*, 90–95.

(323) Diaz, Y.; Sevilla, A.; Mónaco, A.; Méndez, F. J.; Rosales, P.; Garcí, L.; Brito, J. L. Metallic Monoliths of AISI 304 Stainless Steel, Aluminum, FeCrAlloy® and Brass, Coated by Mo and W Oxides for Thiophene Hydrodesulfurization. *Fuel* **2013**, *110*, 235–248.

(324) Yuan, Y. H.; Zhou, X. G.; Wu, W.; Zhang, Y. R.; Yuan, W. K.; Luo, L. Propylene Epoxidation in a Microreactor with Electric Heating. *Catal. Today* **2005**, *105*, 544–550.

(325) noz Murillo, A. M.; T., L. M.; Domínguez, M.; Odriozola, J.; Centeno, M. Selective CO Methanation with Structured RuO_2/Al_2O_3 Catalysts. *Appl. Catal. B* **2018**, *236*, 420–427.

(326) Konishcheva, M.; Snytnikov, P.; Rogozhnikov, V.; Salanov, A.; Potemkin, D.; Sobyanin, V. Structured NiCl/CeO_2/η-Al_2O_3/FeCrAl Wire Mesh Catalyst for Selective CO Methanation. *Catal. Commun.* **2019**, *118*, 25–29.

(327) Konishcheva, M. V.; Svintsitskiy, D. A.; Potemkin, D. I.; Rogozhnikov, V. N.; Sobyanin, V. A.; Snytnikov, P. V. Catalytic Performance and Characterization of Highly Efficient Composite Ni(Clx)/CeO_2/η-Al_2O_3/FeCrAl Wire Mesh Catalysts for Preferential CO Methanation. *ChemistrySelect* **2020**, *5*, 1228–1234.

(328) Dou, L.; Yan, C.; Zhong, L.; Zhang, D.; Zhang, J.; Li, X.; Xiao, L. Enhancing CO_2 Methanation Over a Metal Foam Structured Catalyst by Electric Internal Heating. *Chem. Commun.* **2020**, *56*, 205–208.

(329) Mortensen, P. M.; Klein, R.; Aasberg-Peterse, K. Steam Reforming Heated by Resistance Heating. 2018; European Patent 3574991 A1.

(330) Van Geem, K. M.; Galvita, V. V.; Marin, G. B. Making Chemicals with Electricity. *Science* **2019**, *364*, 734–735.

(331) Wismann, S. T.; Engbæk, J. S.; Vendelbo, S. B.; Eriksen, W. L.; Frandsen, C.; Mortensen, P. M.; Chorkendorff, I. Electrified Methane Reforming: Understanding the Dynamic Interplay. *Ind. Eng. Chem. Res.* **2019**, *58*, 23380–23388.

(332) Dyos, G. *The Handbook of Electrical Resistivity: New Materials and pressure effects*; 2012; pp 1–478.

(333) Hattendorf, H.; Hojda, R.; Naumenko, D.; Kolb-Telieps, A. A New Austenitic Alumina Forming Alloy: an Aluminium-coated $FeNi_{32}Cr_{20}$. *Mater. Corros.* **2008**, *59*, 449–454.

12 TOC graphic

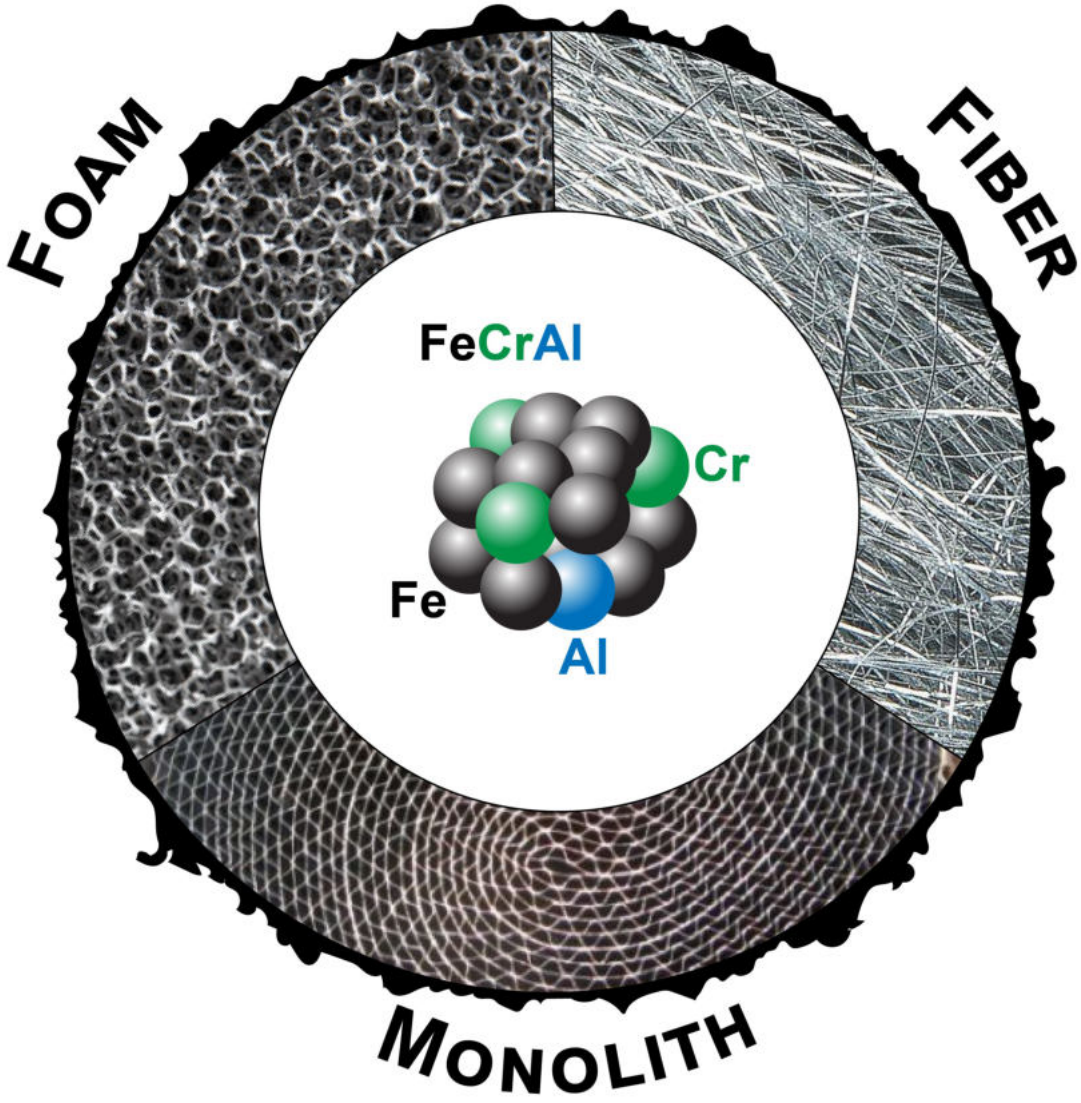
FOAM
FIBER
FeCrAl
Cr
Fe
Al
MONOLITH